Modelling of dynamic pile behaviour during an earthquake using PLAXIS 2D: Embedded beam (row)

Ben van der Kwaak

Delft University of Technology

Delft University of Technology

CRUX

Modelling of dynamic pile behaviour during an earthquake using PLAXIS 2D: Embedded beam (rows)

Master of Science Thesis

By

B. van der Kwaak

Delft, December 2015

To obtain the degree of Master of Science
At the Delft University of Technology

Delft University of Technology
Faculty of Civil Engineering and Geosciences
Section Geo-Engineering

Crux Engineering BV

Student number: 1504525
Project duration: 24 March 2015 – 15 December 2015

Graduation committee:

Prof. dr. M.A. Hicks	*Delft University of Technology*
Dr. Ir. R.B.J. Brinkgreve	*Delft University of Technology*
Dr. F. Pisanò	*Delft University of Technology*
Ir. H.R. Schipper	*Delft University of Technology*
Ir. E. Kaspers	*Crux Engineering BV*
Ing. K. de Jong	*Crux Engineering BV*

Preface

Since the early ’90, earthquakes have been felt in Groningen. After a long period of research, the gas extraction in the area was determined to be the cause. These human-induced earthquakes have grown in intensity over time, with the recent most powerful measured at 16 august 2012 at Huizinge with a magnitude of 3.6 on the Richter scale. My curiosity towards these earthquakes was drawn because I grew up in the very same area where these earthquakes now happen. Also the affinity with both structural and geotechnical aspects of the pile-soil interaction, led to the search for an interesting master thesis topic in February 2015. After several appointments at CRUX Engineering BV and at the section Geo-Engineering of the TU Delft, I found an interesting topic: the modelling of dynamic soil-pile interaction for the Groningen situation, using a FEM program. For this purpose, I have researched the possibilities and limitations of PLAXIS 2D Embedded beam row.

After a period of nine months, the report is finished and a challenging and exciting period came to an end. Especially the research and validation of the complex modelling of dynamic soil-pile interaction during an earthquake turned out to be the main challenge. Without the help and support from many, I could not have succeeded in finishing this master thesis. Therefore, I would like to thank those who contributed to this report or who supported me during the process of graduation, in particular:

- All members of my graduation committee for their input, interest and feedback. Also the discussion and guidance with all the individual members during the several meetings were very helpful.
- Colleagues in Amsterdam from CRUX Engineering BV for their interest, support, discussions, feedback, provided data and information that I required during this research.
- My family for supporting me throughout my time at University.
- My girlfriend for her great and loving support.

The abstract hereafter gives a short insight in the performed research. After the abstract the main report begins.

December 2015,

Ben van der Kwaak

Abstract

In the last few years the research activities on the effect of human induced earthquakes on (piled) foundations has grown enormously. Apart from the complex numerical models for masonry and the effect of earthquake loading on these structures, a lot of research is currently performed on the soil properties and its effect on the wave propagation. However, the influence of these human induced earthquakes on pile foundations and an easy and time efficient FEM calculation method is not yet available or well described in Dutch literature. There are several ways of approximating the soil-pile behaviour during an earthquake. The main one, which is also applied in this master thesis, is by performing 2D FEM analyses on the soil and subsequently the pile behaviour. By performing a 2D analysis, one assumes an infinite long soil profile and structure. It is not possible to model actual 3D soil behaviour of laterally loaded piles correctly, for example the modelling of soil “flow” around the pile. Therefore, it is necessary to test and validate the obtained 2D approximations with for example 3D FEM analysis or real measurement data. In this aspect a study on the possibilities and limitations of the embedded beam (row) within PLAXIS 2D will be performed. Static pushover analysis, free field site response analysis of the Groningen situation and the kinematic loading of the embedded pile will be addressed. The embedded beam (row) within PLAXIS 2D is in fact a 2.5D situation, where the pile (or beam) is connected to the soil elements of the FEM by special interfaces. These interfaces (springs) are defined by the interface stiffness factor, which are determined and validated in previous master thesis projects for mostly axial loading. They depend mainly on the pile to pile distance specified for the embedded beam. In the latest version of PLAXIS (2015) a limiting lateral soil resistance can be defined. With this option plastic behaviour is now incorporated into the 2D pile behaviour. This should give a better approximation of the pile response when compared to 3D calculations or measurements.

The first part of the thesis contains an extensive analysis on the static pushover analysis of an embedded beam in PLAXIS 2D for several pile spacing’s. Based on soil investigation from Groningen, a silty clay layer was defined and used as a one layered soil profile of 20 m depth. During an earthquake, the soil behaviour is assumed to be undrained. Therefore, all the calculations (both static and dynamic) are performed in PLAXIS using the undrained (A) option. In order to define the right effective strength parameters for this model, based on the undrained shear strength, a small investigation was performed. The results from these static pushover analyses were then compared with 3D volume pile in PLAXIS and D-Pile Group calculations. From this comparison the best way of specifying the limiting lateral soil resistance for this thesis was determined. It also became evident that the default lateral interface stiffness factor should be improved, either by making it stress or strain dependent.

The second part consist of performing free field site response analysis in EERA, which is a 1D linear-equivalent site response analysis, and with the FEM-program PLAXIS. Based on KNMI data, which is the Royal Netherlands Meteorological institute, a deconvolution and scaling of the Huizinge earthquake signal was performed based on reports from amongst other Deltares. In EERA and PLAXIS a comparison between the base boundaries was made in order to obtain similar results in both methods. The PLAXIS model boundaries, time stepping, mesh sizes and Rayleigh damping were then further optimized by comparisons of the PLAXIS model with EERA. After the implementation of the earthquake loading in PLAXIS, the behaviour of the embedded beam was evaluated and compared to analytical design methods for kinematic bending moments and pseudo-static calculations with both D-Sheet Piling and PLAXIS 2D. Also the cyclic loading behaviour of the embedded beam in comparison with the 3D volume pile was elaborated. The main conclusion of this thesis is that the embedded beam (row) in 2D does show capabilities for modelling (dynamic) lateral loaded pile behaviour. However, the option of the limiting lateral soil resistance should be optimized in combination with an alternative way of defining the interface stiffness factors. The plastic behaviour of the pile-soil system should be improved of the embedded beam(row) in order to show similar damping behaviour as was obtained in 3D.

Table of contents

List of symbols and abbreviations

A_b	Area pile [m^2]
a	Coverage of reinforcement [m]
	or dimensionless factor which determine the depth dependent relation of shear modulus
a_s / a_{ref}	Peak ground acceleration [g]
$c(')$	(effective) Cohesion [kPa]
c_u	Undrained shear strength [kN/m^2]
$\underline{\underline{C}}$	Global damping matrix
D	Pile Diameter [m]
D_{eq}	Equivalent pile diameter [m]
$\underline{\underline{D}}$	Stiffness matrix
E_{50}	Secant stiffness modulus at half the ultimate stress in an undrained test [kN/m^2]
E_{oed}	Tangent stiffness modulus for primary oedometer loading [kN/m^2]
E_p	Youngs modulus of the pile [kN/m^2]
E_{ur}	Unloading/Reloading stiffness modulus [kN/m^2]
f_{cd}	Concrete compressive strength [kN/m^2]
f_{max}	Maximum frequency component of earthquake signal [Hz]
F_x	Applied vertical pile head load [kN]
$F_{bot;max}$	Maximum axial base resistance [kN/m]
G	Shear modulus [kN/m^2]
G_0^{ref}	Reference shear modulus at very small strains ($\varepsilon < 10^{-6}$) [kN/m^2]
G_{soil}	Shear stiffness of the surrounding soil [kN/m]
G_{sd}	Shear modulus at one pile diameter depth [kN/m]
k_h	Coefficient of subgrade reaction [kN/m^3]
$\underline{\underline{K}}$	Stiffness matrix
$K_{0;nc}$	K_0 – value for normal consolidated soils (default = 1-sin(φ)) [kN/m^2]
K_c	Earth pressure factors of Brinch-Hansen [kN/m^2]
K_f	Interface stiffness at base [kN/m^2]
K_p	Passive earth pressure coefficient [kN/m^2]
K_q	Earth pressure factors of Brinch-Hansen [kN/m^2]
I_P	Pile cross-sectional moment of inertia [m^4]
ISF_{xx}	Interface stiffness factor in axial direction,
	lateral direction and for the pile base respectively [-]
J	Dimensionless empirical constant with values ranging
	from 0.25 to 0.5, determined by field testing [-]
L	Length of the pile [m]
L_a	Effective pile length [m]
$L_{spacing}$	Spacing between the embedded beam row in the out of plane direction [m]
m	Stress level dependency
$\underline{\underline{M}}$	Mass matrix
M_d	Calculated bending moment [kNm]
$M_{n,d}$	Normalized bending moment [-]
M_{kin}	Kinematic bending moment [kNm]
M_p	Plastic moment of concrete pile [kNm]
M_w	Moment magnitude of earthquake, Richter scale
M_{ref}	Moment magnitude of earthquake, Richter scale ($M_w = 3.6\ for\ WSErad$)
N	Normal force [kN]
n	Dimensionless constant based on pile fixities boundaries
	or dimensionless factor which determine the depth dependent relation of the shear modulus
n_h	Unit coefficient of subgrade reaction [kN/m^3]
PI	Plasticity index
PGA	Peak Ground acceleration [m/s^2]
p_u	The ultimate lateral load per unit length [kN/m]
$\frac{p}{p_u}$	Ratio of applied load and ultimate load [-]

R	Pile radius [m]
R_0	Reference pile radius [m]
R_{eq}	Equivalent radius of the pile diameter [m]
R_γ	dimensionless reduction factor based on earthquake magnitude
R_x	Interface stiffnesses in axial and lateral direction based on ISF, Gsoil and Lspacing
R_{inter}	Interface factor between structural elements and soil elements within PLAXIS
$\left(\frac{1}{R}\right)$	Pile curvature [m^{-1}]
$T_{top/bottom;max}$	Skin resistance at top or bottom [kN/m]
$T_{S\ or\ N;max}$	Maximum skin (s) or lateral (n) capacity [kN/m]
T_2	Calculated lateral skin resistance [kN/m]
T_{peak}	Period of peak acceleration for the scaled signal [s]
$T_{peak,ref}$	Period of peak acceleration for the unscaled signal [s]
$\underline{t}^{skin}$	Skin traction
u_s	Maximum soil displacement at soil surface [m]
$\Delta\underline{u}_{rel}$	Relative displacement between embedded pile and soil
V_p	Velocity of P-wave [m/s]
V_s	Velocity of S-wave [m/s]
$v_{s,min}$	Lowest shear wave velocity [m/s]
y	Horizontal displacement [m]
y_{50}	Horizontal displacement at 50% of p_u [m]
z	Depth from ground level [m]
z_{eff}	Effective depth from ground level [m]
α_{ff}	Peak ground acceleration [g]
α_r	Rayleigh damping coefficient
β_r	Rayleigh damping coefficient
β_s	Hysteretic damping ratio
δ	Soil-to-pile stiffness ratio [-]
$d\underline{\varepsilon}$	Incremental strain matrix [-]
ε_{50}	Strain in a triaxial test of 50% of the maximum shear stress [-]
η	Viscosity [kN s m^{-2}]
γ'	Effective soil weight [kN/m^2]
φ'	Effective friction angle [°]
γ	Shear strain [-]
$\dot{\gamma}$	Shear strain ratio [-]
$\gamma_{0,7}$	Shear strain at which G_s=0.72G_0 [-]
γ_{eff}	Effective shear strain during an earthquake with magnitude M [-]
λ_d	Winkler wave number [-]
μ	Characteristic pile wavenumber [-]
ρ	Density [Pa]
ρ_{wap}	Reinforcement percentage [%]
$d\underline{\sigma}$	Incremental stress matrix [kN/m^2]
σ_v'	Effective vertical stress [kN/m^2]
$\nu_{(s\ or\ ur)}$	Poisson Ratio [-]
τ	Shear stress [kN/m^2]
ω	Angular frequency [rad]
ξ	Damping ratio
ξ_r	Rayleigh ramping ratio
Ψ	Dilatancy angle [°]

1. Introduction

The need for knowhow on modelling the effect of earthquakes on existing foundations have grown enormously in the Netherlands over the last few years. The human-induced earthquakes have to be taken into account, not only for the old buildings, but also for new designs of buildings. A lot of research is being done on the shallow foundations of the old masonry building in the area. But an easy to use FEM-method for modelling pile-soil interaction during an earthquake is underexposed. The modelling of the impact of the free field motion during an earthquake on piles is the topic to be addressed in this master thesis, with the function of the 2D Embedded beam row within the FEM program PLAXIS.

1.1 Problem definition

As mentioned in the preface the human-induced earthquake in Groningen is increasing in magnitude in the last decade. The question arises what the influence of these earthquakes is on existing buildings and new designs. In other parts of the world, the magnitude of earthquakes is much larger than in the Netherlands. The difference in magnitude and calculated peak ground accelerations (PGA) originates from the two different types of earthquakes: natural earthquakes and human induced earthquakes. Induced earthquakes can occur near the locations where gas, or an other kind of substance, is extracted from the bedrock. In the Groningen situation, the natural gas is sealed under very high pressure in the sandstone layer at approximately a depth of 3 kilometres. With the gas extraction, the pressure will gradually drop without any consequences on the short term. In time the weight of the soils above the gas field will compact these sandstone layer (gas fields) and lead to subsidence at the surface. In the Groningen province however, there is not just one gas field, but several smaller ones due to the presence of faults. When the gas pressure on the left side of a fault differs from the right side, there is a chance on an induced earthquake, see Figure 1.

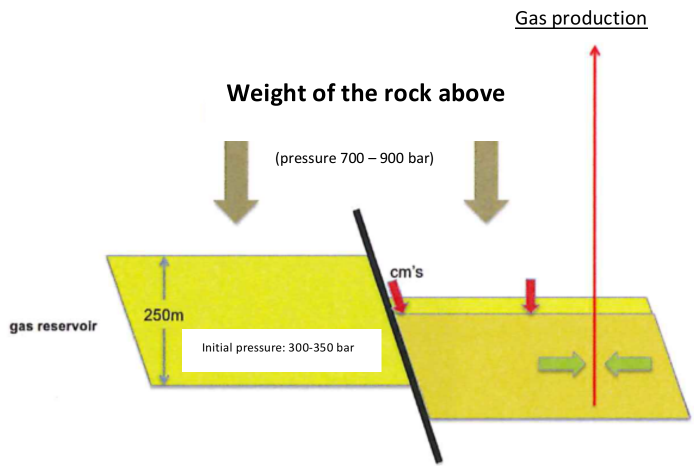

Figure 1 schematization of induced earthquake cause in Groningen (Roijakkers, 2015)

The main difference from natural tectonic earthquakes is that these induced earthquakes occur closer to the surface. When both kinds of earthquakes have the same magnitude, the induced one will have more impact on the existing buildings and soils. The energy of the earthquake has to travel far less, causing more vibrations and displacements at surface level. When calculating the PGA with a return period of 1 in 475 year, it has the same ground accelerations as the most famous earthquakes in Europe (Italy, Greece and Turkey). According to probabilistic seismic hazard assessment (KNMI, 2005) the heaviest PGA will be at Loppersum with 0,42g and near the City of Groningen it is estimated to be around 0,14g – 0,34g. See Figure 2.

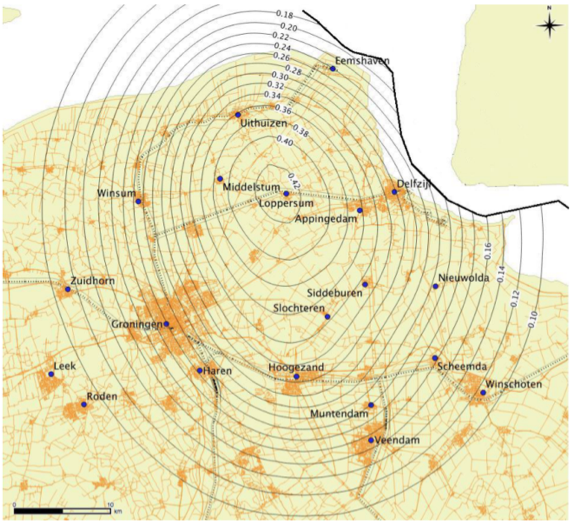

Figure 2 Plot of peak ground accelerations a_{ref} at ground surface with a return period of 475 years (KNMI, 2005)

In other countries the research on soil-pile interaction has been done for quite some time. Standards, like the ASCE 41-13 or FEMA guidelines, can be used for designing buildings and foundations near faults and earthquake sensitive areas. The soil-structure interaction can be defined by the interaction between the structure, its foundation and the soil. Three main factors can be distinguished in this interaction system:

- Foundation flexibility effects: the kind of connection between the foundation and base/the structure (fixed or rotation free);
- Kinematic interaction effects: is the interaction of the foundation (piles and pilecaps) with the soil, due to passive resistance on an embedded foundation or soil loading on piles. This is the loading of the moving soil on the piles;
- Damping effects; the dissipation of energy within the soil-structure interaction system.

Loading of the piles during an earthquake can be caused by:

- Bending and shear forces generated from inertia effects of the superstructure, which are transmitted to the piles through the pile caps;
- Bending and shear forces generated due to deformations induced by the passage of seismic waves through the soil surrounding the piles (Kinematic bending or Kinematic effect);
- Large movements imposed on the piles by soils, which have lost their shearing stiffness (Liquefaction).

In this master thesis the emphasis will be on modelling the soil, with earthquake loading, and its effect on the piles (Kinematic bending or Kinematic effect). Because the piles do not directly follow the free field motion during an earthquake, extra deformation, bending and stresses are induced. In literature some information can be found in which different techniques are specified to perform dynamic or pseudo-static analysis on the lateral pile behaviour during an earthquake. Some obtained methods from this literature are specified below:

- Dynamic Winkler method, for both kinematic and inertia loading;
- Pseudo static analysis where the maximum soil displacement is applied on piles, mainly for kinematic loading;
- Pseudo static push-over analysis, mainly for inertia loading;
- Analytical simplified formulations, for both kinematic and inertia loading;
- Numerical FEM, for example like incorporated in PLAXIS.

Most of these methods use many assumptions and simplifications for several soil and earthquake aspects. The main simplification, in most methods, is the use of a 2D situation. This however is only true if the soil and specified structures are stretched over a long length in the out of plane direction, like a dyke or sheet pile wall.

Modelling soil-pile behaviour in 2D does not incorporate actual 3D soil behaviour, since the soil can not flow around the pile in the 2D model (because the soil and the structural element in the 2D model is supposed to be of infinite length). However, performing 2D analysis is very time efficient and with the right assumptions the pile is able to approximate the 3D behaviour. This can be done in several ways, for instance by applying a strength reduction of the structural element to take the pile-to-pile distance into account. Most of the time the 2D pile behaviour is validated with actual measurement data or with 3D FEM analysis, resulting in a factor applied on the soil or pile stiffness in 2D to match the behaviour in 3D.

In this thesis the numerical FEM program PLAXIS will be used for performing the static analysis, site response analysis in the Groningen situation and investigate the kinematic effect on piles during an earthquake. In PLAXIS the soil is modelled as a one layered clay profile. One of the options for modelling the earthquake is by displacing the base of the FE model with certain acceleration. Modelling the dynamic system in a 3D FE model, will take a long time to calculate. This time could be minimized by using a 2D representation of the system, which is done often in geotechnical engineering to safe time. The software of PLAXIS will be used in this thesis for the 2D and 3D representation of the (dynamic) system. Herein the function of the embedded beam (rows) will be used and its applicability in a dynamic loading situation will be researched. However, as specified above, this 2D static pile behaviour of the embedded beam should be validated in order to check how well the approximated behaviour is in comparison with other calculation methods based on actual measurement data and 3D FEM PLAXIS calculations.

In PLAXIS 2D, the displacement of the soil is superimposed on the pile with the embedded beam option. The principle of the embedded beams in PLAXIS is shown in Figure 11. First the finite element mesh is generated and afterwards the embedded beam is added as an extra layer into the model. Between the beam-"layer" and the soil-layer(s) are interfaces, which represents the interaction of the beam with the soil by which the forces and displacements of the beam element can be calculated. This embedded beam in 2D has been validated for axial and lateral loading in previous graduation projects by Sluis (2012) and Hermans (2014). However, in these projects the loads on the pile were assumed to be static and no limiting lateral soil resistance was specified. A new recently implemented feature in the latest version of PLAXIS 2015 for the Embedded Beam is the option to define the maximum lateral skin resistance. In this way, plastic behaviour in the pile-soil interaction can be incorporated in the 2D embedded beam and approximate the 3D pile-soil behaviour.

1.2 Research objectives

The goal of this thesis is to analyse the possibilities and limitations of the embedded beam in PLAXIS 2D when used for modelling soil-pile interaction during an earthquake, with application to the Groningen case. A start will be made by performing static lateral pushover analyses of the embedded beam in 2D, after which a dynamic acceleration time history will be applied at the bottom of the soil profile. In order to achieve this main goal, the following sub-objective/activities can be specified:

- Evaluate the behaviour of the embedded beam with a lateral (static) pile head load and evaluate the influence and determination of the later slider;
- Evaluate the soil behaviour during an earthquake (free field site response);
- Evaluate the behaviour of the embedded beam during earthquake loading;
- Compare and validate the behaviour of the embedded beam using a PLAXIS 3D calculation and performing calculation with D-Sheet Piling and D-Pile Group.

1.3 Research boundaries

In the previous sections the scope of this master thesis is described. Because of the complexity and broad underlying subject of this thesis it is important to clearly describe the limits of the research. Here the main boundaries are listed, throughout the report more assumptions and limitations will be mentioned.

- Groundwater flow, time dependent soil behaviour and liquefaction of the soil are not taken into account;
- No installation effects of the modelled piles will be taken into account and the piles are made of concrete;
- No complete buildings will be implemented in the FE model, only the foundation piles (embedded beams). So realistic structure-pile-soil interaction is not taken into account;
- The embedded beam will be evaluated for free rotation/displacements at the top for the static loading case with lateral load and fixed rotation in dynamic loading case;
- One continuous soil layer is assumed based on soil data and empirical correlations of the Groningen situation, for both the static and dynamic calculations;
- The piles are only subjected to lateral loads, the combination of axial and lateral loads are not taken into account;
- All the analyses are performed on single piles, so no pile groups are modelled;
- Only comparison between the 2D FEM calculations and 3D FEM calculations / D-Systems is possible, no real test data is available.

1.4 Research approach and thesis outline

In Figure 3 the structure of the research approach is shown, on which the structure of the report is based. In chapter 2 a theoretical background on laterally loaded piles, limiting soil resistance in clays, earthquake engineering and FEM analysis is evaluated based upon the literature study. After this, the results from the sub objectives are evaluated. In chapter 3 the influence of the lateral slider and behaviour in 2D, when a static load is applied, is described. Chapter 4 contains the performed free field site displacement in order to determine the dynamic load on the piles during a certain earthquake in Groningen after which the FEM dynamic model is built in the next paragraph and the result of this kinematic loading on the embedded beam is evaluated. Finally, in chapter 5 conclusions and recommendations on the possibilities and limitations of an embedded beam row in earthquake loading are given, followed with topics for further research in chapter 6.

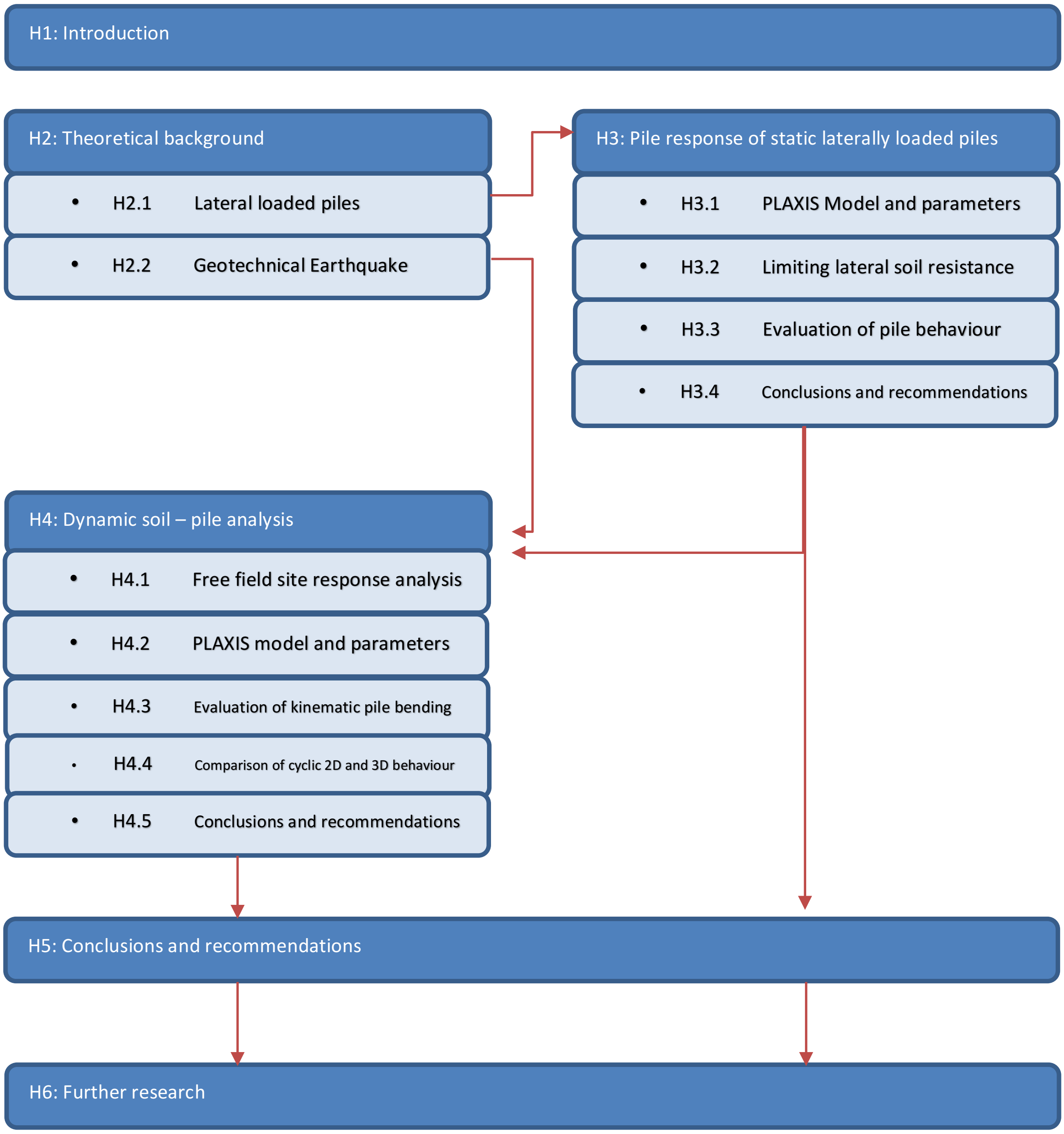

Figure 3 Schematisation of thesis outline

2. Theoretical background

This chapter gives an overview of the important theories used and applied in this research. In paragraph 2.1 the pile behaviour during lateral loading is described as well as different methods for the limiting lateral soil resistance. This paragraph also gives an overview of the applied method for pile modelling in the FEM program PLAXIS. The limiting lateral soil resistance is used in chapter 3 and 4 for determination of the lateral skin resistance in the FEM program PLAXIS for the 2D embedded beam (row). Paragraph 2.2 describes the soil behaviour during earthquakes and calculation methods for kinematic bending in foundation piles.

2.1 Laterally loaded piles

Lateral loads on piles can be divided into two types, which is either an active or passive passive lateral load. An active lateral load is applied at the head of the pile or pile cap (construction), for example wind loading on a high-rise building or piles in bridge abutments. A passive lateral load is applied over the length of the pile when soil is displaced and acts as a force on the pile, for example a pile near an embankment, excavation or due to earthquake ground excitation. Most of the pile-foundations are applied to provide axial bearing capacity to ensure the building is supported sufficiently (prevent settlement of the construction). The largest component of this axial load is the self-weight of the construction and the load-component of, for example, wind. In many cases, the magnitude of the horizontal loads in relation to the applied vertical loading is small, so no additional design calculations are performed. In other loading cases however, near an embankment or due to earthquake loading, the horizontal loading may prove critical in the design. This chapter, and subsequent paragraphs, will discuss the design methods for active loading, although some of the features are also applicable for passive loading (for example, the limiting soil resistance).

When a pile is loaded laterally, normal stresses in front of the pile will increase and decrease behind the pile. Displacements in front of the pile will be radially away from the pile and radially towards the pile behind it. It is possible for a gap to open up between the back of the pile and the soil, when the soil in front of the pile has a wedge type of failure mechanism, which can be seen in Figure 4. At greater depth of the pile, the soil will eventually fail and flow around the pile (see Figure 4, right). One or more failure mechanisms can occur, when the lateral load is too high. The type of mechanism is dependent on several factors, but the main one is pile stiffness. A stiff pile, with free pile head, will rotate at a certain depth. This type will mostly occur with short piles, whereas longer piles will probably fail as a result of too much bending moment. Failure mechanisms therefore depend on stiffness of the pile, length of the pile and connection at pile head. The flow around the pile is incorporated in 3D FEM calculation programs like PLAXIS, when a single pile is assumed or pile-to-pile distance larger than 8 times the diameter of the pile.

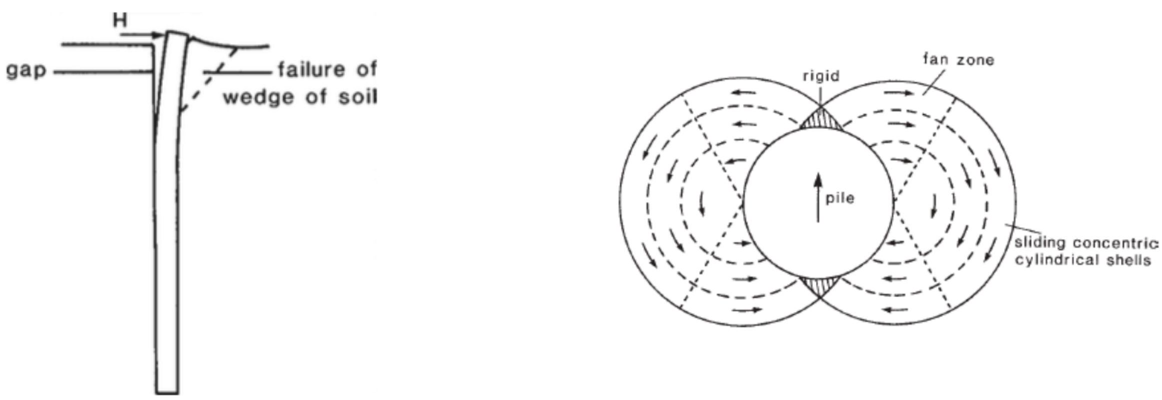

Figure 4 Deformation of pile (left) and soil around a pile (right) under active lateral load (Fleming, et al., 2008)

2.1.1 Design methods for laterally loaded piles

Many theories of determining the bearing capacity and pile displacements of laterally loaded piles can be found in literature, for either cohesive of non-cohesive soil types. This section gives an overview and summary of the theories applicable in this study, based on Broms (1964), Matlock (1970), Randolph & Gouvernec (2011), API RP 2A-WSD (2010) and Fleming, et al. (2008).

2.1.1.1 Limiting soil resistance of laterally loaded piles

The load displacement behaviour can be described by so called p-y curves, which describes the relationship between the load per unit length of the pile (P) and the deflection (Y). The ultimate lateral load per unit length p_u has to be determined in order to work with these p-y curves. For cohesionless soils, equations (1) and (2) by Broms (1964a) is often applied.

$$p_u = 3 * K_p * \sigma'_v * D \tag{1}$$

$$K_p = \frac{1+\sin(\varphi')}{1-\sin(\varphi')} \tag{2}$$

Since for this study the soil is a one layered silty clay, the methods for the limiting soil resistance are only elaborated for the cohesive soil methods. For cohesive soils, the lateral bearing capacity depends in most theories on the undrained shear strength c_u. The bearing capacity varies between 8 and 12 times $c_u * D$, except for shallow depths where the bearing capacity is lower. A value of 12 is associated with rough piles, however a value of 9 is most used in design. Depending on the type of clay, uniform or normally consolidated, two limiting lateral resistance profiles can be distinguished (Randolph & Gouvernec, 2011):

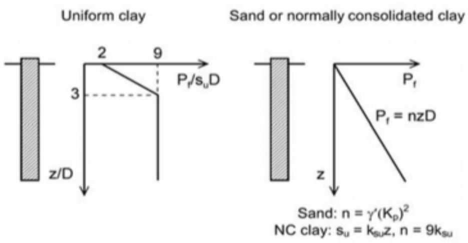

Figure 5 Limiting lateral resistance profiles (Randolph & Gouvernec, 2011)

A uniform clay assumes a constant c_u value in the soil, so there is no stress dependent factor, whereas in the normally consolidated clay the c_u is depth dependent and increasing with depth. For the normally consolidated clays, the limiting lateral resistance is determined by 8 to 12 times $c_u * D$, where c_u is depth dependent . For uniform clay the profile of limiting pressure is linearly increasing from 2 times $c_u * D$ at surface level to 9 times $c_u * D$ at a depth of 3 pile diameters, where c_u is taken as an average or at reference stress of 100kPa. Below 3 times D the limiting pressure is 9 times $c_u * D$. Equation (3) and (4) describes this profile, much as was originally suggested by Broms (1964b):

$$p_u = \left(2 + 7 * \frac{z}{3D}\right) * c_u * D \quad for\ z < 3D \tag{3}$$

$$p_u = 9 * c_u * D \quad for\ z \geq 3D \tag{4}$$

Internationally the API standard (2010) is often used, which has a different approach for the lateral bearing capacity for especially cohesionless soils. For cohesive soils the API suggest a set of equations similar to Broms. The ultimate lateral load per unit length varies between 8 and 12 times $c_u * D$, while the initial limiting pressure at ground level is 3 times $c_u * D$.

$$p_u = \left(3 * c_u + \gamma' * z + J * \frac{c_u * Z}{D}\right) * D \quad (5)$$

$$p_u = 9 * c_u * D \quad \text{for } Z \geq Z_r \quad (6)$$

In which c_u is the undrained shear strength, γ' the effective soil weight, J a dimensionless empirical factor based on field testing with values ranging from 0.25 till 0.5 based on the stiffness of the soil. After a certain depth below surface, specified by $Z_r = \frac{6*D}{\frac{\gamma' * D}{c_u} + J}$, the limiting soil resistance becomes constant with depth based on equation (6).

In case of non-cohesive soil, p_u can be calculated for shallow and deep depths with use of a graph with a dimensionless coefficients C1, C2 and C3. Further information for these non-cohesive soils can be found in API RP 2A-WSD (2010).

Another method for determining the limiting soil resistance is a method developed by Brinch Hansen. In essence it is the same as the model of Blum, but the calculation of the ultimate soil resistance is different. According to Brinch Hansen, this ultimate soil resistance is depth dependent and can be calculated using equation (7):

$$p_u(z) = \left(\sigma_v' * K_q + c * K_c\right) * D \quad (7)$$

For incorporation of undrained behaviour, the cohesion should be replaced by the undrained shear strength in this method.

2.1.1.2 Deformation behaviour of lateral loaded piles

The lateral deformation behaviour of piles is often modelled by springs attached to the pile with a certain stiffness k_h [kN/m^3]; the coefficient (modulus) of subgrade reaction. Various methods for determining k_h have been developed in the past, of which three are described in this paragraph. First of all, the relatively simple linear coefficient of subgrade reaction, after that the more advanced method by Ménard, p-y curves and finally FEM. Poulos & Davis, (1980) gave an overview of the developed methods by various authors. For stiff overconsolidated clays, k_h is independent of depth.

Broms (1964a) related k_h to the secant modulus E_{50} according to equation (8). Using Skempton (1951) with E_{50} equal to 50 to 200 times the undrained shear strength c_u, equation (9) is obtained. Davisson (1970) suggested a more conservative value according to (10).

$$k_h = 1.67 * \frac{E_{50}}{D} \quad (8)$$

$$k_h = 80 \textit{ to } 320 * \frac{c_u}{D} \quad (9)$$

$$k_h = 67 * \frac{c_u}{D} \quad (10)$$

For soft cohesive soils and all cohesionless soils, it is assumed that k_h increases linearly with depth according to the following relationship:

$$k_h = n_h * \frac{z}{D} \quad (11)$$

For cohesive soils, various values for n_h are found in literature (see Table 1). Terzagi (1955) presented values for n_h for cohesionless soils (Table 2).

Soil type	n_h [kN/m^3]	Reference
Soft NC clay	163-3447	Reese and Matlock, 1956
	271-543	Davisson and Prakash, 1963
NC organic clay	179-271	Peck and Davisson, 1962
	179-814	Davisson, 1970
Peat	54	Davisson, 1970
	27-109	Wilson and Hilts, 1967

Table 1 Typical values of n_h for cohesive soils (Poulos & Davis, 1980)

Soil type	Relative density		
	Loose $D_r < 0.33$	***Medium*** $D_r = 0.33$-0.67	***Dense*** $D_r > 0.67$
Dry sand	2425	7275	19400
Sand under water	1386	4850	11779

Table 2 Typical values of n_h for cohesionless soils after Terzaghi, 1955 (Poulos & Davis, 1980)

Ménard developed an empirical method for determining k_h as given in equation (12). It is based on in-situ test with a pressiometer. In equation (12), R and R_0 are pile radius and reference pile radius of 0.3m. E_p is the modulus of elasticity determined with a pressiometer test, or can be related to a CPT test: $E_p \approx \beta \cdot q_c$. Finally, α and β are rheological factors depending on soil type (see Table 3)

$$\frac{1}{k_h} = \frac{1}{3E_p} * \left[1.3 * R_0 \left(2.65 \frac{R}{R_0}\right)^{\alpha} + \alpha R\right] \tag{12}$$

Soil type	α [-]	β [-]
Peat	1	3.0
Clay	2/3	2.0
Silt	1/2	1.0
Sand	1/3	0.7
Gravel	1/4	0.5

Table 3 Values for α and β according to Ménard (CUR 228, 2010)

The API recommends the use of so called load transfer functions, instead of using a coefficient of subgrade reaction. A load transfer function is a predefined load-displacement behaviour, which is incorporated in the springs defining the stiffness and strength of the soil. Based on test data from laterally loaded piles the load-displacement behaviour is fitted with the so called p-y curves (Matlock, 1970). This p-y curves describe the relationship between the load per unit length of the pile (p) and the deflection (y). For cohesive soils equation (13 and 14) is specified as:

$$\frac{p}{p_u} = 0.5 * \left(\frac{y}{y_{50}}\right)^{\frac{1}{3}} \tag{13}$$

$$y_{50} = 2.5 * \varepsilon_{50} * D \tag{14}$$

With p_u and ε_{50} known, the p-y curve can be used to determine y [m] for a given p [kN/m] and visa versa. The ratio dp/dy represents k_h. For non-cohesive soils there is a different strategy, which can be found in API RP 2A-WSD (2010).

2.1.2 Software for designing pile foundations

In the previous paragraph some design methods and models where presented, which are implemented in software packages. For horizontally loaded piles, software packages like *D-Pile Group* or *D-Sheet Piling* from the D-series of Deltares can be used. Apart from these packages, finite element software like PLAXIS is being used more and more in engineering practice. PLAXIS is not based on standards, but uses numerical methods and constitutive relations to simulate soil and structural behaviour and soil-structure interaction, whereas the D-Series is based on the EUROCODE and API standards.

2.1.2.1 D-Pile Group

In D-Pile Group the interaction between the pile and the surrounding soil is described by lateral and axial soil springs along the pile. This is similar to the way it is done in D-Sheet Piling, but in D-Pile Group it is done in a three-dimensional space. The non-linear relation of these springs is based on design rules from either the NEN or API codes. To model the interaction between the piles and the soil multiple models are available:

- Poulos model;
- Plasti-Poulos model;
- Cap model;
- Cap soil interaction model;
- Cap layered soil interaction model.

In this thesis the validation of the 2D FEM model, will be partly done by using the Cap Model in a D-Pile Group calculation. This model uses elasto-plastic springs according to the API-rules and includes cap interaction. The Cap model does not include interaction between the soil and piles.

Therefore, the use of the cap model is limited to single piles or pile groups with large spacing. In PLAXIS 2D and 3D there are no trailing piles modelled, so the cap model is appropriate for comparing with the FEM analyses.

2.1.2.2 D-Sheet Piling

D-Sheet Piling is a program which can be used to calculate pile behaviour during active and passive lateral loads. The program can be used for either sheet pile walls or for single piles. In the same manner as in D-Pile Group, the beam element is connected to the soil profile via elasto-plastic springs. In case of lateral soil displacement working as a load on the beam, the stiffness of the soil is specified by the modulus of subgrade reaction based on Ménard, see 2.1.1.2, and the strength of the soil by the Brinch Hansen method, see 2.1.1.1.

2.1.3 FEM Analysis: PLAXIS

PLAXIS 2D and 3D are finite element software packages. Forces and displacements of soils and structures are described by a coupled system of (partial) differential equations. In PLAXIS 2D the model can either be plane strain or axisymmetric. Various material models are used to describe the soil behaviour. Structures can be made by multiple point-, -line- and plate elements. For modelling foundations in PLAXIS in 2D a plate element, node-to-node anchor or embedded beam (row) can be used.

In 3D these foundations can either be modelled by an embedded pile or by a volume pile, which is a volume with the material properties of a certain pile type. In the next sections the material models and embedded beam modelling, which are used in this thesis, are elaborated.

2.1.3.1 Material models

The relation between stress and strain can be given by mathematical expression of different material models. The stress of a point in a continuum is defined by the stress components acting on three mutually orthogonal planes passing through a point. These planes are taken perpendicular to the ones of the coordinate system. In the finite element model of PLAXIS a Cartesian system (x, y, z) is used to describe the stress states. For a detailed description of the stress and strain tensors and description of the different soil models one is referred to Brinkgreve, et al. (2015), Forsythe & Wasow (2004), Kramer (1996) and Verruijt (2008).

The relation between stress and strain can be denoted by equation (15):

$$d\underline{\sigma} = \underline{\underline{D}} * \mathrm{d}\underline{\varepsilon} \tag{15}$$

Where D is the stiffness matrix, which describes the stress-strain behaviour of the continuum. For elastic-plastic behaviour, this constitutive relation is formulated as increments of stress and strain. In general six responses can occur, see Figure 6 the different responses are named (a) to (f).

Elastic behaviour is defined by the two lines (a) and (b). The straight line of (a) is showing the linear elastic behaviour, whereas the curved line (b) shows nonlinear elastic behaviour. The plastic behaviour can be divided into three responses, showed by (c), (d) and (e). Line (c) shows perfect plastic behaviour, so no extra load can be taken by the soil. (d) and (e) show respectively strain hardening and strain softening. The lines marked by (f) show the behaviour for elastic unloading / reloading. Different soil models describe different behaviour of the soil, which behaviour will occur depends on material properties, loading paths and stress-strain history.

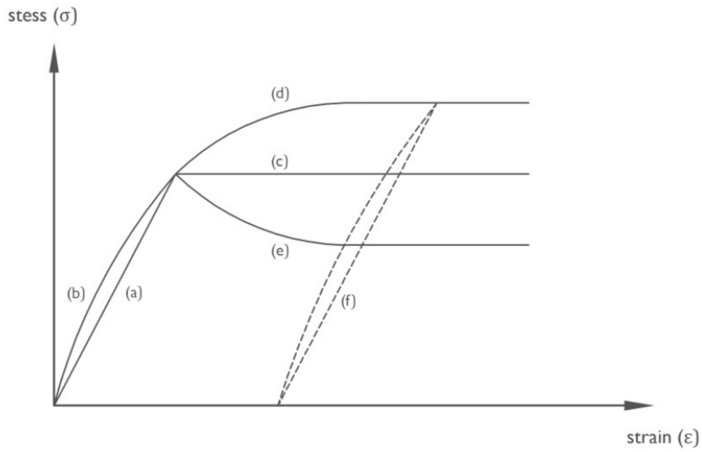

Figure 6 Several stress-strain responses

For modelling the soil behaviour in this study, the Hardening Soil small strain is applied. A description of this model is given below.

Hardening Soil model

The Hardening Soil (HS) model is an advanced model for simulating the behaviour of soft soils as well as stiffer soils. In contrast with the Mohr-Coulomb model the yield surface is not fixed in principal stress space, but as a result of plastic straining the yield surface can develop. This will change the stiffness of the soil after loading and reloading. The Mohr-Coulomb failure surface in combination with a "yield" cap is used in this model, see Figure 7 (left).

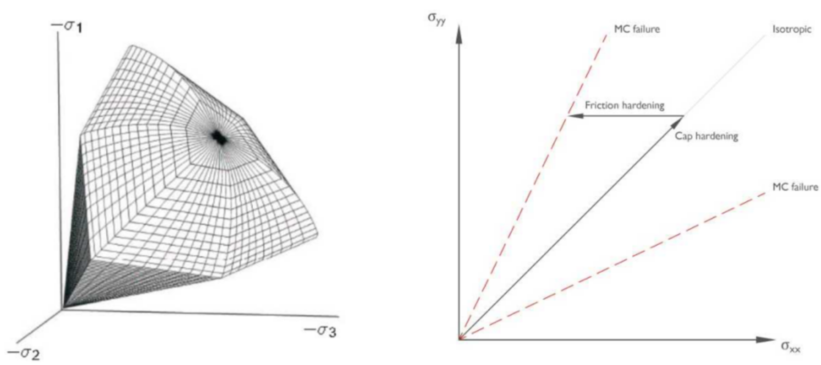

Figure 7 left: HS yield surface with cap presented in principal stress space; Right: Cap- and friction hardening

The following features are incorporated in the HS model:

- Stress-dependent stiffness;
- Shear hardening: plastic strain due to primary deviatoric-loading;
- Compression hardening: plastic strain due to primary compression (loading);
- Taking loading history into account;
- Independent behaviour for unloading/reloading;
- Mohr-Coulomb failure surface with cap.

In addition to the Mohr-Coulomb model, the yield surface is not fixed to a certain stress-state of the soil. As a result of plastic straining, the yield surface will expand, which is called hardening. In this model two types of hardening can be distinguished: Compression- and shear hardening. With both compression and shear hardening, the elastic region is enlarged; see Figure 7 (right). Inside this yield contour the material governs elastic behaviour, where the stiffness is defined by $E_{ur;ref}$. Failure of the soil is still modelled and based on the Mohr-Coulomb criterion. This failure is defined by the parameters: *c'* and φ'.

This HS-model is an improvement of the MC-model and can be used for more accurate predictions of displacements and failure for static types of geotechnical problems both in soft as in stiffer soils. However, this model does not include anisotropic strength/stiffness behaviour, time dependent behaviour (creep) and cyclic/dynamic loading effects.

Parameter	Description
φ'	Effective friction angle
c'	Effective cohesion
ψ	Dilatancy angle
$E_{50;ref}$	Secant stiffness modulus in standard drained triaxial test
$E_{ur;ref}$	Unloading/reloading stiffness (default $E_{ur;ref} = 3 * E_{50;ref}$)
$E_{oed;ref}$	Tangent stiffness modulus for primary oedometer loading
ν_{ur}	Poisson's ratio for unloading/reloading
m	Power for stress-level dependency of stiffness
R_f	Failure ratio (=0.9)
P_{ref}	Reference stress for stiffness (default = 100 kN/m2)
$K_{0;nc}$	K_0 – value for normal consolidated soils (default = 1-sin(φ))
G_0^{ref}	Reference shear modulus at very small strains (ε < 10^{-6})
$\gamma_{0,7}$	Shear strain at which G_s=0.72G_0

Table 4 Input parameters HS model and HS small model

Hardening Soil Small Strain Stiffness model

In addition to the HS-model, the small-strain stiffness relation is implemented according to the formulation of Benz (2007). The assumption of linear elastic unloading/reloading behaviour within the yield surface of the HS model is in reality only applicable for very small strain range. Unloading/reloading stiffness has a nonlinear dependency of strain, with increasing strain. The small-strain relation is based on a modulus reduction curve, formed by the shear modulus G, plotted as a logarithmic function of the shear strain $\gamma_{0,7}$.

These stiffness parameters G_0, known as $\gamma_{0,7}$ are the only parameters that are different from the other HS-model. A hyperbolic law describes the small-strain stiffness. The basic characteristic of this relation is a decrease of stiffness with increase of strains, due to the intermolecular and surface forces within the soil skeleton, see Figure 8.

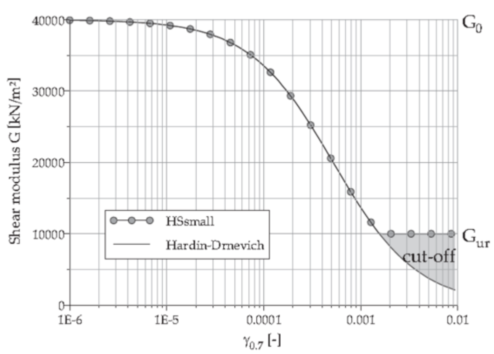

Figure 8 Example of modulus reduction curve

The HS Small model shows hysteretic and damping behaviour with cyclic loading. The principles are elaborated in paragraph 4.1.1. The two extra input parameters for the HS Small model can be seen in Table 4. For small motion amplitudes hysteretic damping will be negligibly small, which is unrealistic compared to actual soil behaviour. Therefore, Brinkgreve, et al. (2007) recommended to add additional Rayleigh damping to incorporate damping at small strains. The same paper shows that hysteretic damping at higher shear strain levels in the HS small model are overestimating actual material damping in clayey materials. A solution to this problem can be found by taking G_0 closer to G_{ur}. A final remark for the usage of HS Small model in dynamic/cyclic loading is that the model does not allow for accumulation of strain or pore pressure.

2.1.3.2 Modelling a pile in PLAXIS 2D

Within the FEM program PLAXIS there are several ways of modelling a pile in 2D. With all these methods it is important to realise that in a 2D finite element model the model is assuming an infinitive length in the out of plane direction. The modelling in 2D can be either plane stress or plane strain, in PLAXIS 2D in this thesis a plane strain situation is assumed. This means that the strain in normal, out of plane, direction is fixed and thus zero. As was mentioned in the introduction, the modelling of pile behaviour in 2D is an approximation of actual 3D behaviour. However, several ways of modelling a pile in PLAXIS 2D can be done by:

- Volume elements (+interfaces)
- Plates (+interfaces)
- Node to node anchors (+plates)
- Embedded beam row

The most important factor for determining which of these methods is best, is the ratio between the centre-to-centre distance of the piles and the pile diameter. Globally, three kinds of pile rows can be distinguished and are shown in Figure 9. For a relation (or ratio) of pile spacing over diameter of 1, the behaviour is similar to a wall. At the other end, where this relation goes to infinity, single pile behaviour is assumed. In between both relations, a pile row is modelled.

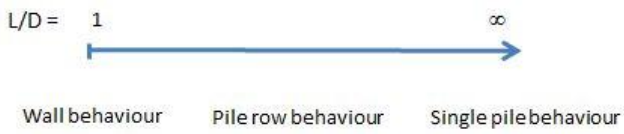

Figure 9 Pile behaviour based on pile to pile distance (L) in relation tot the diameter of the pile (D)

Piles are 1D elements, but the stress state of the surrounding soil is a 3D phenomenon and as such it is not possible to model piles with high accuracy in a 2D model. Since no installation effects are considered, the pile is so called, wished in place. Using a 2D soil model causes some unavoidable changes/simplifications in geometry, because the reality is 3D. Some of these drawbacks, when volume elements or plates are used, are specified below:

- An infinite wall is modelled; however, the skin area may be different from the actual pile row. To obtain a correct transfer of forces to the skin you may need to adjust the R_{inter}. This in turn may influence the generation of an unrealistic shear plane;
- Soil flow around and in between the piles is not possible, since a wall is modelled. This can cause unrealistic behaviour in especially lateral loading;
- The bearing capacity of the shaft and wall (pile) tip cannot be directly controlled;
- It is difficult, or almost impossible, to obtain a realistic load-displacement behaviour both in axial and lateral direction. Some methods, for example reducing the stiffness of the wall to simulate a certain pile-to-pile distance, can be used by trial and error to obtain a proper result.

These problems can be overcome, to a large extend, by using the embedded beam row for modelling pile row behaviour. However, more input is required such as the strength of the shaft friction and the tip resistance. In the next paragraph the embedded pile is further explained.

2.1.3.3 PLAXIS Embedded beam (Rows)

The embedded beam (row) is a function within PLAXIS, which implements a beam that can cross soil volume elements at any arbitrary location and orientation. This beam is connected to the surrounding soil by means of special interfaces, which describe the skin and foot resistance. Although this beam does not occupy a volume, a particular volume around the pile (elastic zone) is assumed in which plastic soil behaviour is neglected. The size of this zone is based on the input of the (equivalent) pile diameters. The embedded beam almost behaves as a volume pile, because of this zone (Dao, 2011). But on the contrary to volume piles, the embedded beam does not influence the finite element mesh as generated from the geometry model. The mesh refinements are therefore lower and save calculation time. However, the installation effects of the pile are not included into the embedded beam. Only piles, in which installation process results in low disturbance (bored piles for example), can be effectively modelled with this beam. Both in 2D and 3D the embedded beam or pile are available. In the PLAXIS manual the Embedded beam (row) is referred to the 2D version of the embedded pile in 3D.

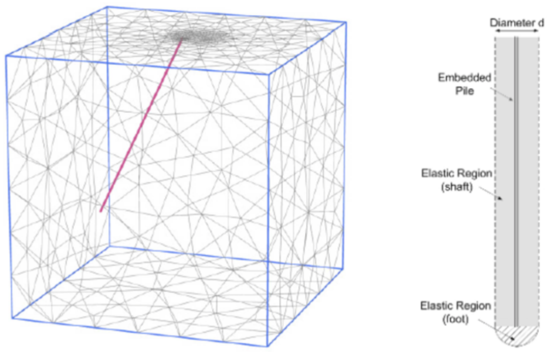

Figure 10 Embedded pile in 3D mesh and elastic zone around embedded beam (Brinkgreve, et al., 2015)

The special interfaces of the embedded beams model the soil-structure interaction. The interaction between the soil and shaft is modelled by means of line-to-volume interface elements, the interaction between soil and base by point-to-volume interface elements. These interface elements determine the strength and stiffness of this interaction. Validation of the embedded beam row (In earlier versions of PLAXIS named: embedded pile row) was done by several people: Dao (2011), Hermans (2014) and Sluis (2012). Outcome of these validations have resulted in various improvements of the embedded pile in PLAXIS 2D/3D, see paragraph 2.1.3.5. An elasto-plastic model is used to describe the behaviour of the special interfaces. The interface is divided into skin resistance (in unit of force per circumference per length) and tip resistance (in unit of force). These two resistances provide the bearing capacity of the pile in axial direction, which is an input parameter in PLAXIS. Both interfaces have failure criteria, where a distinction between elastic and plastic behaviour is specified. The skin traction ($\underline{t}^{skin}$) at the interface is described by the initial skin traction ($\underline{t}_0{}^{skin}$) and force increments at the integration points ($\Delta\underline{t}^{skin}$):

$$\underline{t}^{skin} = \underline{t}_0{}^{skin} + \Delta\underline{t}^{skin} \tag{16}$$

The constitutive relation between the skin friction increments and the relative displacement increments ($\Delta\underline{u}_{rel}$) is given by the material stiffness matrix ($\underline{\underline{K}}^{skin}$) of the interface element:

$$\Delta\underline{t}^{skin} = \underline{\underline{K}}^{skin} * \Delta\underline{u}_{rel} \tag{17}$$

With $\Delta\underline{u}_{rel}$ the difference between pile displacement and soil displacement. A full description of the embedded pile in 3D can be found in Brinkgreve, et al. (2015). Moreover, since in this thesis the embedded beam row is used, the next paragraph will give a short elaboration on the 2D embedded beam (row).

2.1.3.4 Principle of the 2D embedded beam (row)

Recently the embedded beam (row) with new features has been implemented in the 2D version of PLAXIS. Incorporation of a limiting lateral skin resistance and elasto-plastic behaviour of the beam is now available. The properties of the embedded beam row are similar to the 3D embedded pile; however, the implementation in a 2D space is different and therefore described below. This description is mainly based on Brinkgreve, et al. (2015).

The idea behind the embedded beam row in PLAXIS 2D is visualized in Figure 11. The pile is separated from the 2D model, which makes the soil mesh continuous. Special interface elements between the mesh and embedded pile are used for the soil-structure interaction. The difference between implementing an embedded beam in 3D and 2D is the fact that in 2D a beam row is schematized. Because a 2D plane strain model represents a slice of 1m, which is supposed to be repetitive. Therefore, the pile is also repetitive and a row of piles in the out-of-plane direction, with a pile spacing of 1 meter, is modelled.

The soil-structure interaction is described by interface elements between the embedded beam and the mesh. Along the pile there is a line-to-area interface, at the base there is a point-to-area interface, see right of Figure 11. The interface is represented by springs with numerical stiffnesses in axial and lateral direction (R_S and R_N). In axial direction, the force in the spring is limited by using a "slide" with a maximum force $T_{S;max}$. This represents the skin capacity of the pile and is an input parameter. In lateral direction there is also a maximum force in the latest version of PLAXIS 2D 2015, given by $T_{N;max}$, which is also an input parameter. The point-to-area interface at the base takes care of the end bearing. This is represented by a spring with numerical stiffness and a "slide" representing a maximum base resistance $F_{bot;max}$. This definition of the interface elements makes it impossible to use the embedded beam row for calculating the bearing capacity, because this is an input and not a result of the calculations.

The load-displacement behaviour is partially a result of the calculations. It is an interaction between pile stiffness, soil stiffness and interface stiffness, as shown in Figure 11. Default values for interface stiffnesses R_N, R_S and K_F are determined by PLAXIS 2D, which define the load-displacement curve.

The formulas to obtain values for R_N, R_S and K_F are derived by Sluis (2012). Overruling of these default values gives the user the ability to fit the load-displacement curve of the embedded beam row with for example measurement data from a pile load test.

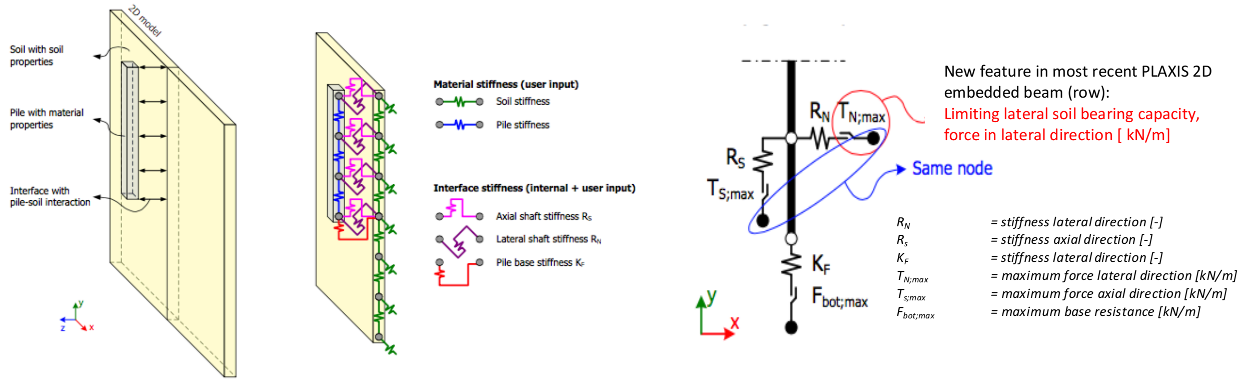

Figure 11 (left) 2D pile modelling using an embedded beam row with special interface stiffnesses; (right) Elastic springs and plastic slides for modelling soil-structure interaction (Sluis, 2012)

The interface stiffnesses (R_s, R_n and K_f) are related to the shear stiffness of the surrounding soil (G_{soil}) according to:

$$R_s = ISF_{RS} \frac{G_{soil}}{L_{spacing}} \tag{18}$$

$$R_n = ISF_{Rn} \frac{G_{soil}}{L_{spacing}} \tag{19}$$

$$K_f = ISF_{Rn} \frac{G_{soil} * R_{eq}}{L_{spacing}} \tag{20}$$

Based on research (Sluis, 2012) the interface stiffness factors for the embedded beam rows are specified and by default applied in PLAXIS 2D:

$$ISF_{RS} = 2{,}5 * \left(\frac{L_{spacing}}{D_{eq}}\right)^{-0{,}75} \tag{21}$$

$$ISF_{RN} = 2{,}5 * \left(\frac{L_{spacing}}{D_{eq}}\right)^{-0{,}75} \tag{22}$$

$$ISF_{KF} = 25 * \left(\frac{L_{spacing}}{D_{eq}}\right)^{-0{,}75} \tag{23}$$

For $|t_s| < T_{max}$ the shear stress will remain elastic. For $|t_s| = T_{max}$ will show plastic behaviour, ensuring elastic perfectly plastic behaviour of the interface. With t_s being the shear force. In the same way as the shear force, the interaction of the pile with the soil at the foot is described by a linear elastic perfectly plastic interface element. Also F_{max} is an input parameter of the embedded beam, which is the maximum force allowed at the pile foot.

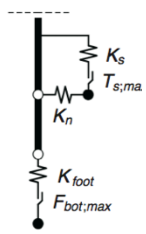

Figure 12 Stiffness of the embedded interface element for piles

The (axial and lateral) skin resistance T_{max} can be modelled in three ways:

- Constant/linear over the length of the pile;
- Multi-linear, to take inhomogeneous or multiple layers into account;
- Layer dependent, which relate skin resistance to the strength properties.

The embedded pile material data sets, so the specification of the axial and lateral skin resistance, involve only the pile bearing capacity. This means that the material data set does not include the stiffness response of the pile and soil (or p-y curves). It only specifies the point where the behaviour becomes perfectly plastic. The stiffness response is the result of the pile length, equivalent radius, bearing capacity and stiffness of the soil layers surrounding the pile. In general embedded piles are not meant to be used as laterally loaded piles, because the transverse forces t_s was not limited in the special interface element that connects the pile to the soil. This transverse force is only limited by failure of the surrounding soil (outside the elastic zone). However, in the new version of PLAXIS 2D (2015) the lateral plastic slider was introduced in the form of a specification of limiting lateral soil resistance. This is supposed to improve the behaviour of the laterally loaded embedded pile.

2.1.3.5 Validation of embedded pile for lateral loading

Since this thesis is about laterally loaded piles in static and dynamic situations, the capabilities and limitations of the embedded beam for lateral loading are important. Different researchers and master thesis projects have evaluated the behaviour of the embedded pile. For axial loading this resulted in the implementation of the elastic zone. The pile behaviour for axial loading can be modelled quite good by the embedded beam (Sluis, 2012). The embedded beam was initially developed for axial loading, but users tend to use it also for lateral loading (Brinkgreve, et al., 2012). Even though it was discouraged in the PLAXIS manual, it seemed that the embedded pile might have lateral-bearing capabilities.

This was investigated during a master graduation project by Dao (2011). The embedded pile was mainly compared with the volume pile in PLAXIS 3D. The embedded pile was able to resemble the volume pile in the same test conditions. It gave good results when modelling a rough pile, but the embedded pile overestimated the capacity for smooth piles. A rough pile is modelled with an interface factor (R_{inter}) of 1, which means that the soil sticks fully to the pile. This overestimation is probably caused by the absence of a maximum skin resistance, or soil resistance, in lateral direction. Such a maximum soil resistance is present in axial direction, but was not available for PLAXIS embedded pile in lateral direction. In the same research by Dao (2011), the embedded pile was compared to measurement data from "Centrifugeproef GeoDelft". In this case an embankment was constructed with 5 consolidation phases and the effects on a nearby pile were measured. Conclusions were that settlements, horizontal displacements and bending moments in the pile are overestimated in early consolidation phases and underestimated in later consolidation phases. Comparing the embedded pile with the volume pile gave similar results. It is also concluded that the comparisons between the PLAXIS 3D model and the real test are limited due to the lack of measured data and the unknown condition of the pile head connection.

Based on Sluis (2012) the behaviour of the 2D embedded beam (row) was analysed and compared for axial and lateral loading of the pile. They were compared to PLAXIS 3D embedded pile. Based on the difference between the 3D, 2D and EUROCODE displacement curves, Sluis gave a formulation of the interface stiffness factor (ISF) for axial loading. A general conclusion from Sluis is that the displacement of an embedded beam (row) gives very good results when compared with the 3D average soil displacements. It was also concluded that this soil displacement was independent from the determined ISF factors. With large pile spacing's however it is impossible to fit the 2D pile displacements with the 3D embedded pile. Where a plate element gives less realistic results, when $L_{spacing}/D$ (= centre-to-centre distance between piles in pile row / pile diameter) is greater than 2, the application area of the embedded beam row starts. For $L_{spacing}/D$ of 2 untill 8, the embedded beam row can be used.

When $L_{spacing}/D$ is larger than 8, in general a single pile is assumed. A better approach for calculating this behaviour is than the use of a 3D model, for example with a 3D embedded pile or volume pile. Although the results on soil displacement are good, the modelling of pile displacement is not. For large pile spacing the pile displacement is unrealistic, for small pile spacing a plate gives similar results (Sluis, 2012).

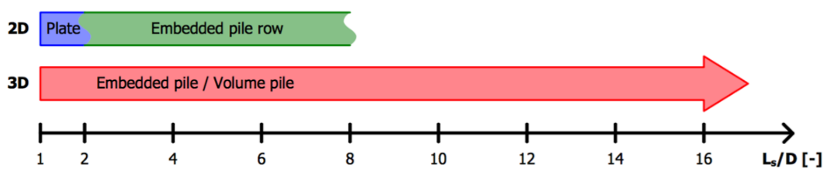

Figure 13 Application areas of PLAXIS 2D and 3D modelling a pile row with various structural elements (Sluis, 2012)

2.1.4 Conclusions

Since this thesis is about modelling a 3D reality in 2D, it is important to analyse the limitation of the 2D model. One of these limitations is in the load-displacement behaviour; in 3D the displacement will have a component in x-, y- and z direction (see Figure 14), whereas in 2D there is only a component in y- and x direction. Sluis (2012) showed in his thesis that the average 3D soil displacement is the same as the 2D soil displacement. The pile displacement should be the same in 3D and 2D, which is realised by the interface stiffness factors of the embedded beam. In the thesis of Sluis (2012) it was concluded that the embedded beam with large pile spacing, $L_{spacing}/D$ larger than 8, was not able to model the correct 3D pile displacement/forces. It therefore did not add new possibilities to the existing 2D pile modelling in PLAXIS 2D. This could be explained by the fact that the effect from Figure 4 (flow of soil around a pile in 3D) is not taken into account in this factor and that the ISF was mainly based on axial loaded piles. The ISF is by default the same for axial and lateral direction.

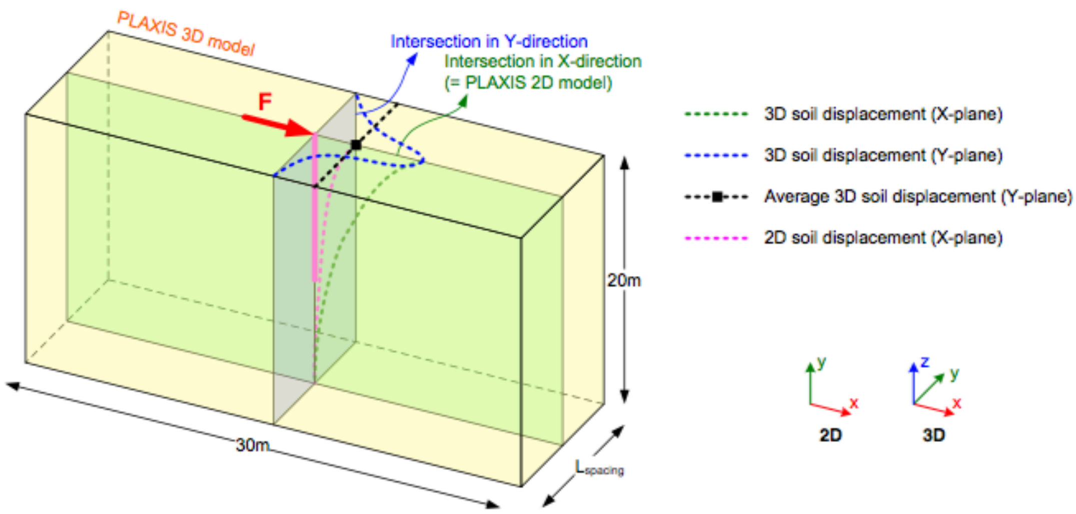

Figure 14 Comparison load-displacement behaviour for 2D and 3D (Sluis, 2012)

In the new release of PLAXIS 2D (2015), a limiting lateral skin resistance was implemented to deal with the modelling of failure of laterally loaded piles and larger pile spacing (or single piles).

2.2 Geotechnical earthquake engineering

In chapter 2.1 the static loading situation and the theoretical knowledge for this study is explained. In chapter 2.2 the theory for the dynamic loading of the embedded piles is elaborated. Earthquakes are caused by vibration of the earth's surfaces, when stored deformational energy is suddenly released. These stored energy is generated by a gradually build-up of stresses due to continental drift of tectonic plates or they can be human-induced. The latter for example when gas is extracted from rock leading to a stress reduction and collapse of the rock. Most severe earthquakes are near the boundaries of the continental plates (inter-plate) or active faults (intra-plate). In the upcoming subparagraphs the behaviour of the soil during an earthquake is explained, after which some methods are described for calculating kinematic induced bending moments of (embedded) piles.

2.2.1 Seismic wave propagation

Once there is a sudden release of energy, after an earthquake, stress waves start propagating through the Earth's crust, causing soil deformations, which can be described along the wave propagation through solids theory, for which most information described below is found in Kramer (1996) and Verruijt (2008).

A variety of wave types can occur when considering the soil to react to local disturbances as an elastic solid. This makes the resulting ground motion quite complex to determine. However, in general there are two basic types of waves that can be distinguished: body waves and surface waves. Most important body waves are P-waves (also denoted as pressure waves or primary waves) and S-waves (also denoted as shear waves or secondary waves). These waves are called body waves, because they can pass through the interior of the earth. Surface waves are only observed close to the surface of the earth and they are subdivided into Love waves and Rayleigh waves. These waves are the result of interaction between body waves and the surficial earth material. In this thesis the emphasis will be on the body-waves, due to the fact that in the Groningen situation the surface waves have not yet been measured for the relatively shallow earthquake (Kruse & Hölscher, 2010).

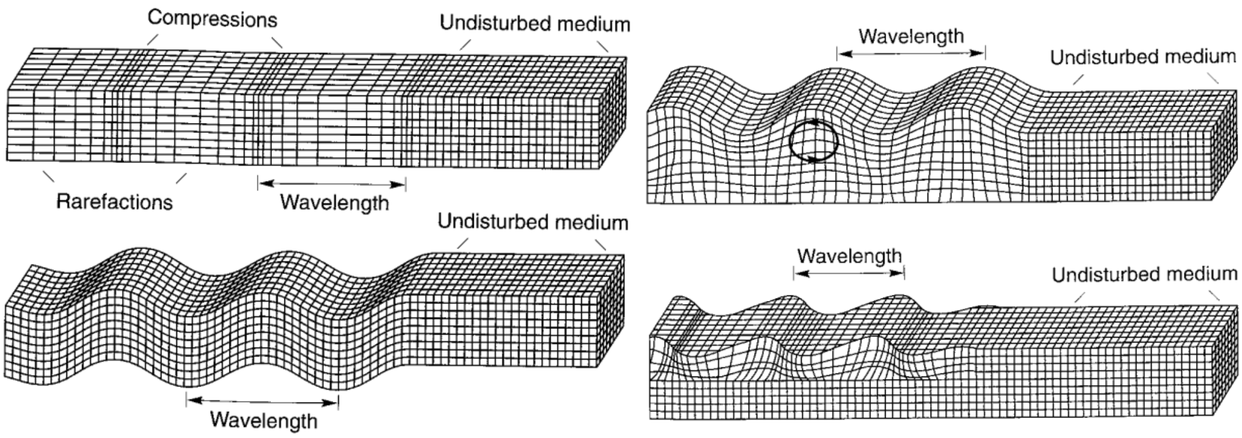

Figure 15 Compression body wave (top left) ; Shear body wave (bottom left) ; Surface Rayleigh wave (top right) ; Surface Love wave (bottom right) (Kramer, 1996)

The P-wave causes a series of compressions and dilations of the material through which it travels, see top left of Figure 15. The motion of the particles, subjected to these P-waves, is parallel to the direction of traveling wave. The P-wave is the fastest wave and is the first to arrive the site considering; the velocity of the P-wave for a 1D problem is defined by the following equation:

$$V_p = \sqrt{\frac{E_{oed}}{\rho}} = \sqrt{\frac{G(2-2\nu)}{\rho\,(1-2\nu)}} \qquad (24)$$

The S-wave causes shearing deformations of the materials through which it travels, see bottom left of Figure 15. The motion of the particles, subjected to these S-waves, is perpendicular to the direction of the traveling wave and can be divided into vertical and horizontal components. This movement will induce shear displacements of the material, so S-waves can only travel through elastic materials. The shear resistance of soil and rock is usually less than the compression-dilation resistance; Therefore, an S-wave travels more slowly through the ground than a P-wave. Its propagation speed can be obtained by the following equation:

$$V_s = \sqrt{\frac{G}{\rho}} \tag{25}$$

2.2.2 Free field site response analysis

Seismic waves will propagate from the source, earthquake ground shaking, till ground level. The characteristics of the seismic wave are modified when it travels through the soil deposit, which acts as a filter. The soil will amplify the acceleration wave signal at some specific frequencies and will damp the signal at some other. Several methods can be used to evaluate this soil effect on the seismic motion:

- Attenuation relationship approach;
- Soil coefficient approach;
- Site response analysis.

The first two are simplifications of the real soil distribution, whereas the site response analysis requires more information to identify the soil layer distribution, mechanical properties of the soil and hydraulic condition. It is preferable to perform the site investigation until the depth of the actual rock or rock-like formation and determine the index properties, stiffness and strength of the soil layers above this rock by in situ tests or laboratory tests. A ground response analysis of the soil deposit is mostly used in a preliminary study for the dynamic analysis of a structure. Seismic response of the buildings or structure is influenced by geological and geotechnical properties of the underlying / supporting soil. Most applied is the free field site response, which means that the occurred motion in the soil layer of interest is evaluated by applying a bedrock signal in the absence of any structure or excavation. This can either be a 1D linear-equivalent site response analysis or a finite element free field site response. The earthquake signal that is used for these analysis in traditional earthquake engineering only takes the horizontal acceleration signal (SH waves) into account, due to the assumption that by successive refractions in the soil (Snell's law of refraction), the considered seismic waves are bent into vertical propagating waves. A short introduction into these two free field site response analysis methods is shown here, the results of the performed free field site response of this study is shown in chapter 4.1. It should be noticed that earthquake engineering involves a high degree of uncertainty in different parts of the ground response and determination of:

- Soil stratigraphy and material properties (site investigation and laboratory testing);
- Site topography (like the level of the bedrock and any slopes at ground level);
- Ground water table (also site investigation);
- Earthquake characteristics:
  - Duration
  - Peak acceleration
  - Frequency content
  - Magnitude

1D linear-equivalent site response analysis

There are multiple one-dimensional linear-equivalent algorithms incorporated into different software packages, for example EERA, STRATA, DEEPSOIL or SHAKE2000. Most of these programs are using the same theoretical background, see manual of EERA (Bardet, et al., 2000).

In this study the EERA plugin for excel is used. A short introduction in how this program works is described below, using the information mentioned in the manual (Bardet, et al., 2000).

Seismic excitation levels can be found from a site-specific probabilistic seismic hazard assessment. This was also done for the Groningen situation by KNMI (2005). The surface motion levels (PGA values) are calculated based on local soil conditions that determine the transfer function for surface motion due to bedrock motion. The model consists of (coupled) first order linear (ordinary) differential equations based on Kelvin-Voigt solid/relation, in which shear stress depends on shear strain, shear modulus, viscosity and shear strain rate:

$$\tau = G\gamma + \eta\dot{\gamma} \tag{26}$$

This model has visco-elastic material properties, were a viscous-damper and elastic spring are parallel, see Figure 16.

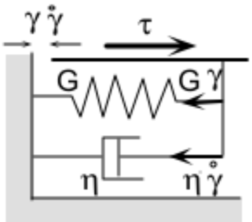

Figure 16 Stress-strain model schematization of equivalent-linear model

Shear strain is dependent on the horizontal displacement u(z,t) for a certain depth z and time the system of equations can be solved. For detailed formulation of this theory one is referred to the EERA manual (Bardet, et al., 2000) and Kramer (1996).

The non-linear and hysteretic stress-strain during cyclic loading is approximated in EERA, see Figure 18. In the hysteretic stress-strain behaviour, the influence of plastic deformation due to cyclic loading is taken into account. In Figure 18 (left), one can see that with zero stress there still is strain. This means plastic deformation of the material. The right graph of Figure 18 displays the dependency of hysteretic damping on the strain level of the material (the higher the strain, the higher the damping calculated by the iteration within EERA). This is due to more energy dissipation with large displacements. For a multi-layered soil deposit, transfer functions are derived based on boundary conditions at surface level and interface conditions. During an iterative procedure for convergence of strain level and associated shear modulus and damping percentage, the equivalent linear approach is executed.

This equivalent linear iterative approach can be described by the following steps:

1. Determine initial G_0 and ξ_0 for small strain;
2. Calculate soil response and determine amplitudes of maximum shear strain γ_{max} in every layer
3. Determine γ_{eff} by:
$$\gamma_{eff}^{i} = R_{\gamma}\gamma_{max}^{i} \tag{27}$$
With R_{γ} = (M-1)/10 a dimensionless reduction factor based on earthquake magnitude of Richter scale (M). R is input in this calculation process and equal in all layers;
4. Calculate the new equivalent linear values for G_{i+1} and ξ_{i+1} based on the effective shear strain calculation;
5. Repeat steps 2 till 4 until values for the shearing modulus and damping ratio are sufficiently alike in all ground layers.

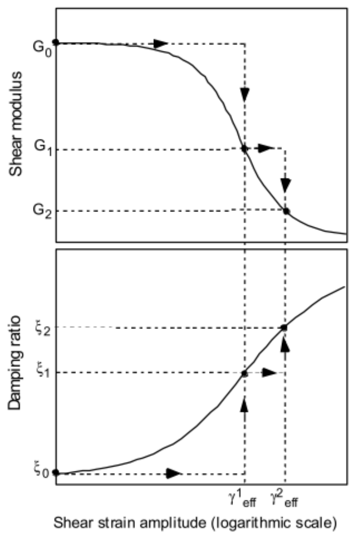

Figure 17 Iteration process for shear modulus and damping ratio based on shear strain

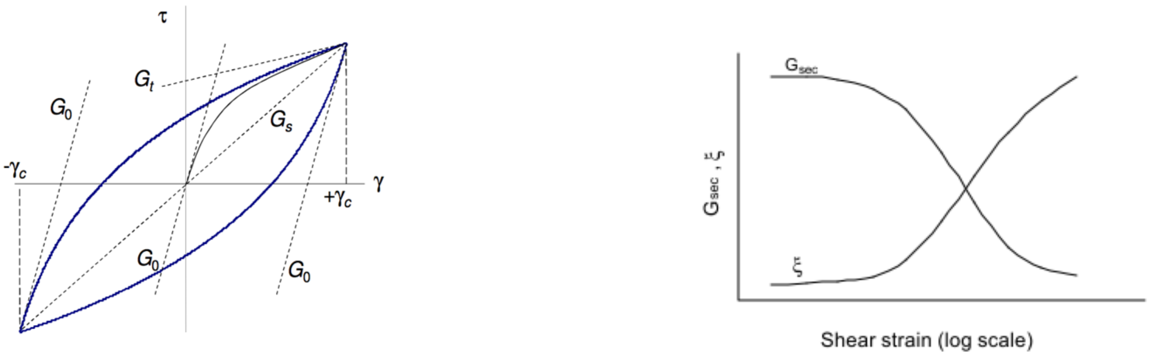

Figure 18 Equivalent-linear model; left: Hysteretic stress-strain curve; right: Variation of shear modulus G_{sec} and damping ration ξ dependent shear strain

The soil behaviour observed in the right picture of Figure 18 is valid for all kinds of soil. It shows the variation of shear modulus and damping ratio for different shear strain levels. The secant shearing modulus, according to $G_{sec} = \frac{\tau_c}{\gamma_c}$, decreases with increasing strain. The equivalent linear damping ratio ξ has the same energy loss as the hysteretic permanent ground deformation, ξ increases with increasing strain. For taking into account the frequency on the stress-strain relation, one is referred to the manuals and information of the two models (SHAKE) within the EERA.

Finite element free field site response analysis

In a 2D/3D finite element model the free field site response can account for different types of waves to develop in the continuum. This will lead to a more accurate representation of the actual surface motions due to bedrock excitation compared to an 1D analysis. Also the site geometric properties (slopes and or discontinuous soil profiles) affecting the wave field can be included. By using nonlinear advanced soil models, it is possible to account for nonlinear soil constitutive behaviour. This behaviour is not included in the equivalent linear site response analysis mentioned above. Although this FEM method can give a more accurate representation, a drawback could be the higher computational effort.

A finite element free field site response is often performed to check the model boundary disturbances, appropriate time steps, performance of the chosen soil model and sensitivity to mesh coarseness.

In order to perform a free field site response analysis in PLAXIS 2D or 3D, one has to define:

- A representative geometry model;
- Appropriate constitutive model (i.e. Linear elastic, Hardening Soil small strain, etc.) to reproduce the actual behaviour of the soil;
- Input motion at bottom of the soil model;
- Generate a mesh according to the minimum required length of the element;
- Boundary conditions at the sides and bottom of the model;
- Appropriate calculation parameters.

It should be noted that any soil model is a simplification of the actual soil behaviour, even the most advanced models, and they involve a number of limitations. The difference between these two methods, PLAXIS and EERA, can be described by, amongst other:

- 1D in EERA instead of 2D or 3D in PLAXIS;
- No hardening within EERA, whereas within PLAXIS with the Hardening Soil small strain model, both cap and shear hardening is incorporated;
- Equivalent linear soil behaviour in EERA, instead of non linear behaviour within PLAXIS;
- In EERA the analysis is performed in the frequency domain, whereas in PLAXIS the analysis is performed in the time domain.

2.2.3 Damping of propagating waves in the model

With the propagation of waves through the subsoil (and structure within the subsoil) energy is dissipated along the way. There are different factors causing this damping and most of them are frequency dependent. Important damping factors in this thesis are summarized below:

- Material damping, either by the soils / structural stiffness and strength properties;
- Damping from the interface between the pile and soil, which is strongly nonlinear;
- Soil radiation damping, transport of energy to the far field;
- Refraction.

Apart from these factors, there are many other factors which should all be included into the mathematical model used in the FE model. However, since the physical background of many of these factors are still unknown, two types of damping in the FE model are used to approximate the damping of the system. For PLAXIS these two methods consist of Newmark time integration damping and Rayleigh damping. The parameters for the Newmark time integration damping are not changed in this thesis and are left to the default values. The values used in PLAXIS are set to a minimum to allow for an unconditionally stable calculation and no extra numerical damping. Only Rayleigh damping is considered. For this approach the PLAXIS model is simplified as a (coupled) damped mass-spring system.

Rayleigh damping is frequency dependent and defined by a certain damping percentage for two target frequencies, resulting in the so-called Rayleigh damping coefficients α_r and β_r. The damping matrix C in PLAXIS is a function of the mass and stiffness matrices. The global damping matrix is formed by collecting the element damping matrixes:

$$\underline{\underline{C}} = \alpha_r \underline{\underline{M}} + \beta_r \underline{\underline{K}} \tag{28}$$

The damping is proportional to the mass and the stiffness per element. These coefficients are also related to the damping ratio. A larger α_r means that the lower frequencies are stronger damped, whereas with a larger β_r the higher frequencies are damped stronger.

The Rayleigh coefficients can be evaluated by means of the following relation with the angular frequency (ω) and damping ratio(ξ_r):

$$\xi_r = \frac{\alpha_r}{2\omega} + \frac{\beta_r}{\omega} \tag{29}$$

Rayleigh damping is in engineering practice mostly between 0.5% and 2% for both the first and second target frequencies. There are different methods mentioned in literature to select appropriate Rayleigh parameters for different target frequencies. In this study the first calculations were performed based on the method mentioned by Hudson, et al. (1994) where the first target frequency is set equal to the fundamental frequency of the soil profile and the second frequency is the first odd number of the ratio: fundamental frequency of the input signal / fundamental frequency of soil profile (Kottke & Rathje, 2009).

	Frequency [Hz]	Damping [%]	Rayleigh α	Rayleigh β
fundamental frequency of soil profile	1.15	-		
fundamental frequency of input signal	9.4			
Target 1	1.15	1		
Target 2	9	1		
			0.128	**3.13E-04**

Table 5 Determination of Rayleigh damping parameters

The applied Rayleigh damping curve applied in PLAXIS is shown in Figure 19. It is important to notice that the Rayleigh damping does not allow for large gradients in the damping curve. So it is not possible to damp a narrow frequency range.

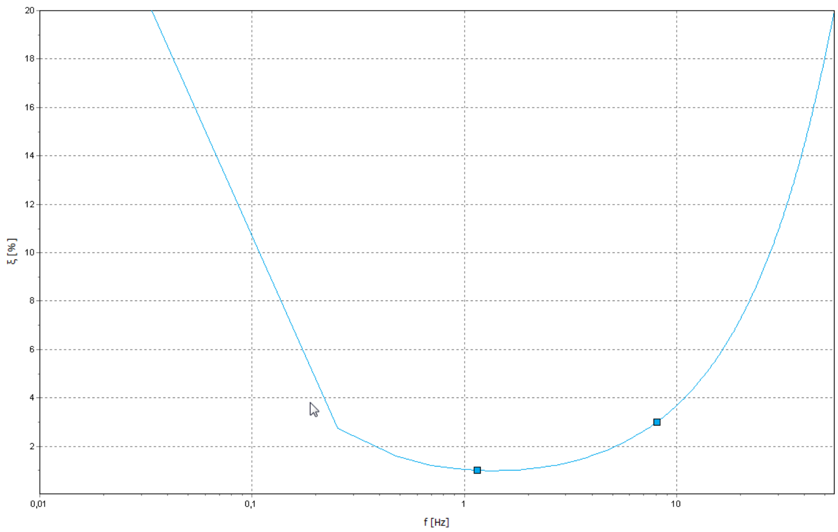

Figure 19 Example of Rayleigh damping curve from PLAXIS input

2.2.4 Design methods for kinematic bending moments

During an earthquake, several mechanisms in the ground and superstructure can occur. This motion of the ground can induce extra forces and bending moments in the pile foundations. As specified before, the dominant ones are kinematic and inertia loading. These loads induce extra forces and bending moments in the piles due to respectively the soil displacements and the response of the superstructure during the earthquake on the foundation. In this thesis the focus lies on the kinematic loading. This simplified situation will give the best insight in the behaviour of the embedded beam in a dynamic loading situation, since several structural factors of the superstructure are outside the scope of this thesis.

In many design guidelines and codes, the effect of kinematic loading is often not taken into account. Only with specific soil conditions and consequence classes of the superstructure, an analysis of the kinematic loading is required. In most cases this is justified, since the inertia loading predominant on pile design in earthquake engineering. The specification and literature of the methods for the inertia loading is more extensive than the one for kinematic loading. Based on an overview of several design methods for kinematic bending moments mentioned in Mylonakis & Nikolaou (2002) and Nikolaou, et al. (2001) an overview is given below.

The most important assumption in all of these methods is that the pile is modelled as a flexural beam and the bending moment in the pile is calculated by the well known formula:

$$M_{kin} = E_p * I_P * \left(\frac{1}{\mathrm{R}}\right) \tag{30}$$

Key problem here is the determination of the pile curvature (1/R) for computing the bending moment. In the paper of Mylonakis & Nikolaou (2002) several methods for obtaining this curvature are presented with the corresponding closed-form expressions. These methods are specified below:

- Margason & Holloway (1977)

This is one of the first methods for determining kinematic pile bending, which calculates the pile curvature by:

$$\left(\frac{1}{\mathrm{R}}\right) = n * \frac{u_s}{L^2} \tag{31}$$

In which n denotes a dimensionless constant based on the pile fixities boundaries. For a pile with one end fixed at pile head, $n = 2$. u_s is the maximum soil displacement at soil surface and L is the length of the pile. The main assumptions and limitations of these methods are specified below:

  - A long pile that follows the exact same motion of the free-field site displacement;
  - The shape of the deflected pile is approximated by a circular arc;
  - The soil-pile interaction is ignored, so no incorporation of soil-pile relative stiffness, excitation frequency and radiation damping;
  - Difficult to determine u_s accurately;
  - Applicable for one layered soils, so no interfaces;
  - The method implies pure bending of the pile (n=2), thereby neglecting the influence of shearing on the pile response.

- NERHP (1997)

This is a modified version of the method specified above. Also in this case, the pile curvature follows exactly the free-field site displacements, which is specified by the formula:

$$\left(\frac{1}{\mathrm{R}}\right) = \frac{\alpha_{ff}}{{V_s}^2} \tag{32}$$

In which the α_{ff} is the peak ground acceleration and V_s is the shear wave velocity of the soil profile. The assumptions for this method:

- Only vertically propagating shear waves due to the earthquake excitation;
- The rest of the assumptions are the same as for the Margason & Holloway (1977)-method.

- Di Laora & Rovithis (2014)

The first two methods ignored the soil-pile interaction. This major effect is often simplified as linear independent springs attached to the beam, so called Beam-On-Dynamic-Winkler Foundations (BDWF). A BDWF is characterized by a given distribution of stiffness and damping coefficients with depth. One of the most recent and most applicable method for this study is the method specified by Di Laora & Rovithis (2014) in which the soil has a depth dependent shear modulus specified by:

$$\mathrm{G}_s(z) = \mathrm{G}_{sd} * \left[a + (1-a) * \frac{z}{d}\right]^n \tag{33}$$

This model description with pile and soil is shown in Figure 20. The pile head is rotationally fixed and the pile is embedded in an inhomogeneous continuous layer, where the pile is a solid cylindrical beam with linear elastic properties. In this model, d is the diameter, L is the length of the pile. Ep and ρ_s are respectively the elastic modulus and mass density of the pile. The Poisson ratio ν_s and the hysteretic damping ratio β_s are assumed constant with depth.

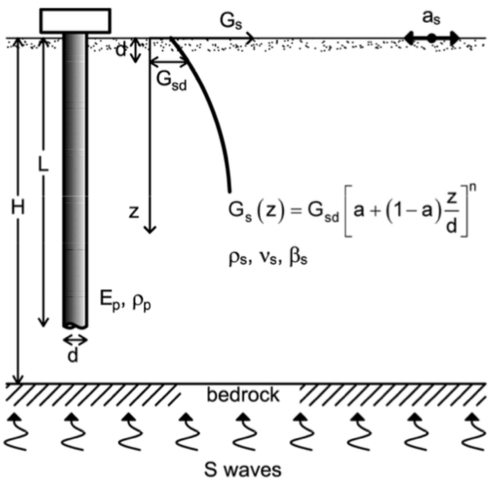

Figure 20 A single elastic fixed-headed pile embedded in a continuously inhomogeneous layer

Depending on the soil type, *a* and *n* are the dimensionless factors, which determine the depth dependent relation of the shear modulus. In this study the shear modulus with depth is approximated linearly, therefore assuming a = 0,5 and n = 1 in equation (33). Apart from a fully numerical analysis, a closed form expression is obtained based on the effective soil curvature as a measure of pile-head curvature. The pile curvature is then calculated by following subsequently steps mentioned below:

- The calculation of the wavenumber λ_d under the assumption of a pile-to-soil stiffness ratio δ= 2 results in equation (34):

$$\lambda_d = \left[\frac{k_d}{4 * E_p * I_P}\right]^{1/4} \tag{34}$$

$$k_d = \delta * E_{sd} \tag{35}$$

$$E_{sd} = 2 * (1 + \upsilon) * G_{sd} \tag{36}$$

In which the G_{sd} is the shear modulus at a depth of one times the pile diameter. This shear modulus is than used to calculate the Winkler spring modulus k_d, which is used as input in equation (34).

- Then the calculation of the characteristic pile wavenumber μ with equation (37):

$$\mu = \frac{4 * \lambda_d}{d^{\frac{n}{4}} * L_a * (4 + n) * (a - 1)} * \left[(ad)^{\frac{4+n}{4}} - (ad + L_a - a * L_a)^{\frac{4+n}{4}}\right] \tag{37}$$

The active dimensionless pile length L_a is approximated by 10 times the pile diameter.

- Determine the effective depth with equation (38):

$$z_{eff} = \frac{L_a}{2} = \frac{1.25}{\mu} \tag{38}$$

- Determine the shear modulus $G_s(z)$ with z = z_{eff}

- Calculate the kinematic bending moment at pile head based on equation (38):

$$M_{kin} = E_p * I_P * \frac{a_s}{G_s(z_{eff})} \tag{39}$$

With the peak ground acceleration a_s , which is divided by the shear modulus at the effective depth, the pile curvature is determined. Multiplying this curvature with the properties of the pile, will result in the maximum kinematic bending moment.

Based on numerical analysis, the conclusion of Di Laora & Rovithis (2014) was that this method is able to determine the effective pile curvature, via a simple expression of the active length of the pile.

Apart from these close-formed expressions for pile curvatures, the EUROCODE NEN EN 1998-5 specifies an alternative method to take kinematic pile bending into account. Under certain conditions for the soil and structure, for which the kinematic bending needs to be taken into account, a pseudo-static approach is defined based on the free-field site analysis. A soil motion is then applied on the pile as an equivalent static soil deformation relative to the depth of the pile. The soil motion from the free-field site analysis should be obtained at the point where the maximum relative pile-head and pile-toe displacement occurs.

3. Pile response of a static laterally loaded pile

This chapter describes the behaviour and influence of the limiting lateral skin resistance of an embedded beam in lateral loading situations. In paragraph 3.1 the model and parameters are determined for the FEM program PLAXIS. Also the limiting lateral skin resistance, which is an input for the embedded beam row, is determined based on the theory mentioned in subparagraph 2.1.1. Paragraph 3.2 shows the results and comparison between the 2D embedded beam row behaviour and the 3D volume pile and D-Pile group calculations. This chapter will end in paragraph 3.3 with the conclusions and recommendations for this part of the study.

3.1 PLAXIS model and parameters

For this thesis there is one soil type used for both the static and dynamic lateral loading situations. The soil parameters for a representative clay layer, see Table 6, are based on soil investigation from Loppersum (in the earthquake area of Groningen) and empirical formulas for determination of the undrained shear strength (c_u) (de Jong, et al., 2015). The hardening soil small strain, material model and undrained (A) behaviour is used in the FE model. The undrained behaviour can be modelled in several ways within PLAXIS. This option was selected because of the generally better numerical performance compared to undrained (B) analysis. The undrained (A) means that soil properties are specified by effective strength parameters and the program determines the undrained soil behaviour based on these parameters and pore-pressure generation. The other two options, undrained (B) and (C), are based on total stress analyses where c_u is actually the input parameter for soil properties. The undrained shear strength, in an undrained (A) calculation, is a function of the effective stress parameters and stress state. The depth dependent c_u has to be translated into effective strength parameters by changing the cohesion and/or friction angle to match the determined c_u profile. This was done by matching the failure line (red line in Figure 21) by respectively shifting upwards(downwards) and/or change the angle of the failure line. The value of the undrained shear strength, with the changed effective strength parameters, is obtained from the PLAXIS model by application of a virtual triaxial test within the PLAXIS soiltest facilities. After several iterations, a match was found between the empirically determined c_u and the effective strength parameters (c' and ϕ') shown in Table 6. One has to keep in mind that calculating the c_u from effective strength parameters with the hardening soil model, will lead to a different value than based on the Mohr Coulomb formula shown in equation 40. This principle is shown in Figure 21. In Appendix A, the method for back calculating the effective strength parameters is elaborated.

$$c_u = \sigma_v' * \sin(\varphi) + c * \cos(\varphi) \quad \text{(Mohr Coulomb Model)} \qquad (40)$$

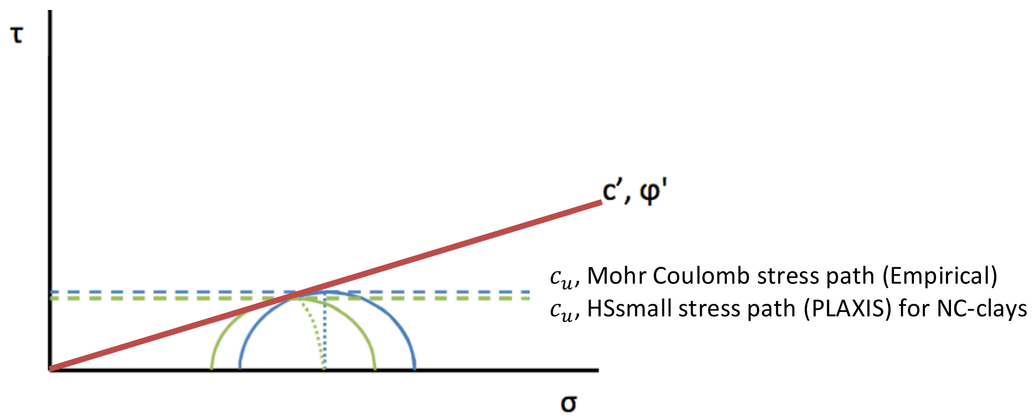

Figure 21 Calculation of c_u with HSsmall effective strength parameters (green)

The importance for the correct undrained behaviour in PLAXIS is to ensure that the limiting soil resistance for the lateral slider is correctly determined. The laterally loaded piles are evaluated for pile spacing 2, 4 and 8 meters. Recalling Figure 13, where the applicability area of the embedded beam (row) was specified by Sluis. Using the mentioned pile spacing and a pile diameter of 0.5 m, the ratio between pile spacing and pile diameter than becomes 4, 8 and 16 respectively, which are inside, on and outside the boundary of the application area specified by Sluis. This was chosen because the behaviour of the pile in this range should improve the pile response due to the incorporation of the lateral skin resistance.

Parameter	Symbol	Clay, poor sandy / silty	Unit
Setting PLAXIS			
Material model	-	HS small	-
Drainage type	-	Undrained (A)	-
Tension cut-off	-	Yes	-
Soil unit weight, saturated	γ_{sat}	18	kN/m^3
Soil unit weight, unsaturated	γ_{unsat}	18	kN/m^3
Soil Parameters			
Secant stiffness in standard drained triaxial test	$E_{50;ref}$	4600	kN/m^2
Tangent stiffness for primary oedometer loading	$E_{oed;ref}$	2300	kN/m^2
Unloading/reloading stiffness	$E_{ur;ref}$	18400	kN/m^2
Stress-level dependency power	m	0.7	-
Cohesion (effective)	c'	5	kN/m^2
Friction angle	φ'	25	°
Dilatancy angle	ψ	0	°
Shear strain at Gs = 0,722G0	$\gamma_{0,7}$	0.00028	-
Shear modulus at very small strains	$G0$	46100	kN/m^2
Poisson's ratio	ν_{ur}	0,2	-

Table 6 Material properties of continuous Clay layer

In this study a relatively stiff and long pile is assumed in the PLAXIS and D-systems models. Since we are only investigating the lateral capabilities of the embedded beam, the pile capacity in axial direction is unlimited and to omit inconsistency a value of $1*10^5$ kPa was applied. The properties of the embedded beam (row) are given in Table 7. The interface stiffness factors are default values calculated by PLAXIS based on formulas derived by Sluis (2012). For both 2D and 3D calculations, the pile is assumed to be a bored concrete pile with a rough interface.

Since undrained behaviour is expected and the soil is modelled by a continuous clay layer, the limiting lateral soil resistance will be calculated according to the methods mentioned in subparagraph 2.1.1.1. For the different methods, as elaborated in Chapter 2, the profiles of the limiting soil resistance can be seen in Figure 22.

Parameter	Symbol	Embedded beam (row)	Unit
Young's modulus	E	3.00E+07	kN/m^2
Unit weight	γ	25	kN/m^3
Predefined pile type	-	Massive circular pile	-
Diameter	D	0.5	m
Area	A_b	0.1936	m^2
Moment of inertia	I_p	3.07E-03	m^4
Axial Skin resistance			
Skin friction distribution	-	Linear	-
Skin resistance at top	$T_{top;max}$	1.00E+05	kN/m
Skin resistance at bottom	$T_{bottom;max}$	1.00E+05	kN/m
Base resistance	$F_{bot;max}$	1.00E+05	kN/m
Lateral skin resistance		Table 8	

Table 7 Material properties of the embedded beam (row)

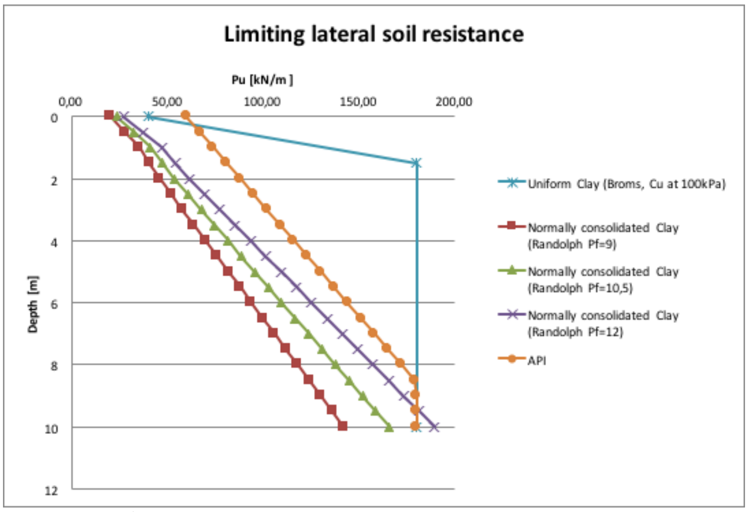

Figure 22 limiting lateral soil resistance profiles, based on soil parameters table 6

The uniform clay assumption and usage of the Broms method was not further used in this study, because of the modelling of a normally consolidated clay. For several other methods of determining the limiting lateral soil resistance, the preliminary results of the embedded beam (row) behaviour during a lateral load were compared with 3D volume pile behaviour and D-Pile Group calculations. Based on these results shown in appendix B en D, the calculated pile displacement and bending moments of the 3D volume pile were in good agreement with the D-Pile Group calculations, which is based on the API method. The maximum strength at a certain depth is determined based on equation (5) and (6) in subparagraph 2.1.1.1. The stiffness is however based on so called p-y curves as specified in equation (13) and (14) in subparagraph 2.1.1.2. The values of the input of the limiting lateral skin resistance in PLAXIS is shown in Table 8.

Lateral skin resistance		
API		
Skin friction distribution	*Multi linear*	
Linear from ground level till -8,5m	60 - 180	kN/m
Below -8,5m	180	kN/m
Pile tip	180	kN/m

Table 8 Lateral skin resistance values for different lateral maximum capacity methods

3.2 Lateral loading by external force

3.2.1 Case properties

To evaluate the behaviour of the lateral slider and the pile displacements of an embedded beam row in PLAXIS 2D with various pile spacing, multiple calculations are performed and compared with PLAXIS 3D Volume pile and D-Pile Group. The used API method for determining the lateral slider of the embedded beam was compatible with the method used in D-Pile Group. D-Systems also uses the specified API p-y curves based on the c_u value of the soil. Calculations in this study are performed, both in 2D and 3D models, with a point load on top of the pile. The height of the FEM model is 20m, the width is 40 m and the out of plane length is the centre-to-centre distance of the embedded beam row ($L_{spacing}$), see Figure 23. The pile has a length of 10 meter and is placed in the middle of the model with linear elastic material properties. The top load in the 2D model is defined by the load in 3D, increasing from 20 kN till 200 kN, divided by $L_{spacing}$ of the 2D embedded beam row, which will lead to a load in [kN/m].

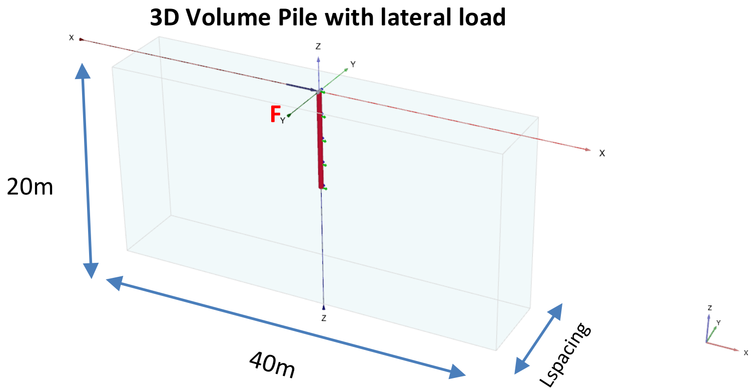

Figure 23 Model for a pile (row) with a single Volume Pile in PLAXIS 3D with various pile-spacing

For the 2D embedded beam, the FEM model and mesh can be seen in Figure 24. The mesh of the 3D model is shown in Appendix D.

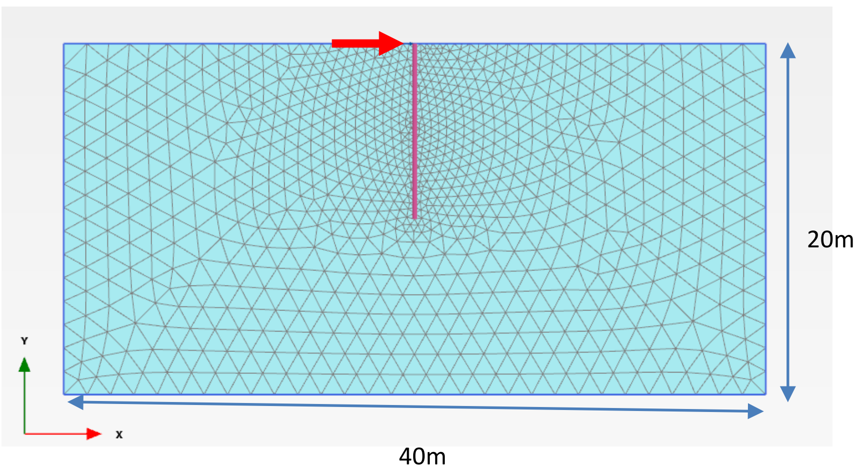

Figure 24 Model and mesh for embedded beam row in PLAXIS 2D for various pile spacing (very fine mesh)

3.2.2 Evaluation of normalized pile displacement and bending moment

For three types of $L_{spacing}$ (2, 4 and 8 meters), the horizontal pile displacements were analysed. In this subparagraph the limiting lateral soil resistance of the embedded beam is based on the API method. The lateral bearing capacity of the pile is 426 kN, based on API method in the D-Pile Group calculation. The applied load at pile head and the calculated bending moment and pile displacement are normalized by the following equations:

- Normalized load $F_{x,n}$, in which F_x is the applied horizontal load and P_{ult} is the lateral bearing capacity based on the API method in this study:

$$F_{x,n} = \frac{F_x}{P_{ult}} \tag{41}$$

- Normalized bending moment M_n, in which M_d is the calculated bending moment, F the applied pile head load and D the pile diameter:

$$M_{d,n} = \frac{M_d}{F_x * D} \tag{42}$$

- Normalized pile displacement $u_{x,n}$, in which u_x is the calculated pile displacement and D the pile diameter:

$$u_{x,n} = \frac{u_x}{D} \tag{43}$$

The results for the pile displacement, with normalized load ratio of 0.235 (100 kN) and 0.47 (200 kN), are compared with PLAXIS 3D volume pile and D-Pile Group, see Figure 25. The development of (normalized) pile displacement and bending moment with increasing loads from 20 kN till 200 kN is shown in appendix C. Also the boundary- and mesh-dependency of the used PLAXIS model are evaluate in appendix C. The validation of the lateral pile behaviour of the PLAXIS model in 2D is done in appendix D with PLAXIS 3D volume pile and a D-Pile Group calculation.

In Figure 25 the results of the normalized pile displacement for different pile spacing can be seen for the standard embedded beam, embedded beam with API skin resistance, 3D volume pile and D-Pile Group calculation. The comparison between the embedded beam and D-Pile Group is only done for a pile spacing of 8 m, because for this pile spacing a single pile is assumed. For small loads, in this study a load up until 23.5 percent of the API lateral bearing capacity (P_{ult}), the displacements of the pile, and thus the occurring maximum bending moments, are overestimated by the embedded beam with and without limiting lateral skin resistance for the pile spacing of 4 m and 8 m.

With a pile spacing of 2 m, the behaviour of the embedded beam is different from the other two methods. In comparison with the 4 m and 8 m, it has a relative higher load per meter in the out of plane direction, but the soil has still the same shear modulus. So the pile will show more displacements and the ultimate skin resistance has much more influence on the results, than compared with larger pile spacing. In 3D this effect can be explained by the fact that pile groups act less stiff than single piles. Another observation of the results is that at 47% of P_{ult}, unrealistic pile behaviour is observed at the pile toe. This unrealistic pile displacement behaviour near the toe of the pile (at a normalized depth of 20 m) is observed for all pile spacing for 2D embedded beam with lateral slider. This movement of the pile toe is named unrealistic, because the soil should behave more stiff near the pile toe due to the increased vertical effective stress.

The effect of a weaker lateral skin resistance is that this unrealistic behaviour will even increase, see Figure 29 in next paragraph. For the pile spacing of 4 m and 8 m, the pile displacements of 2D embedded beam standard, with slider and 3D volume pile are approximately similar for loads up until circa 23.5% of P_{ult}. For loads closer to the lateral bearing capacity, the 2D embedded beam, both standard and with lateral slider, tend to act stiffer (so less displacements).

In Figure 26, the development of normalized bending moment along the pile length for normalized load of 0.235 (100 kN) and 0.47 (200 kN) are shown. The same holds for the magnitude of the normalized bending moments along the pile, as for the normalized pile displacement, for lower loads the results for the different 2D and 3D methods are similar. The higher the load, the more differences in the results of the 3D calculation and the 2D calculations are observed. However, the normalized bending moments along the pile with increasing load tend to be similar for the standard embedded beam. Meaning that the bending moment is directly proportional to the applied load at pile head.

In 3D there is almost no difference in normalized displacement for $L_{spacing}$ of 4 m and 8 m, when the volume pile is modelled as a rough 3D pile without interface. The same should hold for the 2D situation, since a single pile is modelled for the ratio $L_{spacing}/D = 8$. In 3D the load is specified as a point load of either 100 kN or 200 kN, which in the 2D situation is based on $L_{spacing}$ and thus specified as a line load of $\frac{100}{L_{spacing}}$ kN/m. So with larger pile spacing, a smaller line-load is applied on top of the embedded beam, resulting in less displacement when the ISF is kept constant. When looking at the interface stiffness factor, with larger pile spacing the value for ISF becomes lower (so less stiff response and more displacements). It is expected that with larger pile spacing the behaviour of the standard embedded beam should be the same for a single pile (i.e. $L_{spacing}$ = 4 m and 8 m). From this, it can be concluded that the reduction in relative soil-pile stiffness and reduction of the load is not proportional. A decrease in expected displacement due to a smaller load is not compatible with a decrease of soil-pile stiffness. This could be caused by the fact that the ISF is determined for the entire length of the pile and is not depth dependent.

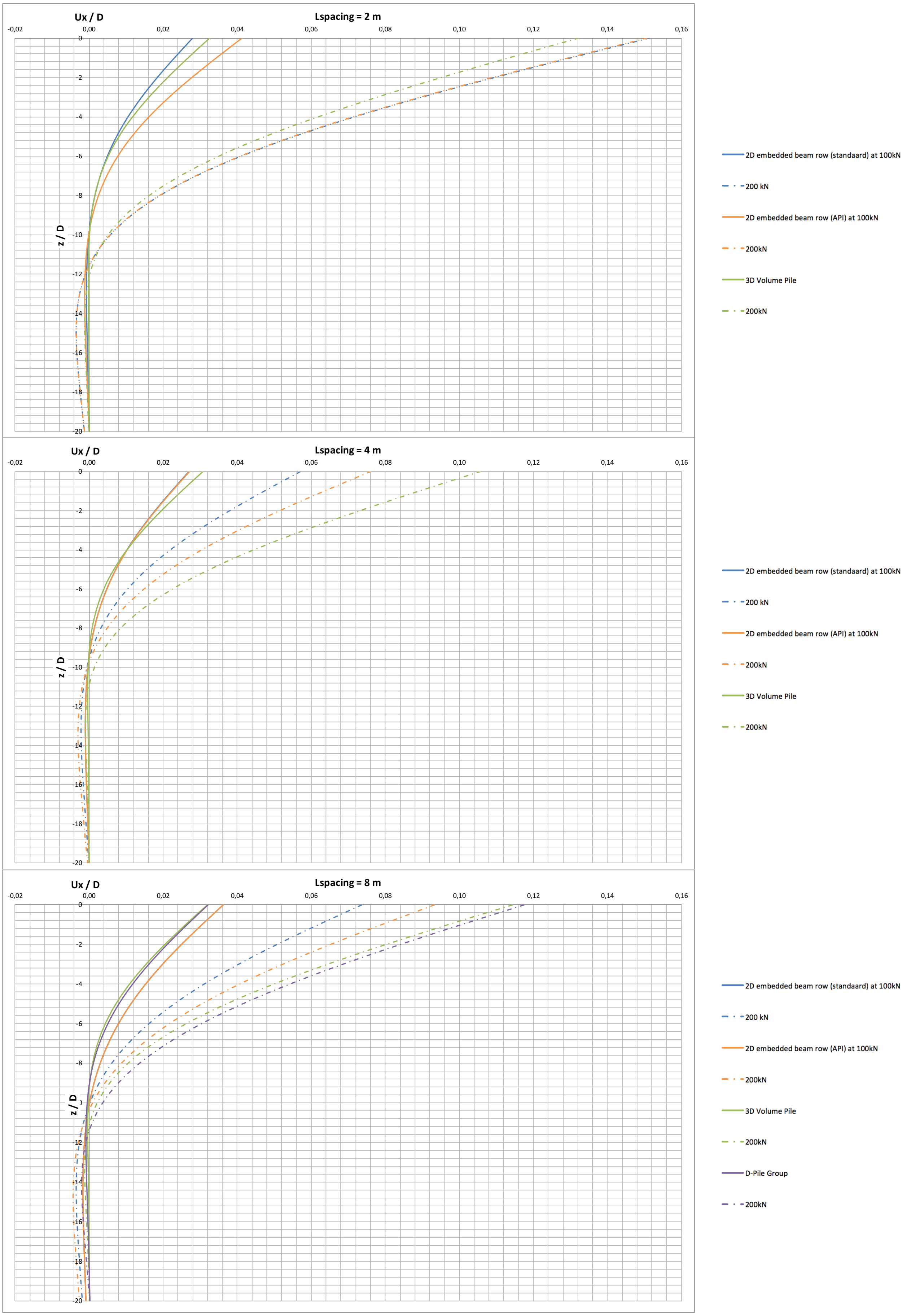

Figure 25 Comparison normalized pile displacement PLAXIS 2D and PLAXIS 3D for different methods and for $L_{spacing}$ of 2, 4 and 8 m respectively.

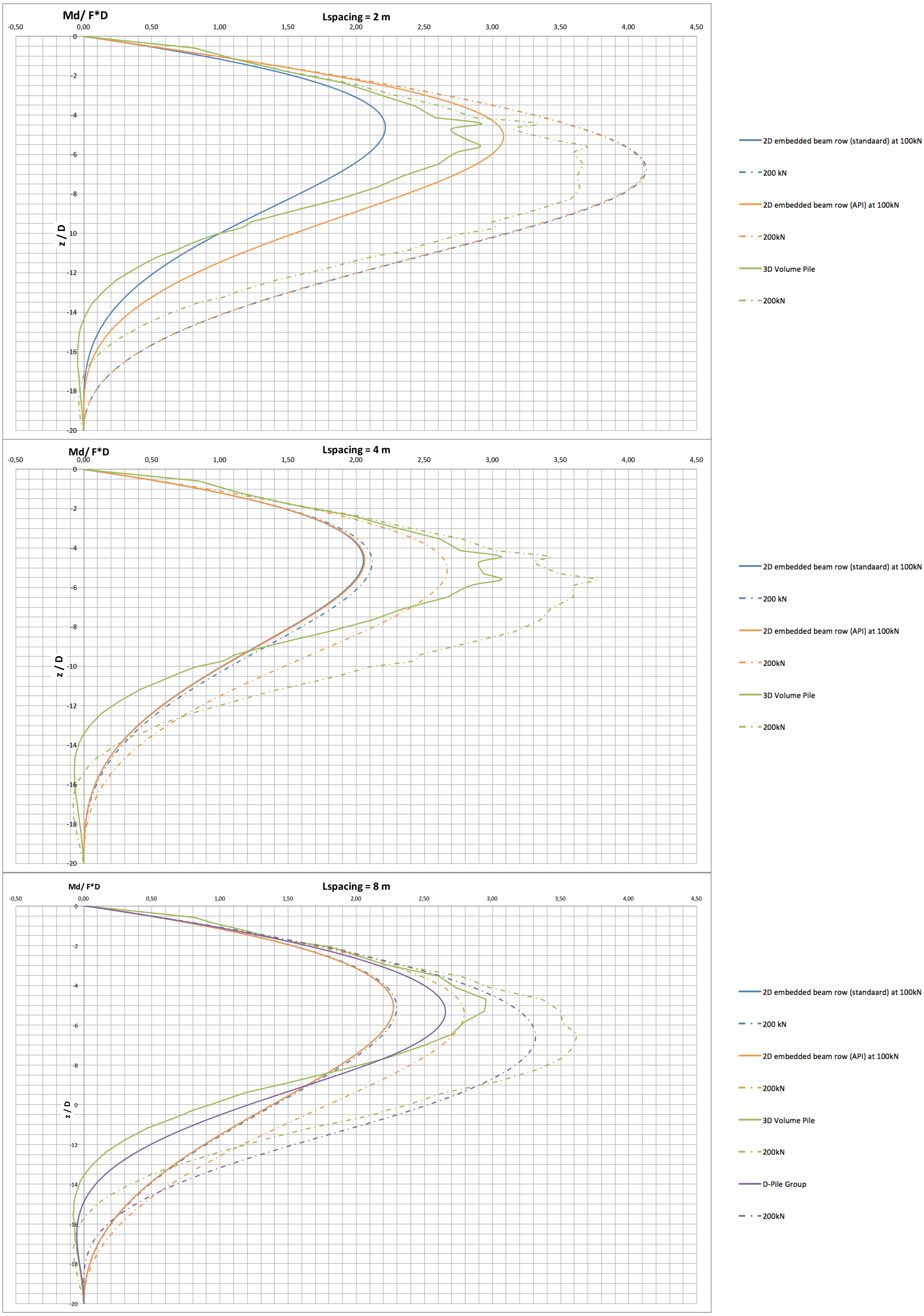

Figure 26 Comparison bending moment with depth of PLAXIS 2D and PLAXIS 3D for different methods and for $L_{spacing}$ of 2, 4 and 8m respectively.

3.2.3 Evaluation of lateral skin resistance of embedded beam row

In the previous subparagraph the influence of the lateral skin resistance on the pile normalized displacement and bending moments are shown for two loading situations. However, the purpose of the lateral slider was to implement a maximum limiting soil pressure, so a maximum strength. To check the lateral bearing capacity for several methods, the pile head in the PLAXIS model was displaced by 0.6m for a pile spacing of 8m. With this experiment the elasto-plastic behaviour of the pile is neglected, so the behaviour of the pile is due to the soil resistance. By displacing the pile head, the development of elasto-plastic / perfectly plastic behaviour is visualised. The results are shown in Figure 27

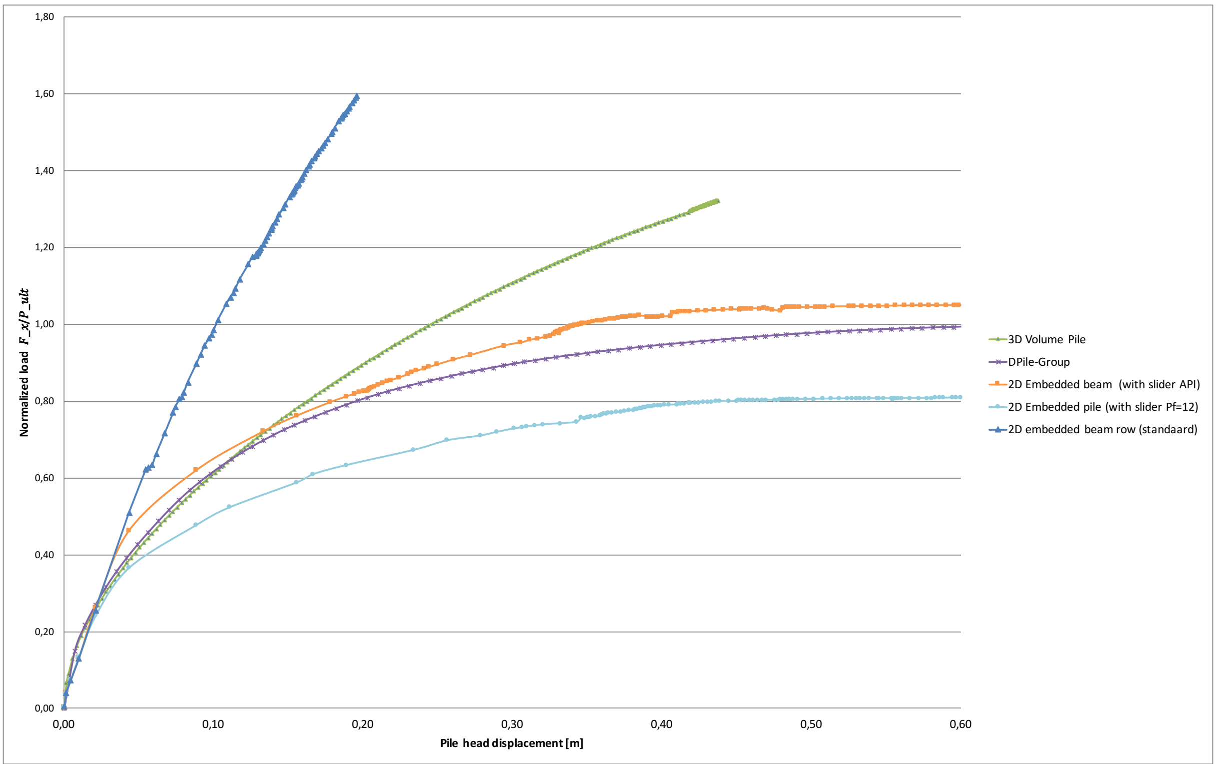

Figure 27 Load-displacement behaviour of PLAXIS 2D, 3D and DPile Group calculations for $L_{spacing}$ of 8m

Based on the performed calculation, the following observation can be made from Figure 27:

- 2D embedded beam (dark blue line) with unlimited lateral resistance (standard) acts too stiff for large loads in comparison with the behaviour of the 3D volume pile (green line);
- The stiffness of the 3D volume pile and D-Pile Group (purple line) show similar behaviour until a load of approximately 59% of P_{ult};
- The difference between the behaviour of the 3D volume pile and the 2D situation with the embedded beam and in D-Pile Group could be caused by locking of the mesh element around the pile in the 3D situation. This will lead to stiffer behaviour of the volume pile.
- The methods of normally consolidated clays with (light blue line), for determining the lateral slider, give significantly lower strength of the pile. This is due to a lower lateral skin resistance in the top of the soil profile;
- The ultimate strength of the embedded beam with API slider and D-Pile Group (which is also based on the API) gives similar results. Only the stiffness differs for lower loads.

So when using the API for determining the lateral slider in PLAXIS 2D, the strength matches the one calculated with D-Pile Group. However, the stiffness calculated with the PLAXIS 2D embedded beam is not comparable to D-Pile Group for lateral loads until approximately 26% of P_{ult}. For these loads, the 3D volume pile and D-Pile Group act stiffer, see Figure 28.

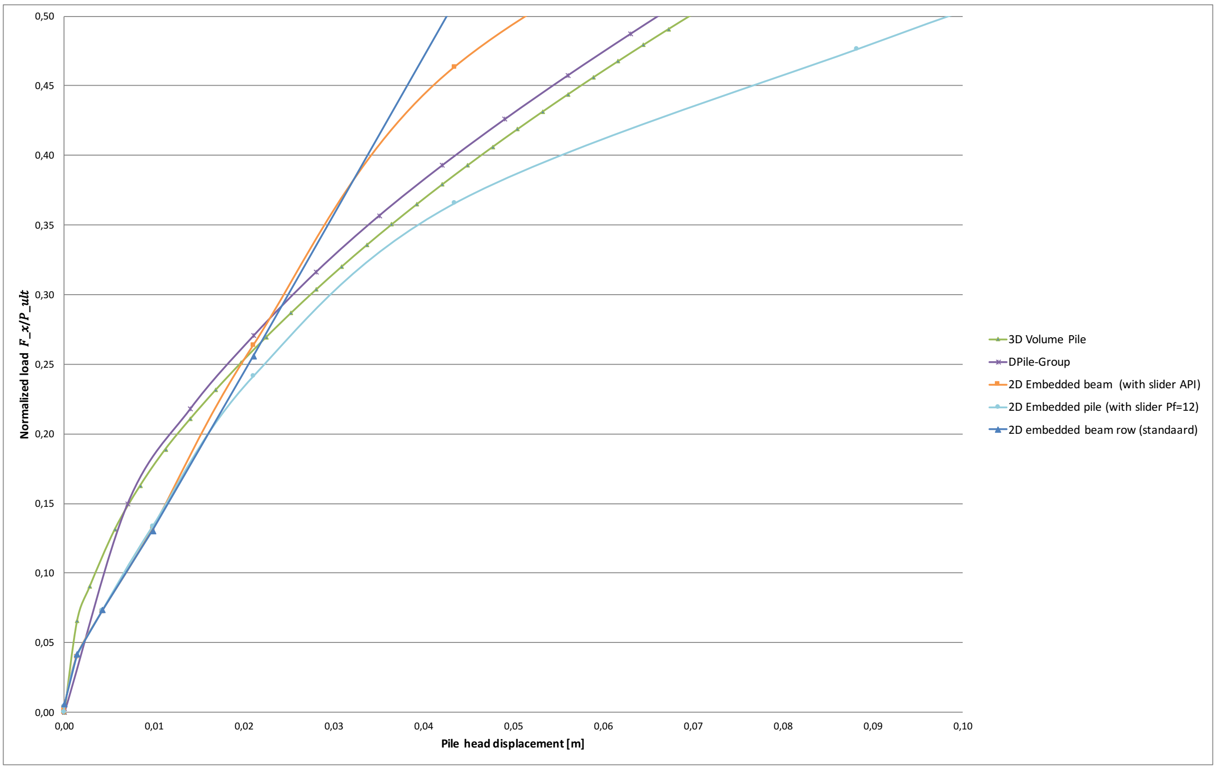

Figure 28 Zoom of Load-displacement behaviour of PLAXIS 2D, 3D and D-Pile Group calculations for $L_{spacing}$ of 8m

The results in Figure 28 show that the embedded beam with a specified lateral skin resistance, follows the load displacement curve of the standard embedded beam until the limiting soil pressure is reached at any point along the pile. This would suggest that the stiffness is not dependent on the lateral slider, for small loads, but is still dependent on the interface stiffness factor. For multiple lateral sliders, the bending moment and pile displacement for a single pile ($L_{spacing}$ = 8 m) and lateral pile head load of 200 kN are shown in Figure 29.

For a pile spacing of 8 m the ISF is 0.3125. In order to check the influence of the ISF, a value of 0.2 was manually defined for the lateral interface. It can be seen that the pile head displacement is now overlying the values calculated with 3D volume pile, however the pile toe gives unrealistic displacements. This would suggest that at the top of the pile the ISF is correct, but too low for the lower part of the pile. The normalized bending moment for the embedded beam with changed ISF is slightly moving towards the 3D Volume Pile and D-Pile Group profile.

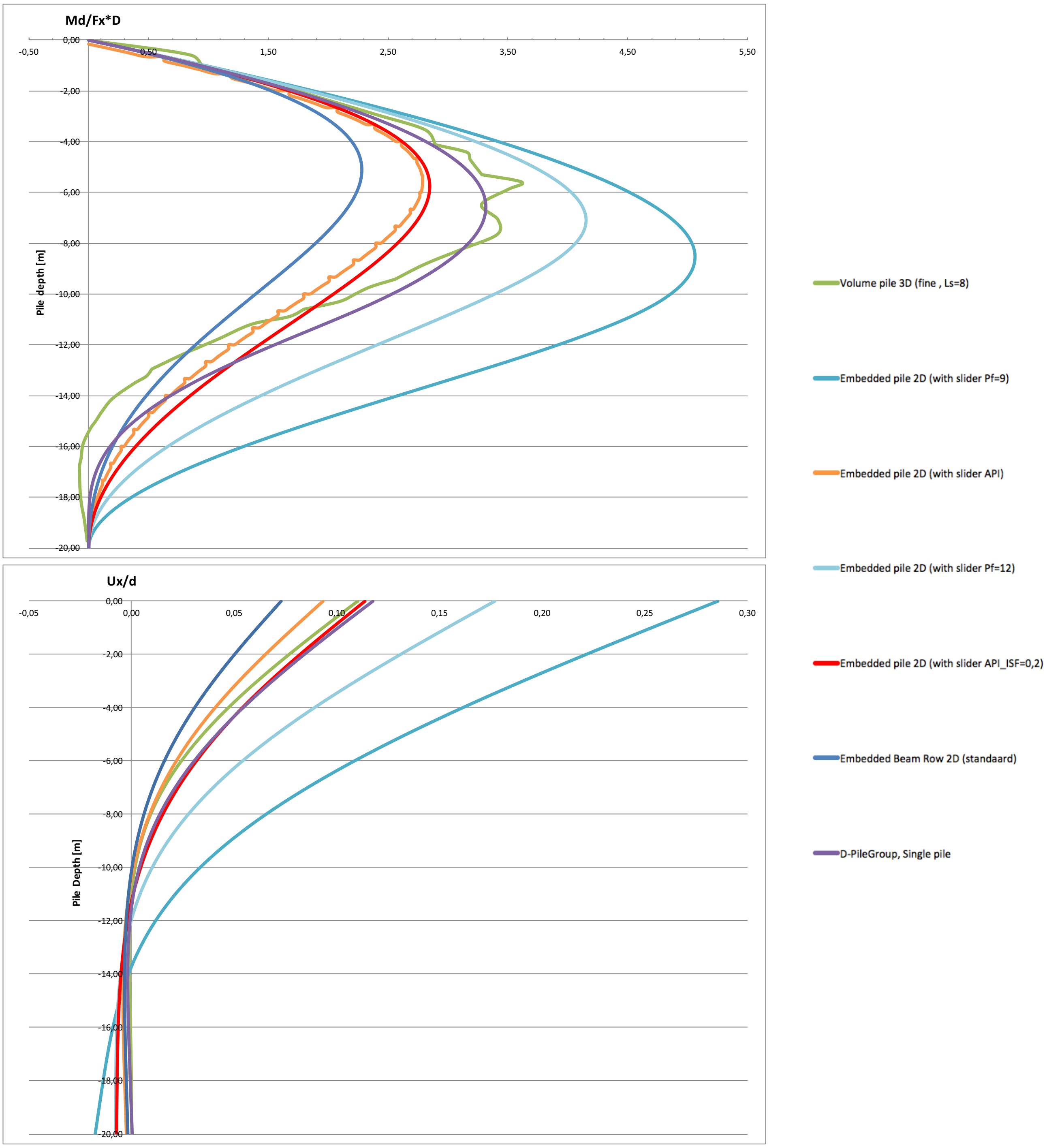

Figure 29 Normalized bending moments and pile displacement along the pile for different lateral sliders for $L_{spacing}$ of 8m

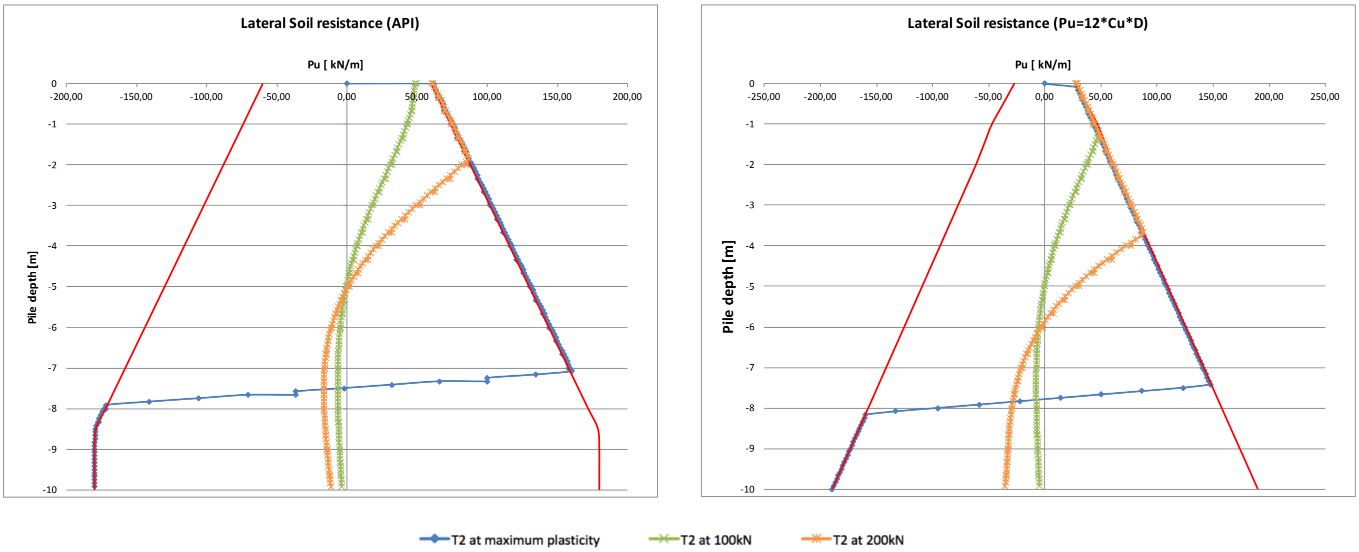

Figure 30 Development of lateral slider (T2) as output from PLAXIS for API and Normally consolidated slider profile

In Figure 30 the calculated lateral resistance (T_2) of the embedded beam is compared for three situations with the input profile (Red lines). It can be seen that at full plasticity all the values of T_2 along the pile are on the limiting soil resistance profile.

The conclusions and observation mentioned above are summarized in Figure 31. With a decrease in pile to pile spacing, the ratio between bending moment and applied load will also decrease, resulting in a downwards movement in Figure 31. This can be explained by the fact that with a smaller pile to pile distance, the stiffness of the soil and pile is stiffer, so there are less displacements resulting in a lower bending moment with a certain load. The only exception to this is the pile to pile distance of 2 m. After a load of about 19% of P_{ult}, the pile starts to slip through the soil, resulting in large displacements and thus large bending moments. This is shown as an increase in the normalized bending moment ratio at higher loads. As mentioned before an explanation can be found in the ratio of line load over shear modulus. The line load is higher for smaller pile spacing, so with the default determination of the ISF the stiffness of the interface of the pile is too weak.

For the standard embedded beam with pile spacing of 4 m and 8 m, the normalized bending moment ratio is the same for different loads. This means that the applied load at the pile head is directly proportional to the resulting bending moment, which can be explained by the fact that no soil plasticity occurs. So no soil-flow around the pile is possible. The incorporation of the limiting lateral soil resistance should improve this plastic soil-pile behaviour, which in this study is only visible for loads at pile head closer to the lateral bearing capacity. This plastic behaviour is taken into account in the 3D calculations and to a lesser extend in the 2D embedded beam with API lateral skin resistance. The result of this plastic soil-structure behaviour is an increase of the normalized bending moment ratio with increasing loads.

The effect of pile spacing and the normalized bending moment is smaller for the 3D calculation than for the 2D embedded beam (row) calculations. After a spacing of 4 m, almost similar behaviour is expected due to the single pile assumption. This effect is visible in the 3D calculations for larger loads, but not so much for embedded beam in 2D.

The results in Figure 32 support the conclusions drawn for the normalized bending moments results. The relation between the normalized displacement and normalized bending moment is as expected: with increase pile head displacement, the ratio of bending moment over applied load will also increase.

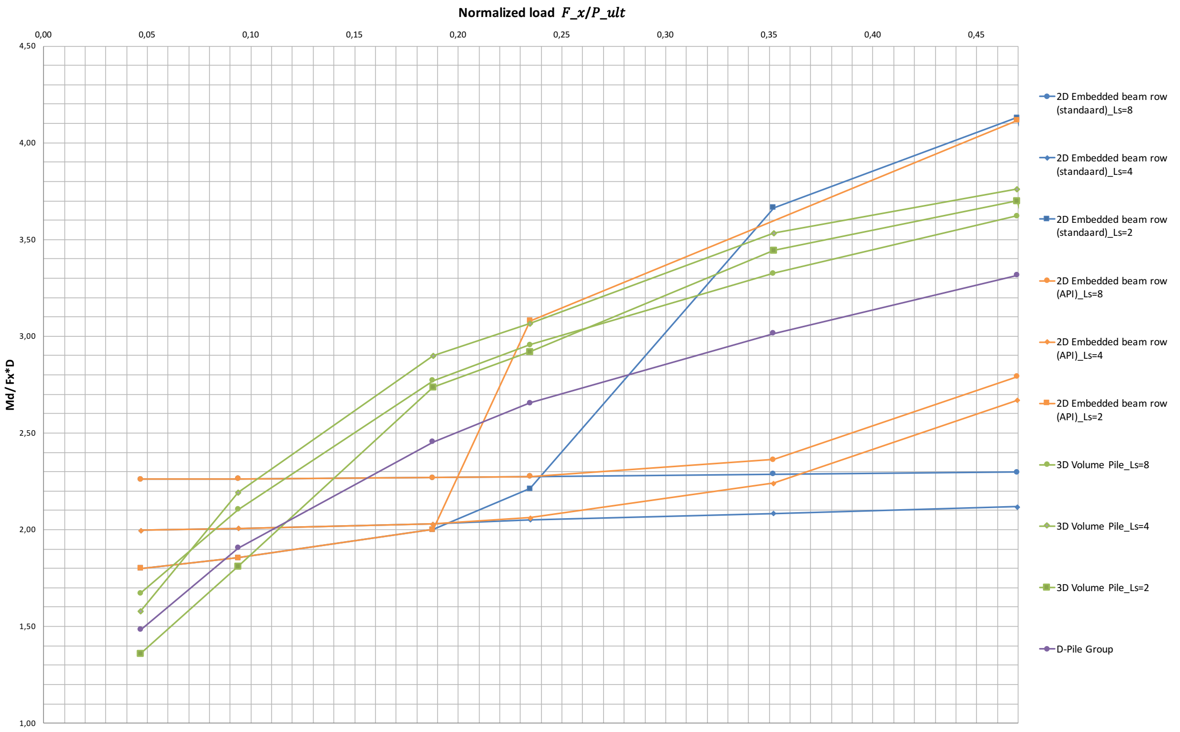

Figure 31 Relation between normalized bending moment and pile head load for different pile to pile spacing

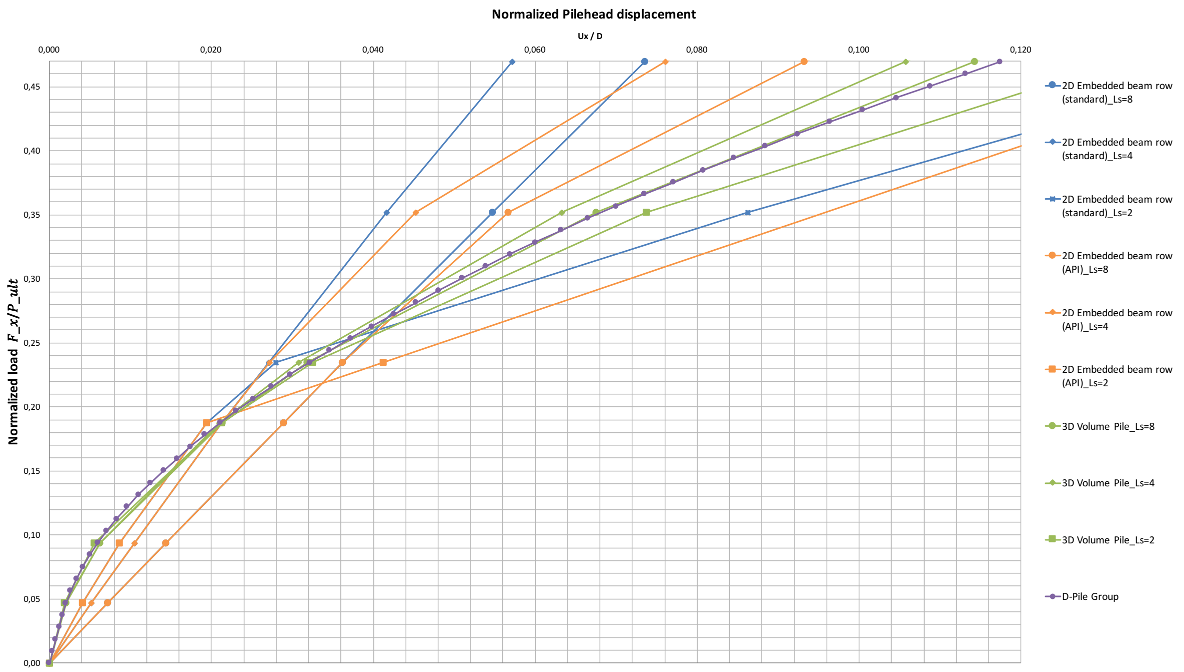

Figure 32 Relation between normalized displacement and pile head load for different pile to pile spacing

3.2.4 Influence of elasto-plastic behaviour of the pile

In order to check the soil behaviour in the 2D and 3D situation, linear elastic material properties were assigned to the circular concrete pile. However, in reality, the pile is not linear elastic, but could also show plastic behaviour. To incorporate this behaviour, a plastic moment M_p was estimated using the relation between acting normal force, bending moment and reinforcement percentage. The interaction diagram of the former Dutch code 1990 was used for the determination of the plastic moment, which is shown in Appendix E. For the calculation done in PLAXIS two situations were evaluated: no acting normal force, which result in a lower limit of the maximum moment, and pile with 500 kN of normal force resulting in a higher plastic pile moment.

Factor diagram	Factor diagram	Normal force acting on pile	Plastic Pile moment
Nd/fcd*Ab	Mp/fcd*Ab*h	N [kN]	Mp [kNm]
0.00	0.09	0	133
0.17	0.12	500	177
0.34	0.13	1000	191
0.51	0.135	1500	199

Table 9 Calculation of plastic moment for 4 different working normal force on the pile

Depending on the normal force, the maximum plastic moment will increase. However, since this experiment is about researching the effect of the plastic moment the lower limit was used as a starting point, after which also a calculation was done with an increased plastic moment. The result is, as expected, that a plastic "hinge" is formed in the pile. For the PLAXIS model a pile to pile distance of 4m was used and the (API) lateral slider was activated. The behaviour of the pile head shown in Figure 33, for several options, is the same as shown in subparagraph 3.2.2 until the maximum plastic moment is reached somewhere along the length of the pile. Around 2 m depth this plastic hinge becomes visible and the upper part of the pile displaces more than the linear elastic piles. The implementation of Mp only defines the strength of the pile, but not the stiffness behaviour of the soil surrounding the pile. What is observed is that the problems with the lower stiffness of the embedded beam is still present, see green line in Figure 33. It can be concluded that based on this result the behaviour of the pile will follow the lines specified by the embedded beam (with or without slider). The only change is a sudden bend in the load displacement curve at the load, where Mp is exceeded and a plastic hinge is formed.

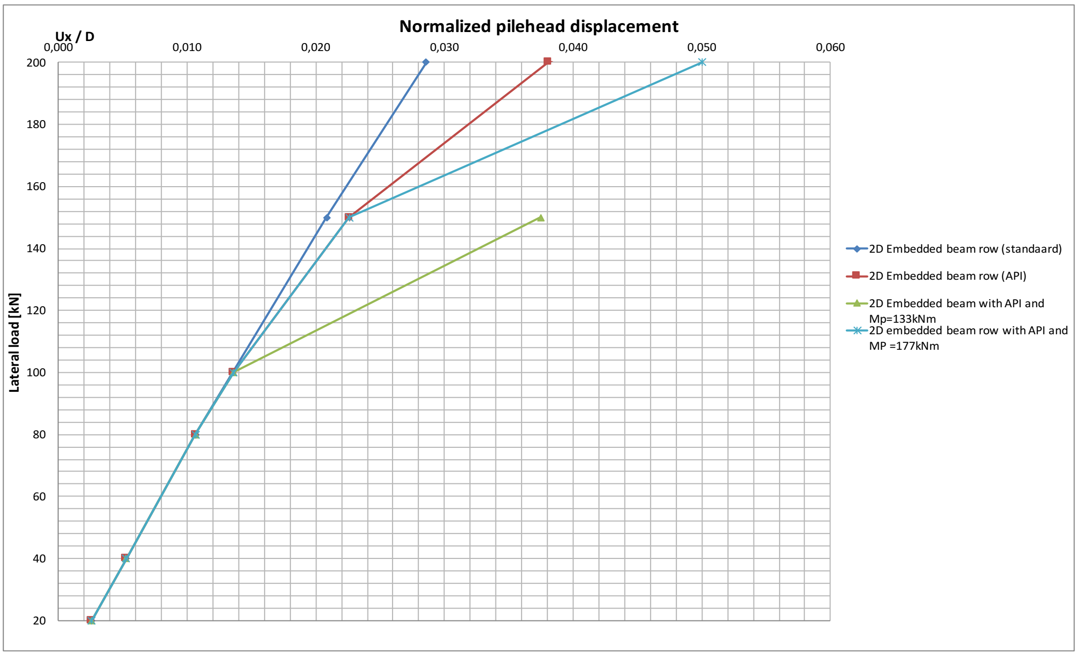

Figure 33 Normalized pile head displacement with increasing load

3.3 Conclusion and recommendations

This chapter described the model for calculating an embedded beam row with lateral loading by an external force on top of the pile, with default values for the interface stiffness factor (ISF). The 2D embedded beam row is analysed for the normalized pile displacement, bending moment and the influence of the lateral slider and compared with 3D volume pile (PLAXIS) and D-Pile Group results.

The first step was to determine the limiting lateral soil resistance, which would be the input for the embedded beam. Since we have a silty soft clay with specified undrained shear strength profile, the limiting lateral skin resistance is based on methods for cohesive soils. In literature it can be found that the early methods by Matlock and Broms overestimate the lateral bearing capacity of pile, in this light the method of the API is an extension of the Broms method and shows better comparison with the 3D volume pile and D-Pile Group calculation in this thesis. The latter is expected, since the D-Pile Group software uses the same method as specified in the API code. For this thesis, with the specified clay layer, it is therefore concluded that the API was the best method for determining the limiting lateral soil resistance. If a different soil, for example non-cohesive or stiffer clays, is applied in PLAXIS, different calculation methods should be used for determining the skin resistance.

After implementation of the API limiting lateral skin resistance, several conclusions could be drawn from the results:

- The pile displacements are overestimated with the default interface stiffness factors for loads until 26% of P_{ult};
- For $L_{spacing}/D < 4$ the normalized pile displacement and bending moment calculated with the 2D methods don't differ that much from one another. They are all in agreement with the calculated 3D volume pile. For this range of $L_{spacing}$, the embedded beam row does not add new or better possibilities for modelling pile behaviour in 2D compared to alternative pile modelling options (like a node-to-node anchor or plate);
- For $L_{spacing}/D > 4$ the different methods also show similar result for small loads and displacements, however the stiffness response of the 2D embedded beams are lower than the 3D volume pile and D-Pile Group;
- For all pile spacing the horizontal pile displacements along the pile in 2D are in better agreement with 3D than the maximum bending moments. In the case of $L_{spacing} = 2$, the bending moments are overestimated in 2D, whereas for $L_{spacing}$ of 4 m and 8 m the bending moments are underestimated in comparison with 3D;
- The ultimate strength of the embedded beam with API lateral skin resistance shows comparable results with the maximum strength of the D-Pile Group calculations for a single pile;
- The stiffness of the embedded beams, with or without slider, for small loads is not consistent with the 3D volume pile and D-Pile Group. Higher stiffnesses (so less displacements) are observed for small loads until 26% of P_{ult} in the 3D situation.

As was shown in subparagraph 3.2.3 the influence of the Interface stiffness factor on the normalized pile displacement and bending moment is still the main issue for small loads. It was shown that the pile head displacement could be matched by reducing the ISF, however this lead to unrealistic pile behaviour of the pile toe. As mentioned before, the determination of the lateral ISF is based on the axial validation of the embedded beam and has the same value. To overcome the unrealistic lateral pile behaviour, the ISF could be made depth or stress dependent. In this way the ISF will be lower in the upper part of the pile and higher near the pile toe. By lowering this ISF, plasticity will occur at lower loads and soil flow around the pile is better approximated. This soil flow around the pile can occur in 3D, however in 2D one need to take this effect into account by applying certain factors on the pile response like the interface stiffness factors.

It is acknowledged that an extensive parametric study of different ISF factors was not performed. However, lowering the ISF did show the expected behaviour. Therefore, the influence of different ISF factors on the pile behaviour will be further researched in the dynamic calculations.

The implementation of the structural properties of the concrete cylindrical pile in the form of a maximum plastic moment of the pile (Mp), will only lead to a sudden bend in the load displacement curve. Until this Mp is reached, the stiffness behaviour is obviously the same as the one observed for the linear elastic pile. Further research on the use of this function, the interaction between the soil properties (lateral slider), the structural properties and the influence on the soil-pile behaviour should be performed. In this research the focus was on the response of the soil, where the implementation of actual elasto-plastic behaviour could lead to a better approximation of the displacements of the pile. With respect to performance based design this elasto-plastic behaviour of the pile could prove helpful in earthquake design, because the focus with this method is on the maximum allowable displacement of the foundation and superstructure

All the 2D calculations are compared with the 3D volume pile and D-Pile Group calculations. In Appendix D the validation between the Volume pile 3D, D-Pile Group and 2D calculations is given. The volume pile shows a good fit with the D-Pile Group calculations, which uses the undrained shear strength in combination with the API code for determining the p-y curves at different depths.

Further research should be done on the adjustment of the lateral ISF factor in combination with the determination of the lateral slider. Since the ISF is used for approximating the 3D pile behaviour, it should be depth/stress dependent. A check should be performed on the influence of this new ISF with respect to the stiffness behaviour for small loads and approximation of the 3D pile behaviour.

Since this study only used one continuous soil layer, with a difficult relation between effective strength parameters and undrained shear strength, more research should be done on different soils and different relations for the limiting soil resistance. The best way of comparing the 2D embedded beam behaviour, would be with measurement data. But since this was not available, similar methods for calculating the pile behaviour were used as validation of pile behaviour in 2D. Further research should be done by validating output of the 2D and 3D calculations with real test data.

4. Dynamic soil-pile analysis with embedded beam row PLAXIS 2D

In the previous chapter the building blocks of the FEM model were explained. In this chapter the model will be extended by adding an earthquake load at the bottom of the FEM model. The way this is done is explained in paragraph 4.1. In the subsequent paragraph 4.2, the obtained PLAXIS model and parameters are described followed by the evaluation of the pile bending moments in comparison with analytical models and D-Sheet Piling calculations in paragraph 4.3. Paragraph 4.4 will show the comparison of the cyclic loading behaviour of the 3D volume pile and the 2D embedded pile with or without slider. This chapter will end with the conclusions and recommendations in paragraph 4.5.

4.1 Free field site response analysis

The free field site response analysis is used to describe the distribution of the shear wave soil motion through the top soil deposit. During excitation of the bedrock, or in Groningen excitation along a fault in the gas field, the free field site response is calculated along a 1D linear elastic frequency domain analysis. This is done with the use of dedicated software for site response (EERA) and with finite element analysis in PLAXIS 2D. In this study a comparison between these two methods is made. In the PLAXIS finite element analysis the HS small material model is used, which is different from the equivalent elastic analysis done with EERA. Nonlinear and hysteretic behaviour is incorporated in the PLAXIS model, but this behaviour is approximated in EERA. A continuous one layered soil profile is assumed, thereby reducing the free field site analysis to a 1D problem. In the following subparagraphs the different aspects of the free field linear- and FE- site response analysis are explained.

4.1.1 Dynamic soil behaviour

Based on the parameters used for the static lateral loading of a pile, the dynamic properties of the soil are described here in more detail. The generally accepted soil model for earthquake loading available in the FEM program PLAXIS is the hardening soil (HS) small strain model if soil parameters are obtained properly, according to Brinkgreve, et al. (2007) and Meijers, et al. (2014). Within this model the hysteretic behaviour is best described, which is an important damping phenomenon in soil materials. However, a proper validation of this model should be performed.

Apart from this HS soil model, it should be mentioned that the chosen soil model does show peculiar behaviour in the top soil layer when it comes to stress dependency in a clay (Besseling, 2012). A new model has become available recently to take this into account: the generalized Hardening Soil model. Since in the beginning of this thesis this model was not available, the results here are based on the HS small strain model. The main parameters and settings in PLAXIS of the continuous one layered soil are shown in Table 6, which are obtained from a selection of a clay layer from soil investigation near Loppersum. The important parameters for the dynamic part are summarized in Table 10.

Parameter	Symbol	Clay, poor sandy / silty	Unit
Soil unit weight, saturated	γ_{sat}	18	kN/m^3
Soil unit weight, unsaturated	γ_{unsat}	18	kN/m^3
Soil Parameters			
Secant stiffness in standard drained triaxial test	$E_{50;ref}$	4600	kN/m^2
Tangent stiffness for primary oedometer loading	$E_{oed;ref}$	2300	kN/m^2
Unloading/reloading stiffness	$E_{ur;ref}$	18400	kN/m^2
Stress-level dependency power	m	0.7	-
Shear strain at Gs = 0,722G0	$\gamma_{0,7}$	0.00028	-
Shear modulus at very small strains	G_0	46100	kN/m^2
Poisson's ratio	ν_{ur}	0.2	-
Average shear wave velocity	$V_{s;30}$	137.5	m/s

Table 10 Dynamic soil parameters for HSsmall material model

Strain dependent characteristics, like the shear modulus and damping ratio, depend and vary on the content of the soil and soil type. In general, soil stiffness shows non-linear behaviour and is both stress and strain dependent. So even in a continuous soil deposit, the soil stiffness varies with depth and its value will decay with an increasing strain level induced by loading. The maximum strain at which linear behaviour occurs is very small (in the order of 10^{-6}) and thus in this situation the soil is purely elastic. The stiffness associated with this strain range is used as the initial stiffness and its value will decay by increasing strain amplitudes. This according to the characteristic S-curves in logarithmic scale, also called modulus reduction curves. Many researchers defined different shear modulus reduction curves and damping curves for different types of soil, based on cyclic strain levels. In this thesis the relationship of G_s / G_0 is used from Hardin & Drnevich (1972) modified by Benz (2007) as is implemented in the PLAXIS Hardening Soil small strain stiffness model.

For deconvolution of the earthquake signal at Huizinge to a depth of 30m, the G_s / G_0 in the EERA analysis was specified by Idriss and Sun (1992) for sand and Vucetic & Dobry (1991) for a clay with PI of 30. In EERA the assumption of a PI=30 for the soil profile defined in this thesis was checked with the secant modulus reduction and damping curves defined by Vucetic & Dobry (1991), see Figure 34.

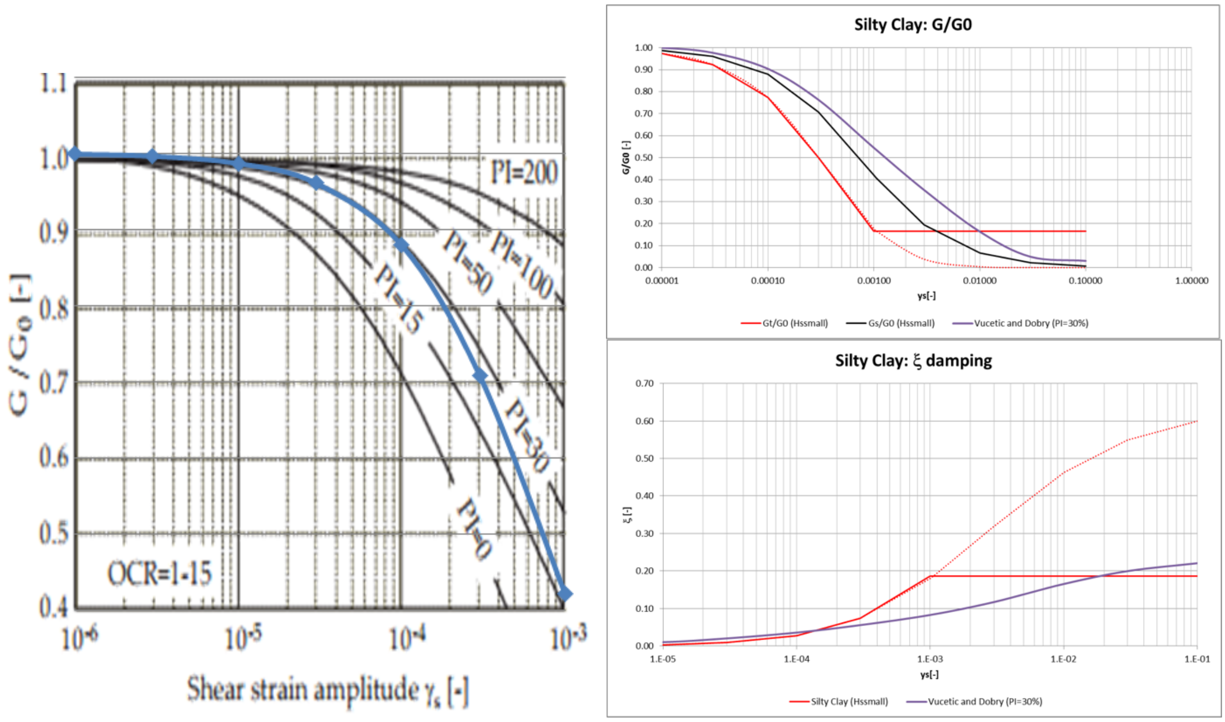

Figure 34 Modulus reduction and damping curves defined for parameters of silty soil in comparison with curves defined by (Vucetic & Dobry, 1991).

What can be observed from the left graph in Figure 34 is that the modulus reduction curves match quite good, but that the damping curve for clay defined by Hardin & Drnevich (1972) adopted by the HS small model in PLAXIS is higher for high strain levels. This was also noted by Brinkgreve, et al. (2007). In EERA the shear modulus and damping curves of the soil are specified manually. In order to compare EERA with PLAXIS, the curves from the HSsmall model were adopted in EERA (continues red line in Figure 34 (right)). Apart from these curves the shear wave velocity (Vs) through the soil material is also of importance. In equation (25) this velocity is linked by the shear modulus and the density resulting in a Vs profile with depth shown in Figure 35.

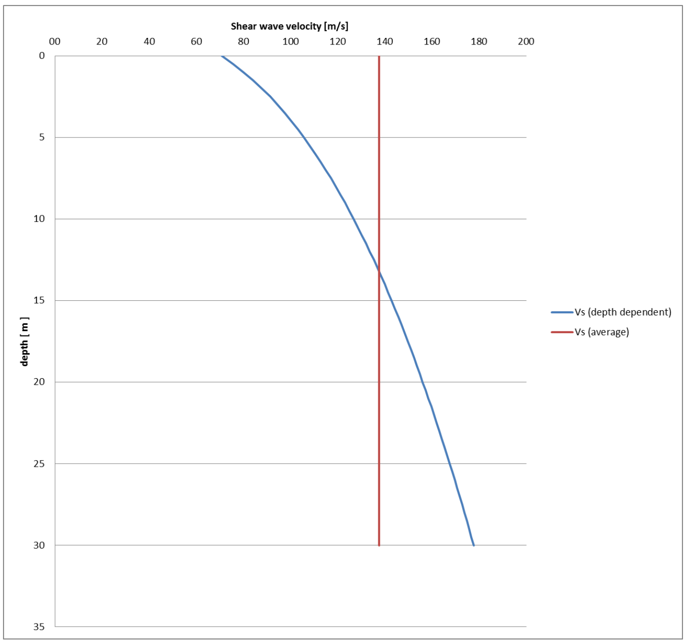

Figure 35 Shear wave velocity profile of homogeneous silty clay layer

4.1.2 Earthquake input signal

In traditional earthquake engineering, the input motion in most analysis for the free field site response contain only horizontally polarized shear waves, which propagate vertically. For this thesis the input signal for both methods was obtained by deconvolution, according to the method specified by Deltares in Meijers, et al. (2014). The signal used was the most severe earthquake measured in Groningen (KNMI, 2005): Huizinge Mw=3.6 on the Richter scale with a PGA of 0.06 g. This signal was measured at the station Westeremden and is specified as the WSErad signal. The recorded signal at ground level was used to back-calculate (deconvolution) the acceleration signal at a depth of 30 m, in this study with EERA and the soil profile at Huizinge. For calculation convenience the signal was reduced and the part from 0.00 to 12.40 seconds was used. The EERA files are shown in Appendix F. The mentioned "bedrock" in this study is referring to the signal in the soil at a depth of 30m below ground level as within motion. The process of the performed deconvolution is shown in Figure 36.

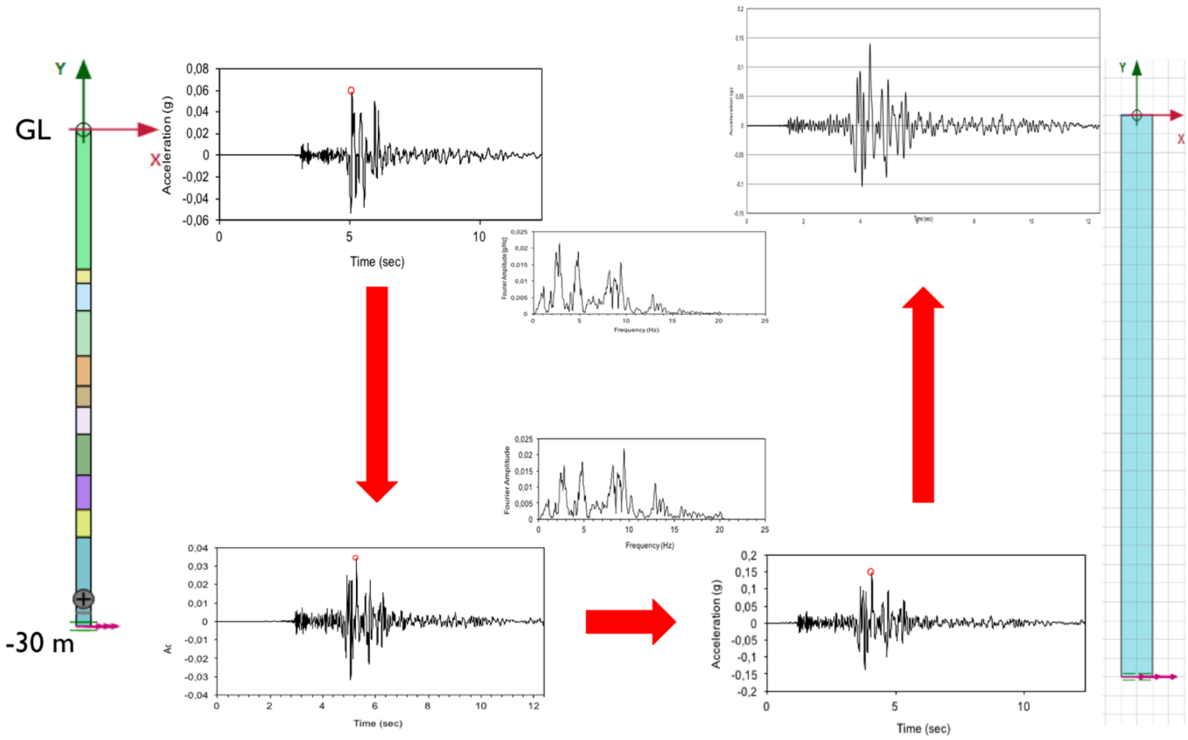

Figure 36 Deconvolution of the measured signal (left); scaling of the earthquake signal and calculating the peak ground acceleration of the continuous one layer clay profile (right)

In Figure 2 the so-called probabilistic seismic hazard contours are shown based on KNMI (2005). It shows the expected maximum PGA values with a return period of 1/475 year. Based on this contour profile one can observe that nearly anywhere in Groningen a PGA of 0.25 g can be expected. However, there are no measured earthquake signals of this magnitude, so the approach of scaling the measured signal at ground level is used here. Based on reports from Dost & Kraaijpoel (2013), Dost, et al. (2013), Visschedijk, et al. (2014) and Meijers, et al. (2014), the signal is scaled in magnitude and frequency in the following way:

- The magnitude of the unscaled signal at bedrock is multiplied by a factor of desired magnitude at ground level divided by the measured magnitude of the WSErad signal;
- The frequency scaling is done by applying the formula:

$$\frac{T_{peak}}{T_{peak,ref}} = \exp\ (0.3(M_w - M_{ref})) \tag{44}$$

By applying the relation (Dost, et al., 2013) for an earthquake magnitude of less than 4.2, as was done by Deltares and de Greef (2015), equation (44) becomes:

$$\frac{T_{peak}}{T_{peak,ref}} = -0.25 * \left(\frac{PGA}{g}\right)^2 + 1.65 * \left(\frac{PGA}{g}\right) + 0.85 \qquad (45)$$

There are some remarks on these time and magnitude scaling:

- These equations (44/45) are based on tectonic earthquakes, the application to the Groningen situation has not yet been validated;
- Equation (45) is only valid for earthquake with a magnitude of less than 4.2 (Dost, et al., 2013);
- Every period, including the peak, has been scaled;
- The outcome of this deconvolution is a very rough approach.

Using the above assumption on scaling, the magnitude at bedrock resulted into a value of 0.146 g and the time step was changed from 0.005 s to 0.0062 s, see signal in Figure 37. As mentioned above the applied deconvolution is a rough approach, however since this thesis is not about defining the exact scaling for earthquake signals, the method applied by Deltares was used as an estimate. For the continuous clay profile, the horizontal ground acceleration and Fourier amplitude spectrum is obtained by using EERA and is presented in Figure 39. The calculated peak acceleration was 0.146 g and the calculated fundamental frequency was 2.79 Hz. This means that the applied signal at -30 m is filtered by the clay deposit, modelled in this thesis.

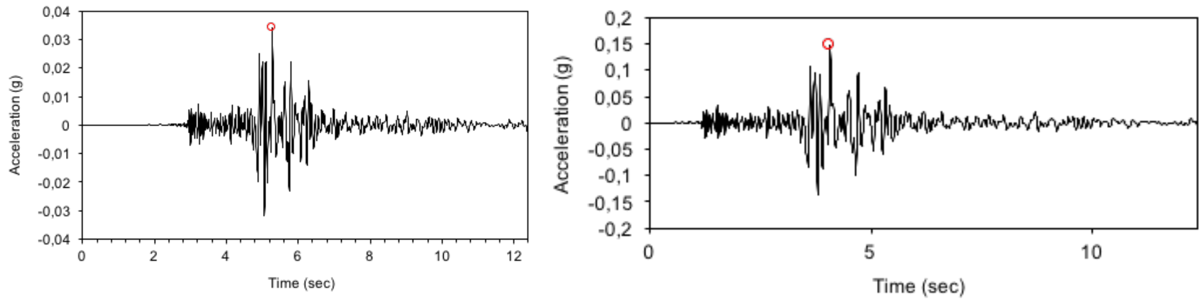

Figure 37 (left) Unscaled WSErad signal at "bedrock" at 30 meters depth; (right) scaled WSErad signal at "bedrock"

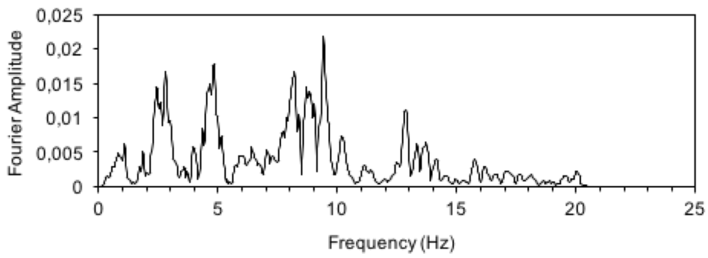

Figure 38 Fourier amplitude spectrum of scaled signal at 30m depth

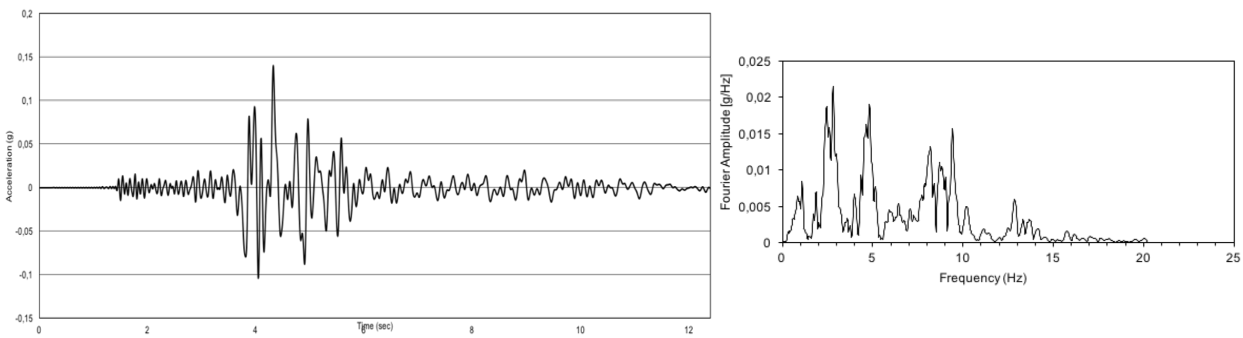

Figure 39 (left) Calculated WSErad hor. Acceleration signal for clay profile with scaled magnitude and frequency; (right) Fourier amplitude spectrum

4.1.3 Calibration of the finite element model

For the site response analysis of the FEM model, EERA was used to compare the soil behaviour during an earthquake signal applied at 30 m depth. This comparison was mainly executed to examine the influence of the boundaries disturbances at the bottom and sides, kind of boundaries chosen in EERA and PLAXIS, mesh size and performance of the chosen soil model. A small study was performed on the influence of the base boundary setting in and the chosen PLAXIS base boundary.

4.1.3.1 PLAXIS model and boundaries

Undrained (A) conditions have been used for the PLAXIS model in both the static and dynamic calculations. The whole soil deposit consists of a fully saturated cohesive soil. Considering that earthquakes act for a very short time, excess pore pressures are generated and cannot dissipate during the seismic motion. In PLAXIS the soil was defined by effective stiffness and effective strength parameters, which are shown in 3.1 and 4.1.1.

Depending on the type of side boundary in 2D, the width of the PLAXIS model was either 1m (ranging from -0.5 m to 0.5 m) or 200 m (-100 m to 100 m) for respectively the tied-degrees-of-freedom boundary and the viscous boundary, see Figure 40. The absorbent boundaries are applied at x-min and x-max of the model. The final model, which was used for all calculations, had a compliant base boundary with an (inactive) interface and viscous side boundaries, see right side of Figure 40.

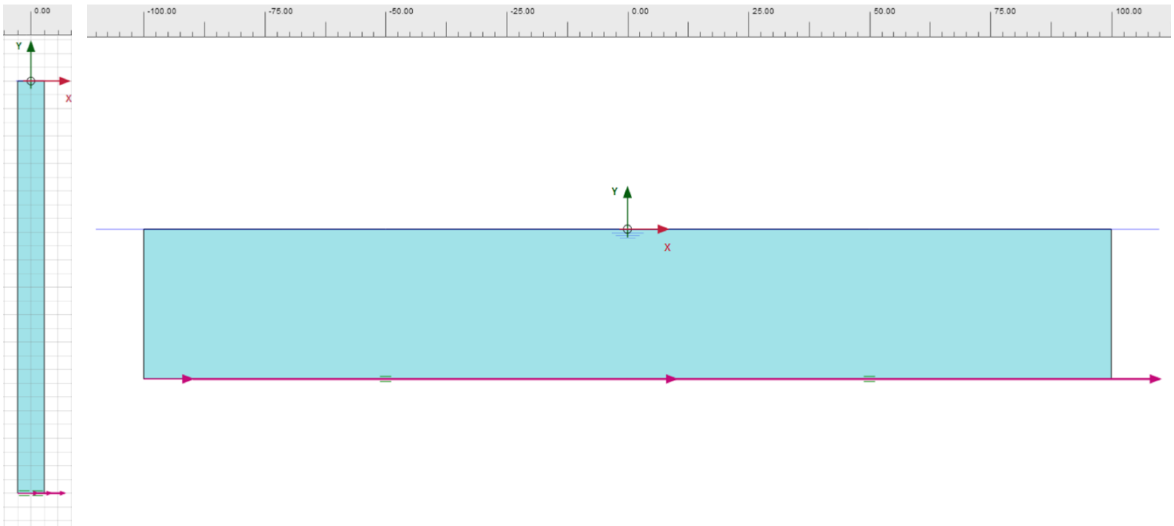

Figure 40 PLAXIS model for tied-degrees(left) and viscous boundary (right)

4.1.3.2 Base boundary in EERA and PLAXIS

In order to determine the best base boundary for the models, a relation between the applied motion in EERA and the application of the motion within PLAXIS had to be defined. It is important to understand the kind of signal that you are implementing in your model. In this case the signal at Huizinge was recorded at ground level, which is an "outcropping" motion. This means that the signal measured is superposition of the incoming and reflective wave, since the interface is a free boundary; no stress accumulation but strain enhancement. When this signal was deconvolved with EERA to a depth of 30m, the obtained signal is an "inside" motion. This means this is the actual motion at that location, which is characterized by the superposition of upward and downward propagating waves. This is true when assuming bedrock at that location.

In this study at a depth of 30 m, the same soil is present and no actual bedrock is specified. Since we only model the upper part of the soil profile, the signal applied at 30 m depth should be half of the total signal calculated at that locations with EERA. So only the upward travelling wave should be applied. In EERA this can be done by setting the input motion to outcrop, whereas in PLAXIS the applied accelogram should be halved manually.

To check both options and to determine the relation between the base boundary in EERA and in PLAXIS a small study was performed. Herein linear elastic soil properties were assumed and the scaled Huizinge signal was applied, see right of Figure 37.

Fully reflective fixed base boundary in PLAXIS in comparison with EERA inside motion

The soil profile of the deconvolution from the Huizinge signal is used in this check for both EERA and PLAXIS with linear elastic soil properties based on the shear wave velocity, see Figure 42. In PLAXIS, Rayleigh Damping was added for target frequencies 1 and 2 of 1% at 9,4Hz, which is the fundamental frequency of the input motion. The base boundary in PLAXIS is set to fully fixed and at 'none' in the dynamic boundaries window, ensuring a fully reflective boundary without damping at the bottom. In EERA the input motion is defined as a "inside" motion, which means that the signal is both the upward and downward travelling wave as the signal should be measured inside the bedrock. This input motion at 30m depth is obtained after a deconvolution of the signal at ground level at Huizinge. The signal used in this comparison is shown in Figure 41. The signal is scaled to a maximum magnitude of 0,146g and the time step is changed to 0,0062 s.

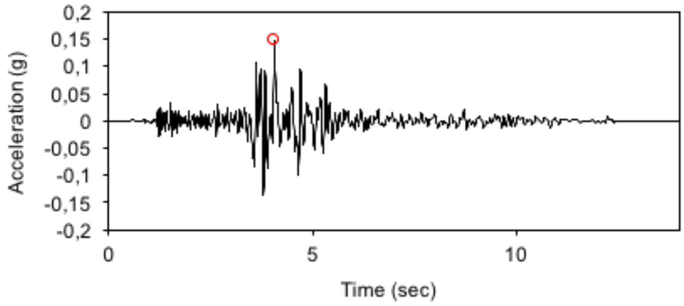

Figure 41 input signal at 30m depth

Fundamental period (s) = 0,73
Average shear wave velocity (m/sec) = 197,93
Total number of sublayers = 17

	Layer Number	Soil Material Type	Number of sublayers in layer	Thickness of layer (m)	Maximum shear modulus G_{max} (MPa)	Initial critical damping ratio (%)	Total unit weight (kN/m³)	Shear wave velocity (m/sec)	Location and type of earthquake input motion	Location of water table	Depth at middle of layer (m)	Vertical effective stress (kPa)
klei	1	0	1	6,8	24,12	1	14,00	130			3,4	47,60
klei	2	0	1	3,4	24,12	1	14,00	130			8,5	119,00
zand	3	0	1	1,0	56,15	1	17,00	180			10,7	151,30
zand	4	0	1	2,0	86,34	1	17,50	220			12,2	177,30
klei	5	0	1	3,3	29,97	1	15,00	140			14,8	219,55
zand	6	0	1	2,2	124,04	1	18,00	260			17,6	264,10
klei	7	0	1	1,5	68,54	1	16,00	205			19,4	295,90
zand	8	0	1	2,0	120,59	1	17,50	260			21,2	325,40
klei	9	0	1	3,0	63,96	1	16,50	195			23,7	367,65
zand	10	0	1	2,5	92,89	1	18,00	225			26,4	414,90
zand	11	0	1	2,0	124,04	1	18,00	260			28,7	455,40
zand	12	0	1	1,5	130,93	1	19,00	260			30,4	487,65
zand	13	0	1	1,5	130,93	1	19,00	260			31,9	516,15
zand	14	0	1	1,5	130,93	1	19,00	260			33,4	544,65
zand	15	0	1	1,0	130,93	1	19,00	260			34,7	568,40
zand	16	0	1	1,0	130,93	1	19,00	260			35,7	587,40
Bedrock	17	0			130,93	1	19,00	260	Inside		36,2	596,90

Figure 42 Soil properties for EERA and PLAXIS

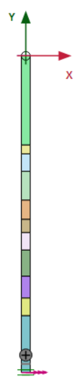

Figure 43 Soil profile within PLAXIS model with Tied degrees of freedom

The results of the time history of the acceleration at ground level is compared between EERA(**black line**) and PLAXIS(**green line**) and shown in Figure 44. This shows that both methods show the same time histories. Figure 45 shows the velocity time history at ground level, the only difference between the two methods is the peak around 4 seconds, where a lower peak velocity is obtained within PLAXIS.

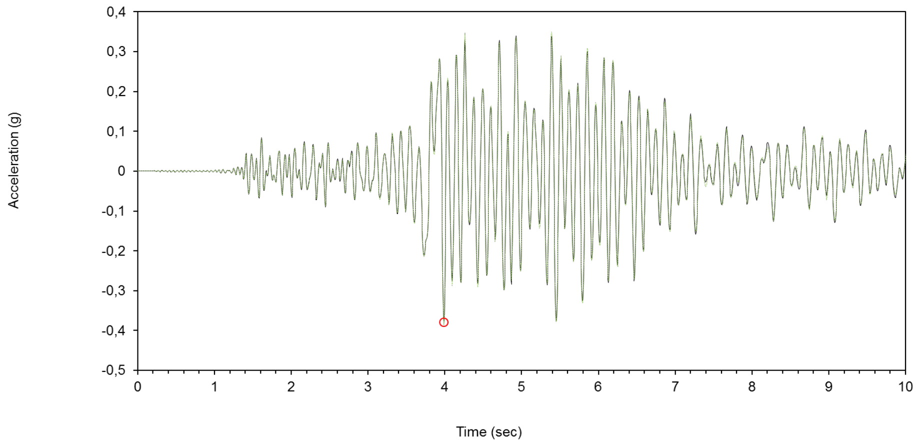

__Figure 44 Acceleration time history at ground level: PLAXIS (Green) and EERA (Black)__

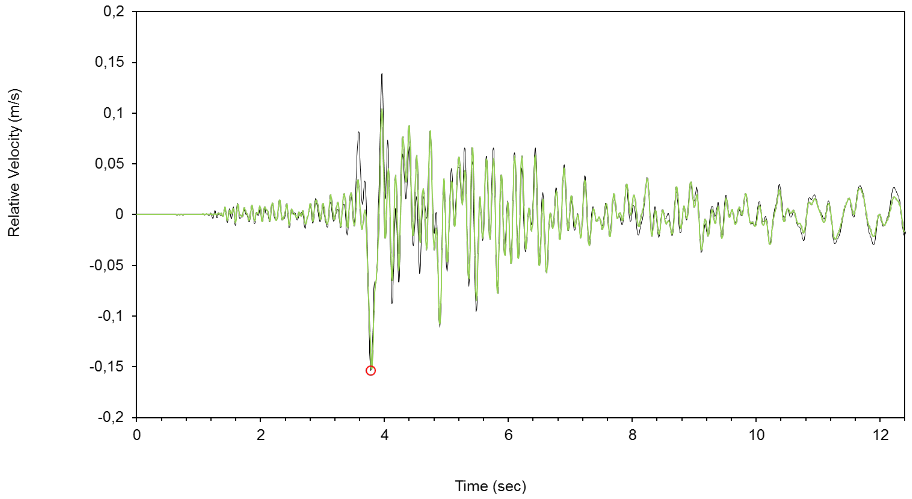

__Figure 45 Velocity time history at ground level: PLAXIS (Green) and EERA (Black)__

The spectral analysis of EERA and PLAXIS is compared in Figure 46 and shows good agreement between both methods.

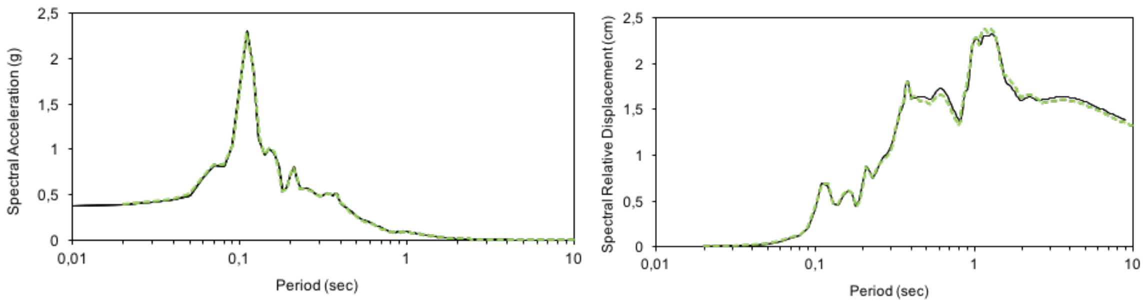

__Figure 46 Spectral Acceleration (left) and displacement (right) analysis EERA (black) and PLAXIS (Green) for fixed base boundary__

Compliant base boundary in comparison with EERA outcrop motion

For this comparison, the same soil profile was used as shown in Figure 42. The only thing changed here is the compliant base boundary within PLAXIS and the selection of an 'outcrop' motion within EERA. This means that only half of the signal is used, since only the upward traveling component of the signal is used. To ensure that only the upward motion is modelled in PLAXIS, a factor of 0.5 is used for the input motion in combination with the compliant base boundary. The results of the time history of the acceleration at ground level is compared between EERA(**black line**) and PLAXIS(**green line**) and shown in Figure 47.

This shows that both methods show similar time histories, although some peaks of the PLAXIS calculation are higher than obtained from EERA. Figure 48 shows the velocity time history at ground level, the same holds as for the acceleration where some peaks are higher in PLAXIS than in EERA, although the differences are very small.

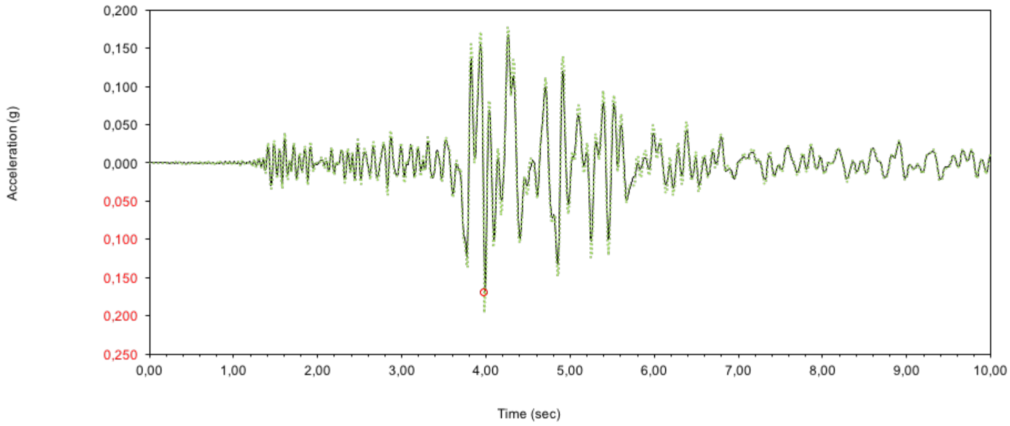

Figure 47 Acceleration time history at ground level: PLAXIS (Green) and EERA (Black)

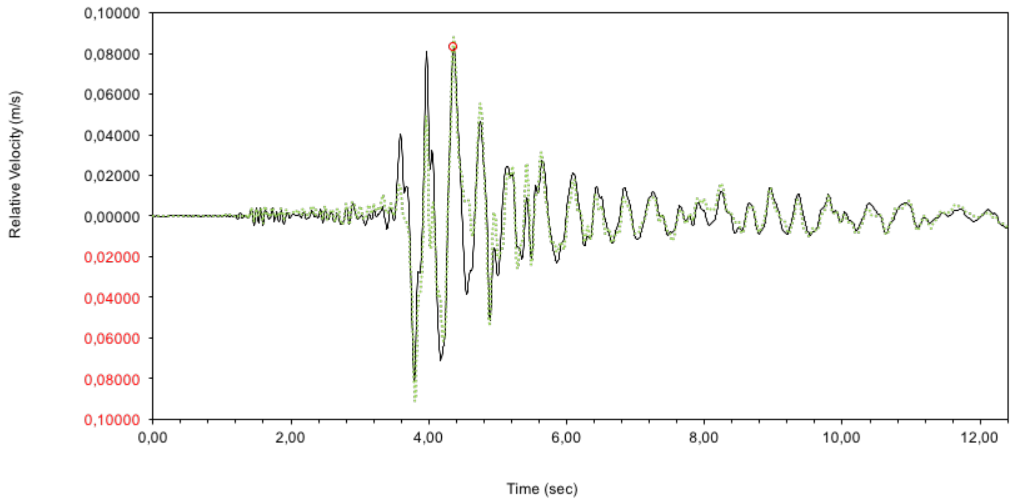

Figure 48 Velocity time history at ground level: PLAXIS (Green) and EERA (Black)

The spectral analysis of EERA and PLAXIS is compared in Figure 49. This also shows good agreement between both methods.

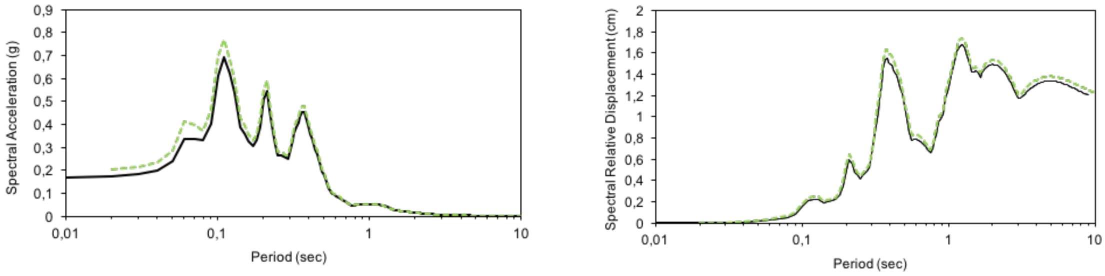

Figure 49 Spectral Acceleration (left) and displacement (right) analysis EERA (black) and PLAXIS (Green) for fixed base boundary

Conclusion on the chosen base boundary and input motion

Since the deconvolution was performed to obtain a 'within' motion, which is both the upward and downward propagating amplitude, the time histories of both EERA and PLAXIS in the site responses could not be matched. Therefore, the different options of the base boundary settings in both programs were further researched. In this subparagraph the relation between the two boundary conditions in EERA, inside or outcrop, and PLAXIS, fixed base or compliant base, are shown. It turned out that for modelling an inside motion in EERA, a fixed base boundary in PLAXIS should be used. However, when modelling an outcrop motion in EERA, a compliant base boundary should be applied with a factor of 0.5 on the input signal.

For this thesis the site response analysis should be performed using the outcrop motion in EERA and the compliant base boundary with a factor of 0.5 on the input motion. The main reason for this is that the signal used in the deconvolution is a signal at ground level, which is an outcrop motion (upward and downward signal). When applied in the FEM model of this thesis, only the upward travelling wave was required since the source of the earthquake or bedrock is not located at 30m depth.

4.1.3.3 Damping

Hysteretic damping of the soil can capture damping at strains larger than 10^{-4} until 10^{-2}, depending on the values of material properties within PLAXIS. Even at low deformation levels, the behaviour of the soil is irreversible. As mentioned in subparagraph 2.2.2 the chosen soil model in PLAXIS, Hardening soil small strain, mostly is used with extra Rayleigh damping in the order of 0.5% till 2%. There are different methods mentioned in literature to select appropriate Rayleigh parameters for different target frequencies. In this study the first calculations were performed based on the method mentioned by Hudson, et al. (1994). The first target frequency is set equal to the fundamental frequency of the soil profile and the second frequency is the first odd number of the ratio: fundamental frequency of the input signal / fundamental frequency of soil profile (Kottke & Rathje, 2009). The applied Rayleigh damping parameters for the FEM model can be found in Table 5. The comparison between EERA and PLAXIS 1D Fourier amplitude spectrum can bee seen in Figure 50. This shows similar spectra between EERA and PLAXIS 1D.

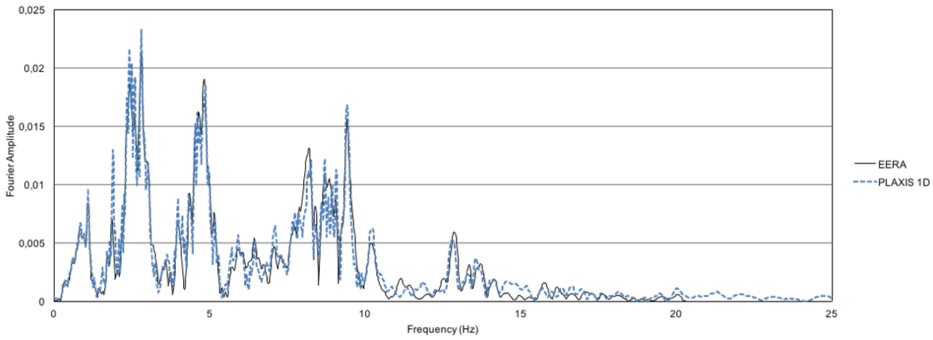

Figure 50 Fourier amplitude spectrum comparison with Rayleigh damping according to Hudson, et al. (1994)

4.1.3.4 Mesh generation and Dynamic time step

For the FE model the size of the mesh-elements discretising the soil profile and the time steps of the dynamic calculation are of importance in order to ensure a proper wave propagation through FE model. As with the damping determination, also for these two important factors many different methods for defining them could be find in literature. The mesh generation in PLAXIS needs to be adjusted in order to comply with equation (46) which can be defined by (Kuhlemeyer & Lysmer, 1973):

$$Average\ Element\ size\ \leq \frac{\lambda}{8} = \frac{v_{s,min}}{8 * f_{max}} \tag{46}$$

With $v_{s,min}$ the lowest shear wave velocity of the soil profile, which can be obtained from Figure 35 : 70.7 m/s. From the Fourier spectrum in Figure 38 the maximum frequency component f_{max} is about 9,4Hz. The average length needed for the PLAXIS FE model is therefore 0.94m. However de Greef (2015) mentioned, based on Visone et al (2008) and Visschedijk et al (2014), that this formula could be changed to $\frac{\lambda}{2}$ as long as within each wavelength λ a minimum of 8 nodes is available to describe the wave properly. The 15-noded equilateral triangular (quadratic) mesh elements used within PLAXIS can be checked to this condition within PLAXIS with the function "mesh quality", which indicated if this condition is met. Applying this rule, results in an average element size of 3.74 m.

The dynamic time step is defined in PLAXIS by a dynamic time interval, max number of steps and number of sub steps. Two conditions need to be met in order to have a proper dynamic time interval. The conditions are depending on the mesh element size and on the number of data points which define the input signal. The last conditions can automatically be implemented by PLAXIS in the phases screen. A general rule of thumb can be used for the first condition:

$$dt\ \leq 0.1 * T_{highest\ mode} = \frac{1}{f_{highest\ mode}} = \frac{1}{20} = 0.05s \tag{47}$$

Dynamic phase		
Dynamic time interval	12.4	s
max number of steps	2000	
sub steps	2	
Δt	0.0031	s

Table 11 Applied dynamic time step in PLAXIS calculations

Some calculations with different time steps were performed and obtained the same results. The time step will automatically be smaller than the specified condition in equation (47), since the data points of the input motion are fixed. The only option to change the time step, without loss of proper implementation of the signal, is by defining a certain amount of sub steps. So both dynamic time step conditions are met, when using the automatic determination of steps and sub steps within PLAXIS.

4.1.4 Comparison between EERA and 2D dynamic free field site response

The input signal, soil profile and settings for the EERA excel plugin can be found in Appendix F. The PLAXIS model conditions, assumptions and properties are mentioned in the previous subparagraph. The same input signal is used for PLAXIS and EERA, see Figure 37. For EERA the soil was defined by 16 layers with the Vs as determined in Figure 35. Bedrock was defined with the same shear wave velocity as the soil layer above and the outcrop motion within the EERA program was selected. The damping properties (curves) in the EERA program were manually changed to match the Hardening Soil Small strain overlay model with the chosen soil parameters, this means using the truncated damping curve. The ratio of effective strain, which can be defined by the magnitude of the earthquake was set at the default value of 0.65, as was also done by Visschedijk, et al. (2014), Meijers, et al. (2014) and mentioned by Kottke & Rathje (2009). In Figure 51 and Figure 52 the time histories of both acceleration and velocity for EERA and PLAXIS 1D and 2D situation is shown. The best fit with EERA was the 1D PLAXIS tied degree of freedom boundaries. However, since in a later stage an embedded beam will be implemented, the PLAXIS 2D with viscous boundaries was also compared to the other two methods. Quite a good fit is observed when comparing the time histories, apart from the expected small differences in the signals phase and amplitudes, especially from 3 till 6s. These differences can have multiple explanations, but are most likely due to the comparison of an equivalent linear elastic soil model with a elasto-plastic Hardening soil model.

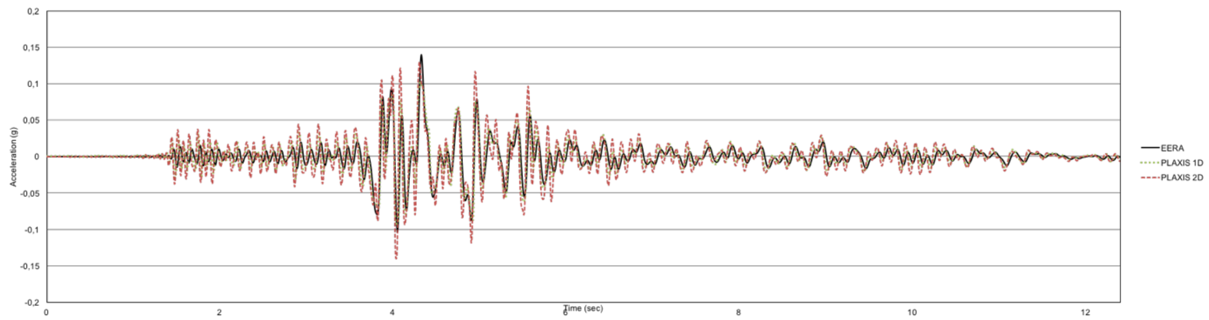

Figure 51 Time history of horizontal acceleration

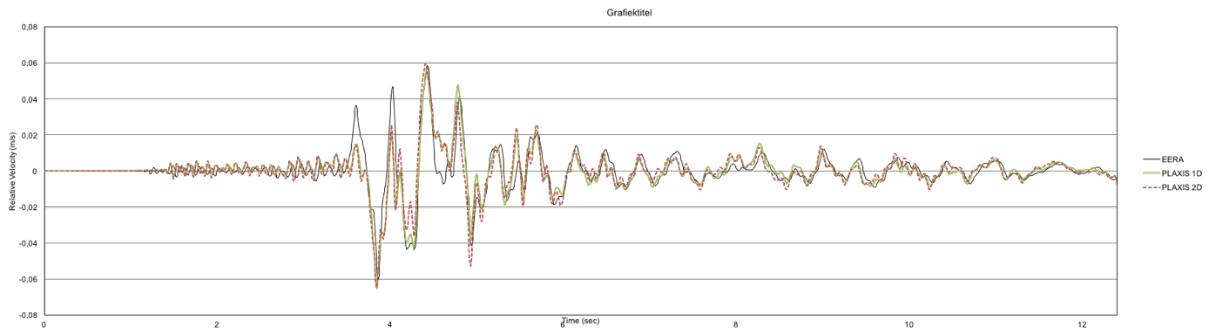

Figure 52 Time history of horizontal velocity

Also the Hardening Soil small strain model introduces some specific behaviour when it comes to dynamic calculations. Much was researched by Besseling (2012) who showed that the accelogram and thus dynamic behaviour is influence by:

- Stress dependency;
- Reset of the deviatoric strain tensor with strain rate reversal;
- Number of dynamic sub steps;
- Undrained/drained analysis of clays;
- Small strain overlay model parameters G_0 and $\gamma_{0,7}$;
- Additional Rayleigh damping.

Apart from the time histories, also a spectral analysis was performed on the PSA (Peak Spectral Acceleration) and Relative displacement. In Figure 53 and Figure 54 the comparison of the different acceleration and displacement spectra are shown. From the comparison between EERA and PLAXIS 1D and 2D, it can be seen that the 2D PLAXIS model shows a higher spectral acceleration for frequencies above 9Hz (around 0.1s period). But in the spectral relative displacement, differences can be found for the small frequencies. A possible explanation can be found in the applied boundary conditions and mesh size within the 2D model. Since a model of 200m width and 30m deep is taken to diminish the interference of the boundaries, the relative mesh size is automatically larger than for the 1D PLAXIS calculation. A solution can be found by reducing the coarseness of the mesh manually, but this will increase the calculation time substantially. Since both PLAXIS 1D and 2D reasonable resemblance with EERA, the applied soil model in PLAXIS (HS small) and boundary conditions specified in this paragraph, were used in the dynamic analysis of this study.

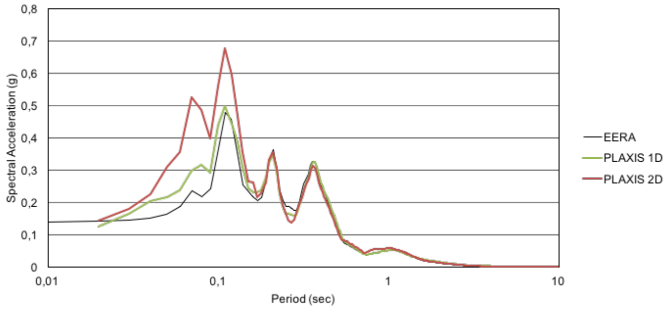

Figure 53 PSA spectrum at ground level

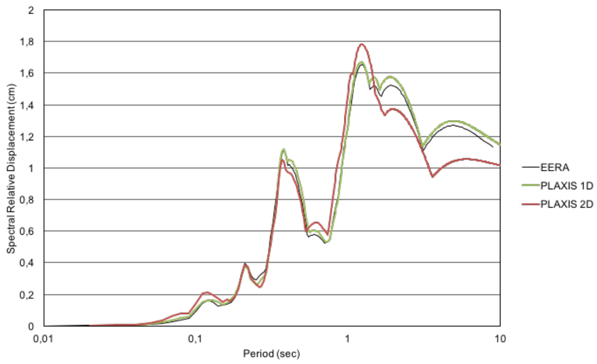

Figure 54 Relative displacement spectrum at ground level

The Fourier amplitude spectra are shown in Figure 55. Up until the frequency of 9.4Hz, the spectrum is quite similar for all methods. As was the case with the spectral acceleration, the amplitude around the fundamental frequency in the 2D PLAXIS model shows different behaviour with EERA and the 1D PLAXIS model.

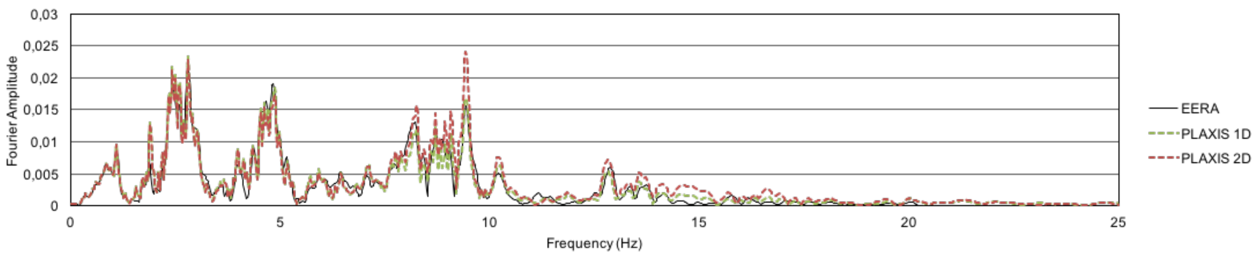

Figure 55 Fourier amplitude spectra of EERA and PLAXIS 1D / 2D

Concluding on the response of the chosen soil profile, the dynamic behaviour in the PLAXIS model is consistent with EERA. This is also expected based on Vucetic (1992), rather an attenuation of the input signal than an increase of PGA is expected based on the soft, low plasticity clayey soil.

4.1.5 Conclusion and recommendations

In order to compare and perform the site response analysis, several investigations have been performed on the use of EERA and PLAXIS in combination with its settings and boundary conditions. For this part the deconvolution and scaling of the Huizinge signal was used as input at 30m depth. For the determination of the base boundary condition, a linear elastic model of the Huizinge soil profile was adopted in EERA and PLAXIS. Since the signal measured in Huizinge was assumed to be at ground level, this could be seen as an outcrop motion. Performing a deconvolution on the signal will obtain an inside motion at 30m depth. However, only the upward wave needs to be modelled in both EERA and PLAXIS. In this thesis it was shown that the compliant base boundary in PLAXIS, with a factor of 0.5 on the signal, and the outcrop motion in EERA selected, could be well compared with each other.

The dynamic behaviour of the soil was compared by its modulus reduction curves, which needs to be specified in the linear equivalent EERA model. Similar modulus reduction curves of the clay deposit with HS small parameters compared with the curves from Vucetic & Dobry (1991) are obtained. However, at high levels of strain the modulus reduction curve from the HS small model is overestimating the damping. Because of this difference, the specified curves from PLAXIS were used in the EERA model for comparison. This is justified since maximum shear strain in the soil profile during the earthquake obtained from EERA is 0.0005, which is within the range where the curves of Vucetic & Dobry are comparable with the ones calculated by the HS small model.

The time histories of both the PLAXIS models and EERA showed similar behaviour, as was the case for the Fourier-, acceleration- and displacement-spectra.

The applied and scaled Groningen signal can be seen as a moderate to weak earthquake signal with a maximum of 0.146g. Further research should focus on the influence of stronger motions on the effects in either EERA and PLAXIS. In this research the applied Hardening Soil small strain model, showed similar behaviour with EERA output. The influence of the improved hardening soil model, generalized hardening soil model, should be a topic for further research when increasing the magnitude of the earthquake.

4.2 Introduction Dynamic PLAXIS model and parameters

In paragraph 4.1 the free field site response analysis was performed in order to obtain a model with the implementation of the earthquake wave propagation. In this paragraph the boundary conditions at the base and sides of the model were determined, as well as the amount of Rayleigh damping, mesh size and time stepping during dynamic calculation. The implementation in this part of the research was the embedded beam row with and without lateral slider. The model and mesh used for this part is shown in Figure 56. The limiting lateral soil resistance of the embedded beam is the same as for the static case. It should be noticed that an error is introduced with this assumption, since the limiting lateral soil resistance will either increase for short applied cyclic loads. But depending on the type of soil, the strength can also seriously deteriorate with increasing loading cycles (cyclic softening / hardening).

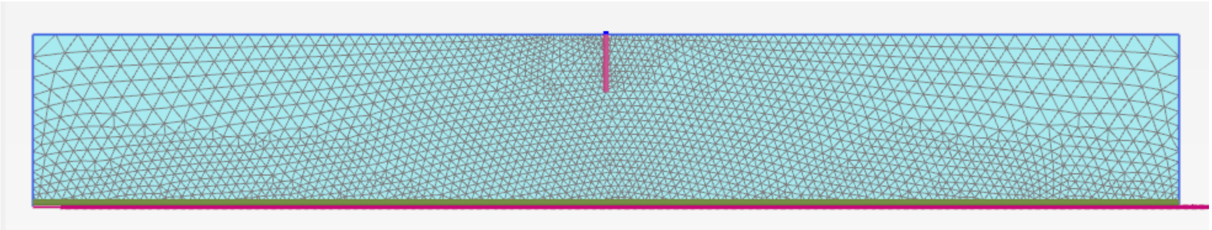

Figure 56 model and mesh for the dynamic calculations

For incorporation of the inertia loading in the model, implementation of real structures is considered very challenging, especially when the superstructure is massive. In some analysis carried out in soil-pile interaction problems, the whole structure is modelled on top of the pile (coupled system). However, when a multi-storey building is considered, the modelling techniques can be challenging and can increase the computational time and costs drastically. Therefore, Liyanapathirana & Poulos (2005) suggested that attaching the superstructure total mass at the cap level of the pile foundation provides sufficient accuracy, at least for initial pile design. In this study the pile cap was modelled with a plate fixed to the pile head with a width of 1m. The weight was based on a bearing capacity calculation, NEN 9997-1, shown in appendix H. This weight was than applied in the analysis on the effect of both the inertia and the kinematic loading. It should be mentioned that this method also has disadvantages. Using this simplified model for the structure does not take structural damping into account. However, the exact modelling of the superstructure is outside the scope of this thesis.

For the kinematic loading, the plate on top of the embedded beam was either fixed in x-direction or in both x- and y-directions. The modelling of the kinematic loading was done by applying a weightless plate on top of the embedded pile, which has no cohesion with the soil. To model this, an interface with a factor R_{inter} of 0.01 was applied underneath the plate. In the case of both fixities in x- and y- direction a very heavy building or structure is assumed, which does not move in case of an earthquake. This situation can therefore be described as an upper bound of the maximum kinematic earthquake loading, since the pile needs to follow the soil movement induced by the earthquake while it is fixed at pile head. Both fixities are visualised in Figure 57.

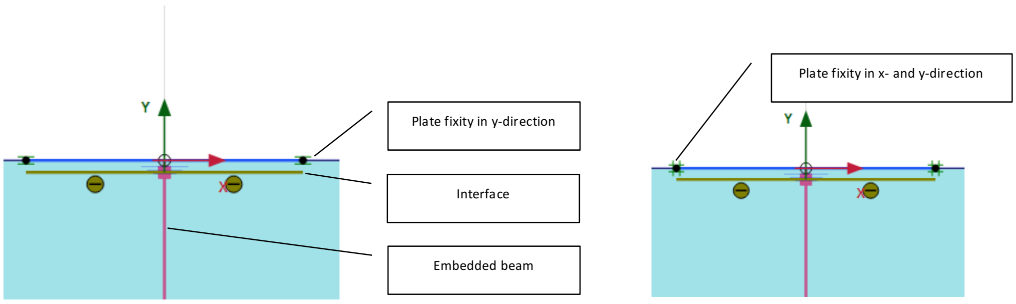

Figure 57 Plate fixities in x-direction (left); Plate fixities in both x- and y-direction (right)

The properties of the pile and the used lateral skin resistance are shown in Table 12. Rayleigh damping was not specified for the embedded beam.

Parameter	Symbol	Embedded beam (row)	Unit
Young's modulus	E	3.00E+07	kN/m^2
Unit weight	γ	25	kN/m^3
Predefined pile type	-	Massive circular pile	-
Diameter	D	0.5	m
Area	A	0.1936	m^2
Moment of inertia	I_p	3.07E-03	m^4
Axial Skin resistance			
Skin friction distribution	-	Linear	-
Skin resistance at top	$T_{top;max}$	1.00E+05	kN/m
Skin resistance at bottom	$T_{bottom;max}$	1.00E+05	kN/m
Base resistance	$F_{bot;max}$	1.00E+05	kN/m
Pile to pile distance	$L_{spacing}$	4	m
Lateral skin resistance			
API			
Skin friction distribution		*Multi linear*	
Linear from ground level till -8,5m		60 - 180	kN/m
Below -8,5m		180	kN/m
Pile tip		180	kN/m

Table 12 Material properties of the embedded beam (row)

The dynamic PLAXIS 2D model, with embedded beam, is clarified in Figure 58. Based on paragraph 4.1 the earthquake loading is defined and applied as vertical propagating Shear waves at the bottom of the model. The 2D embedded beam is connected with the soil by springs, which are defined by the interface stiffness factor mentioned in subparagraph 2.1.3.3. The default values of these ISF are applied in this part of the thesis and the maximum capacity of the interface is specified by the maximum lateral skin resistance based on the API.

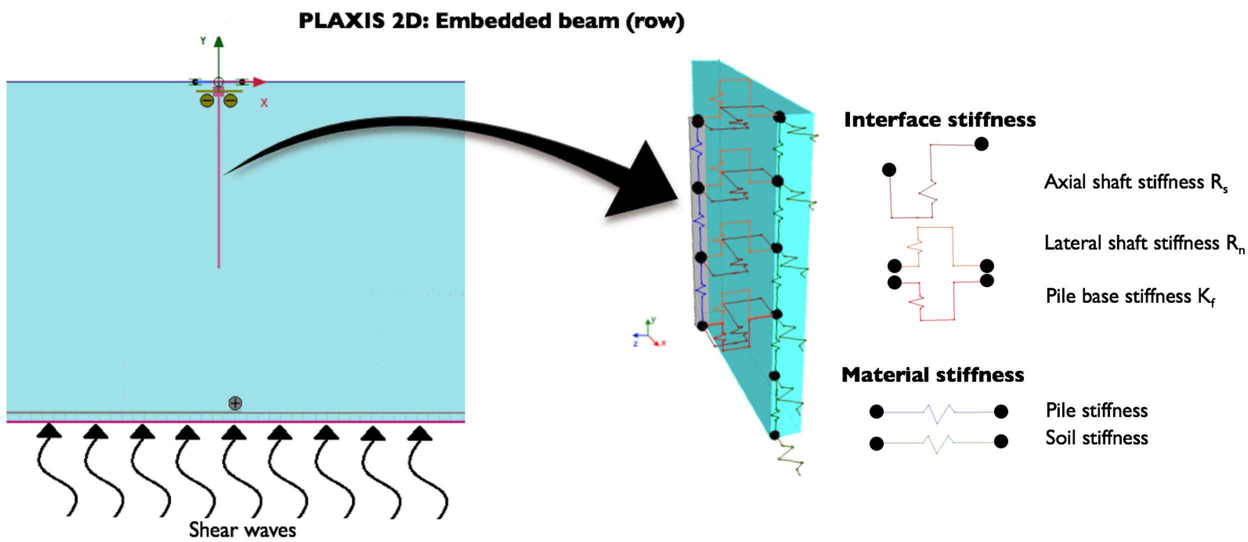

Figure 58 PLAXIS 2D model with 2D pile modelling using an embedded beam row with interface stiffnesses (based on Sluis, (2012))

4.3 Evaluation of the kinematic pile bending moments

In literature several design methods and pseudo static methods were found, the equations for these methods can be found in paragraph 2.2.4, as well as all of their assumptions. In this paragraph the values for the maximum kinematic bending, occurring at pile head level, are shown. In first instance 3D volume pile calculation would be used for comparison with the 2D embedded beam behaviour, however this 3D PLAXIS calculation turned out to be very computational demanding and could not be performed with the available resources.

The closed form design methods are used for calculating the maximum bending moment at pile head, where it is fixed with the pile cap. The main assumption of these methods is a fully flexible pile, therefore it will follow the displacement of the soil during an earthquake. In reality however the relation between the pile and soil is much more complex and depends on key parameters like:

- Type of soil profile;
- Relative pile soil stiffness;
- Slenderness ratio of the pile;
- Pile-head fixity conditions;
- Frequency of excitation.
-

PLAXIS 2D is a FEM program which does take these parameters into account. Therefore, one of the earliest closed form design methods by Margason & Holloway (1977) and NERHP (1997) could not be used for comparing with the 2D embedded beam row results. In this study the method specified by Di Laora & Rovithis (2014) is used. It takes the non homogeneous soil properties, i.e. depth dependent shear modulus, into account in calculating the maximum kinematic bending moment. The resulting bending moment for this study is shown in paragraph 4.3.1.

Other methods, apart from these closed form expression, is the validation like Fan, et al. (1991), where the soil is displaced with a sinusoidal input motion and the observed pile displacement is compared to a so called “kinematic displacement factor”. However, this will require a new analysis in PLAXIS 2D with the implementation of a sinusoidal displacement at the base and is therefore not performed.

In this study a pseudo static method is applied as second validation of the dynamic results, which is based on the provisions mentioned in the EUROCODE 8 NEN EN 1998-5. The maximum soil displacement is calculated with the free field site response analysis and applied on in the model of D-Sheet Piling program and PLAXIS 2D embedded beam. The results of this method is shown in 4.3.2.

4.3.1 Analytical determined kinematic maximum bending moment

Laterally loaded pile response is a complex phenomenon of soil-pile interaction as the behaviour depends on the resistance provided by the surrounding soil and soil resistance depends on the pile deflection. Many factors play a role in this behaviour such as loading type and soil profile. The analytical methods for comparison with the 2D embedded beam is the one specified by Di Laora & Rovithis (2014). For this method a linearization of the shear modulus was specified. The resulting depth dependent shear modulus in comparison with the PLAXIS soil model is shown in Figure 59.

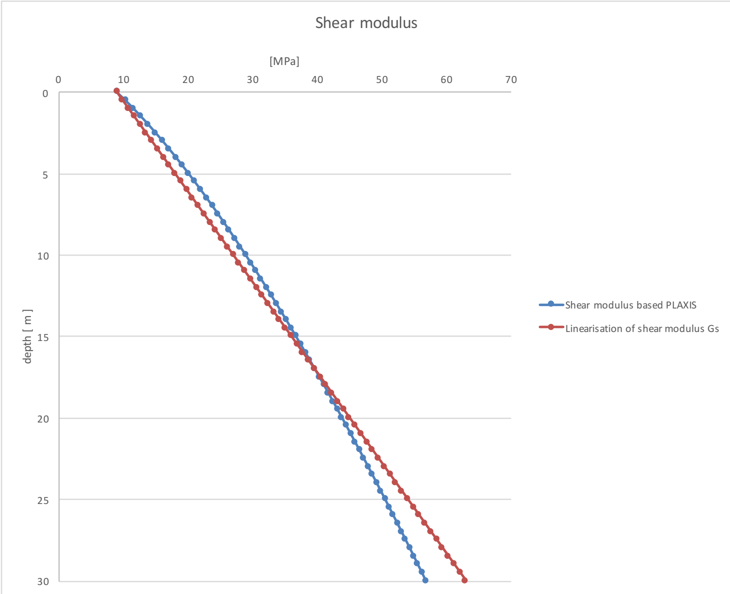

Figure 59 Comparison between shear modulus profile of PLAXIS and the linearized shear modulus

Based on this linearization the maximum kinematic bending moment was calculated, for which the values can be found in Table 13. This method however only gives the maximum bending moment at pile fixity and does not give the full bending moment development along the depth of the pile. Other assumptions are the approximation of the shear modulus and no friction of the pile cap with the soil, resulting in zero shear force at pile head. These assumptions are the same as the one applied in the 2D PLAXIS model.

R. Di Laora and E. Rovithis	Symbols	Values	
Linearized shear modulus	$G_s(z)$	9000 + 1800*z	kPa
proportionality coefficient	δ	2	
shear modulus at 1D under GL	G_{sd}	9900	kPa
young's modulus	E_{sd}	29700	kPa
spring coefficient	k_d	59400	kPa
Winkler wave number	λ_d	0,63377844	m^{-1}
active pile length	$L_a = 10 * D$	5	m
diameter	D	0,5	m
dimensionless inhomogeneity factor	n	1	
	a	0,5	
characteristic pile wavenumber	μ	0,62	
effective depth	$z_{eff} = \frac{L_a}{2} = \frac{1.25}{\mu}$	2,015	m
soil shear modulus	$G_s(z_{eff})$	12,63	MPa
Peak ground acceleration	a_s	0,146	g
Maximum kinematic bending moment	$M_{kin} = E_p * I_P * \frac{a_s}{G_s(z_{eff})}$	10,44	kNm

Table 13 Calculation of maximum kinematic bending moment

4.3.2 Pseudo static kinematic bending moment

The second validation method of the dynamic embedded beam results is the pseudo static approach. In this method the determined maximum displacement during the earthquake signal is used, based on the performed free field site response analysis. The PLAXIS 2D free field site response analysis was used to obtain the time history of the maximum relative displacement of pile head and pile toe, see Figure 60. At 4.3 seconds this maximum is found. The soil displacement profile along the pile corresponding with this maximum relative displacement is shown in Figure 61.

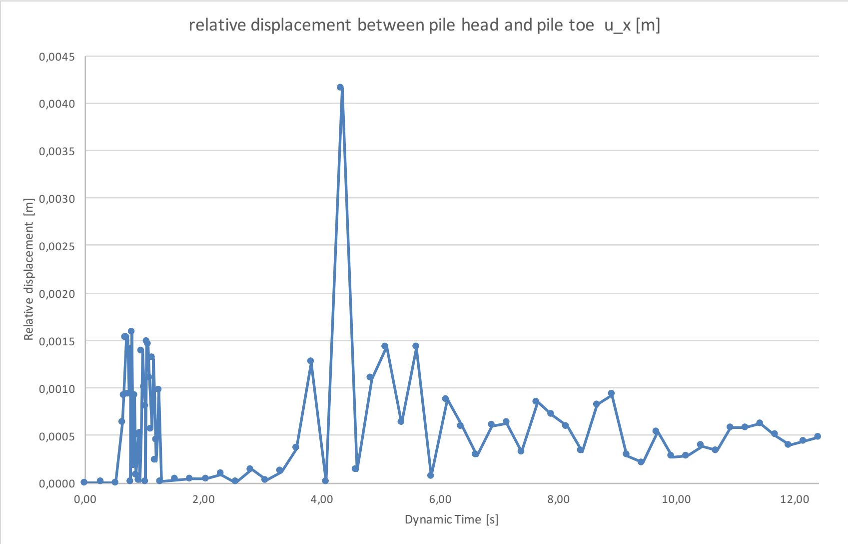

Figure 60 2D PLAXIS relative soil displacement between pile head and pile toe

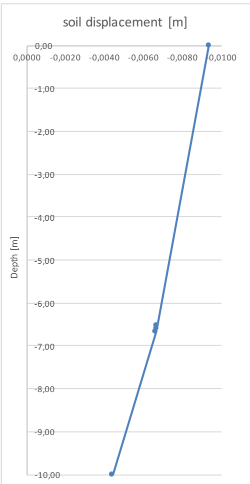

Figure 61 Soil displacement profile at maximum relative displacement (4.3 seconds)

This soil displacement profile was than applied on the pile in both D-Sheet Piling and PLAXIS 2D. D-Sheet Piling is used in this case because it is widely applied software that fulfils the requirement of static lateral soil displacement on piles assessment. For D-Sheet Piling the “single pile”-option was used and the soil subgrade reaction modulus was determined based on Ménard, see the calculation sheet in Appendix I. Both models are shown in Figure 62. In D-Sheet Piling the pile head was only rotationally fixed, whereas in the 2D PLAXIS model an interface between the plate and the soil was specified with very low R_{inter} to incorporate the same fixities at pile head between the pseudo static and the analytical method. The applied prescribed displacement is starting, in the 2D PLAXIS model, just under the plate and ends at pile toe level. In this way the soil is displaced and ensures that the prescribed displacement is not connected directly to the pile.

This will incorporate the interaction between the (displaced) soil and pile.

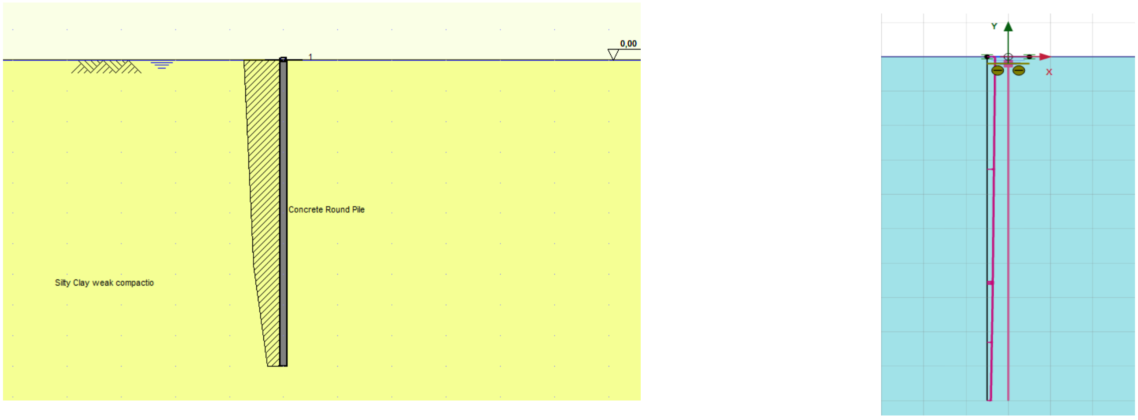

Figure 62 Pseudo static models: D-Sheet Piling (left) and PLAXIS 2D embedded beam (right) with soil displacement

In Figure 62 the pseudo static models are visualised. On the left the model used in D-Sheet Piling and on the right the model used in PLAXIS 2D. The pile fixity is only rotational, see pile fixity in Figure 57 on the left. The resulting bending moments of these two methods are shown in the next subparagraph.

4.3.3 Comparison between analytical, Pseudo static and PLAXIS dynamic calculations

The results from the dynamic 2D embedded beam analysis were obtained by implementing the embedded beam in the soil profile and earthquake signal specified in paragraph 4.1. The signal of 12.4 seconds applied at the base, induced a soil displacement acting as a load on the embedded beam. The maximum bending moment at pile head is obtained at the same time as for the maximum relative displacement mentioned in 4.3.1, 4.3 seconds. The results of the analytical, Pseudo static and fully dynamic analysis were analysed and compared for the (kinematic) bending moment along the pile, shear force distribution and pile displacement, see Figure 63.

It can be seen that the 2D Embedded beam row in the pseudo static situation acts to stiff in the upper part of the pile, showing more shear force compared with D-Sheet Piling, and less stiff for the deeper part of the pile, showing less shear force. Hereby assuming that D-Sheet Piling provides the most realistic behaviour in this case. The maximum kinematic bending moment is higher for the PLAXIS 2D embedded beam row, with or without slider, compared to the D-Sheet piling. This can be explained by the shear force distribution as aforementioned. The loading is still in the elastic part of the soil-pile behaviour and nowhere along the pile is the limiting lateral soil resistance reached, see Figure 66. The soil-pile stiffness is thus dependent on the interface stiffness factor specified by the pile spacing. As was the case with the static pile loading, this supports the conclusion that the ISF should be made depth dependent. The effect of lower or higher ISF, constant with depth, is shown in paragraph 4.3.5.

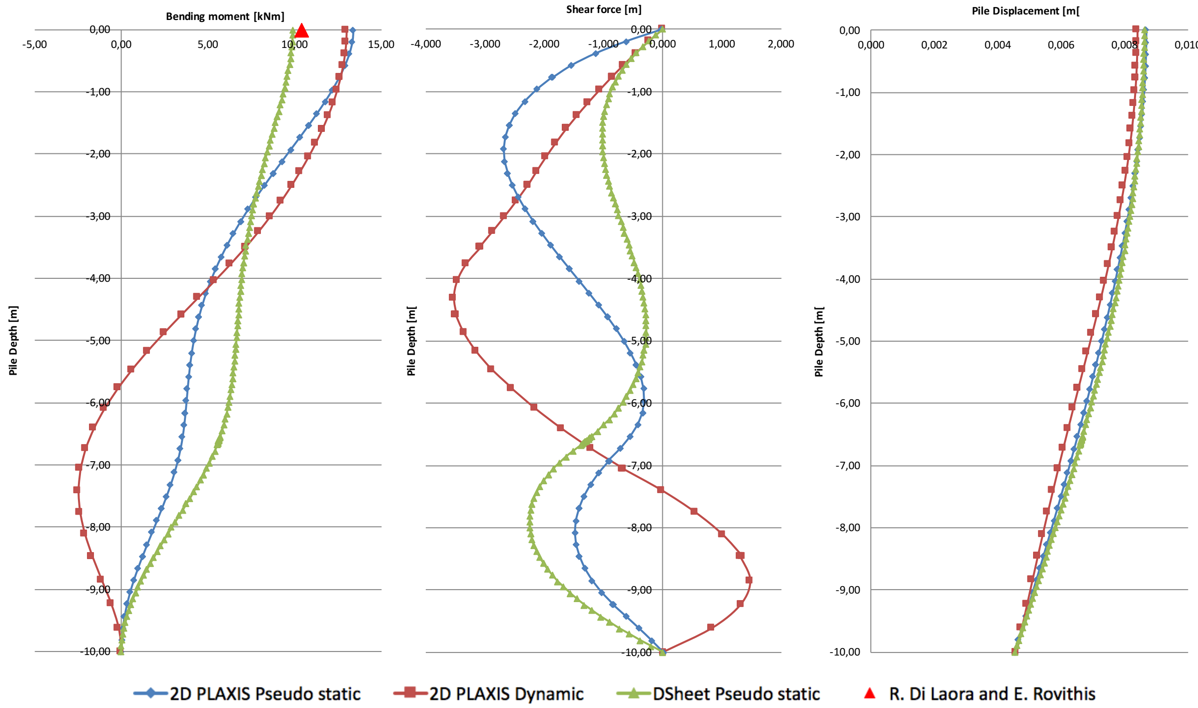

Figure 63 Comparison of (kinematic) bending moment(left), shear force(middle) and pile displacement(right) between the three methods

The obtained bending moment, shear force and pile displacement distribution in the dynamic calculation are somewhat different. The maximum value of the bending moment at pile head do match, but still show too high values compared with the analytical and D-Sheet Piling calculations. The difference between the dynamic and pseudo static 2D PLAXIS results can be explained by the fact that the soil movement in the dynamic calculation is constantly changing, influencing the calculated bending moment of each time step.

The shear forces along the pile are also larger for the 2D embedded beam calculation compared to D-Sheet Piling, which results in larger bending moments in the upper part of the pile. It can be observer that for the upper part of the embedded beam the shear force is overestimating the shear force of D-Sheet Piling, but from 5.5 m downwards the shear force is underestimated.

The results above were calculated with a pile spacing of 4 m of the embedded beam row. The effect of pile spacing was also evaluated for pile spacing of 2 m and 8 m. The time history of the maximum bending moment at pile head for these different pile spacings are shown Figure 64. For larger pile spacing the maximum bending moment increases, as was also the case for the static lateral load in chapter 3.

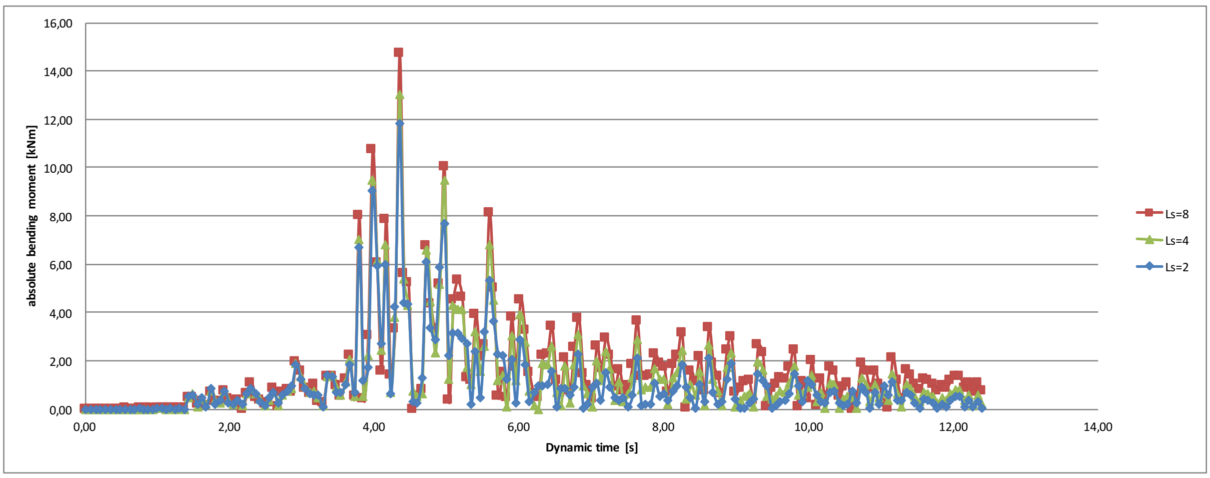

Figure 64 Time history of maximum kinematic bending moment at pile head for pile spacing 2, 4 and 8m

Apart from the calculations performed with the plate only fixed in vertical direction, the plate was also fixed in both directions, see right side of Figure 57. The resulting maximum bending moments are far higher for this option, since the pile needs to follow the entire free field site displacements. This modelling can be seen as a simplification of a very high weight and rigid superstructure, which does not move during the earthquake.
The same can be observed as with the rotational fixity only, the 2D embedded beam row shows more shear force and bending moment at pile head in comparison with D-Sheet piling. This is probably because of too soft behaviour of the embedded beam interface.

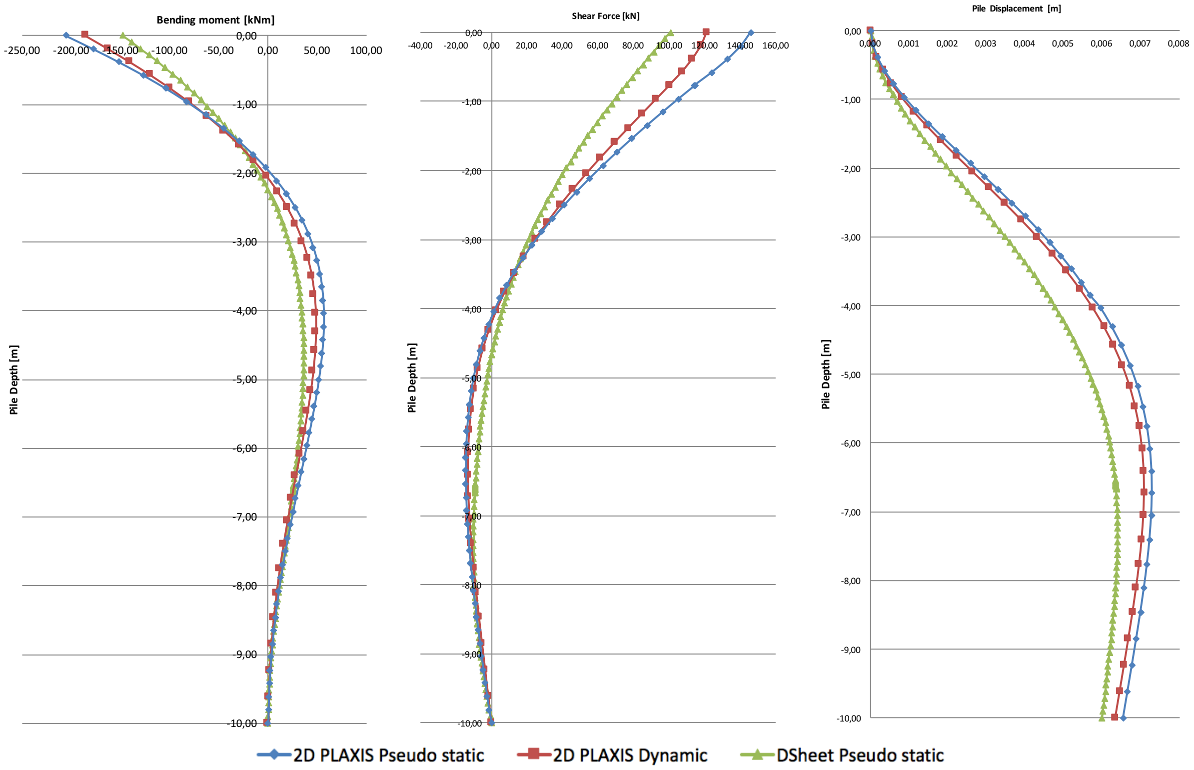

Figure 65 Comparison of (kinematic) bending moment(left), shear force(middle) and pile displacement(right) between the three methods for fixed plate and pile head

For both the fixity in only y-direction and in x-, y-direction the development of maximum skin resistance is shown in Figure 66. The lateral slider is not activated along the length of the pile, not even for this worst case scenario when the plate is fully fixed. In the static loading situation, see paragraph 3.2, it was shown that the behaviour of the pile for small loads is depending on the interface stiffness factor. So for the specified earthquake of 0.146 g, the same conclusion can be drawn as in the static situation. The effect of different values for the interface stiffness factor is elaborated in the next subparagraph.

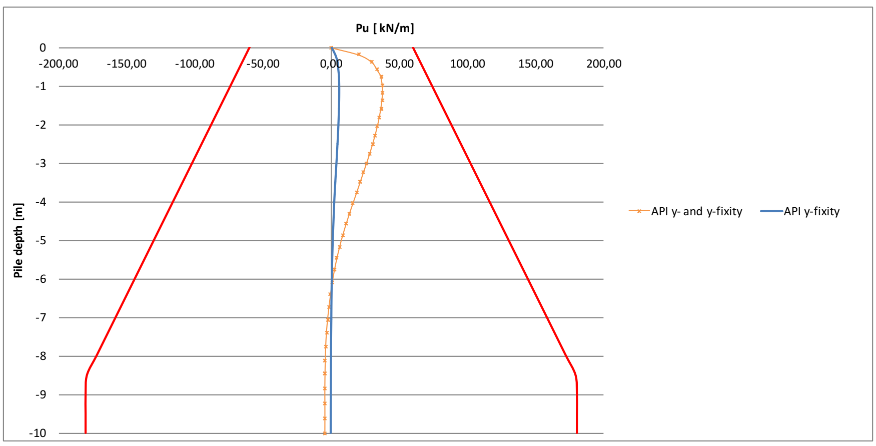

Figure 66 Development of lateral skin resistance along the length of the pile

4.3.4 Influence of changed ISF factor on pseudo static 2D embedded beam

The soil displacement causing the bending moments in the pile in the pseudo static calculations do not activate the limiting lateral soil resistance of the embedded beam. Therefore, the stiffness of the interface (soil-pile) is depending on the interface stiffness factor. The influence of several values for this ISF factor is researched and the results are shown in Figure 67. For a lower stiffness factor, the shear force distribution could be matched better with the D-Sheet Piling calculation. However, although the bending moments and shear force distribution could be matched for the upper part of the pile with an ISF of 0.1, the values for the lower part of the pile decreased as well. With higher ISF factors, the shear force distribution, and thus the bending moments increased. This can be explained by the fact that with an increased soil stiffness, more shear force is transferred to the pile and thus more bending moments occur along the length of the pile.

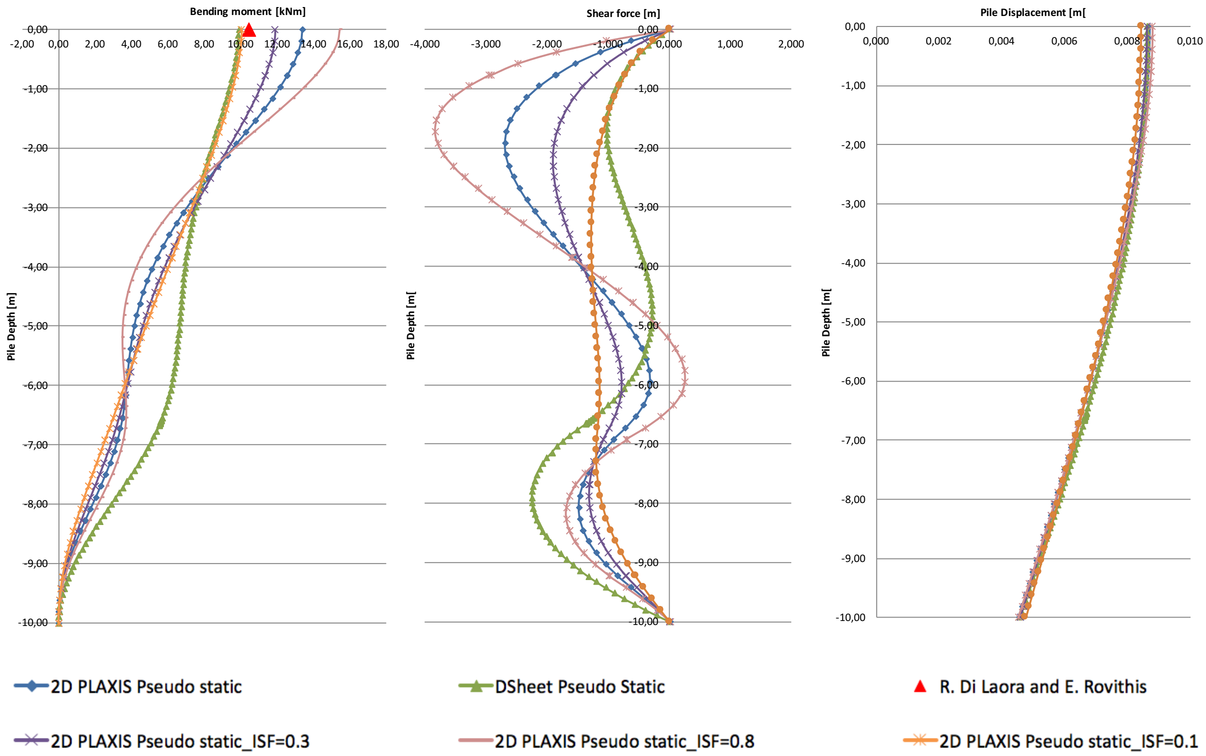

Figure 67 Comparison of (kinematic) bending moment(left), shear force(middle) and pile displacement(right), for several ISF.

4.4 Evaluation of the kinematic and inertia pile bending moments of embedded beam row

Although the emphasis in this study was on the kinematic loading, the applied soil loads in the dynamic situation did not activate the limiting lateral soil resistance of the embedded beam. To check the influence of extra inertia loading on the pile, several calculations were performed.

The inertia load during an earthquake was simulated by applying a certain weight to the plate which was fixed to the embedded beam row. The time history of the maximum bending moment at pile head is compared for different pile spacings. The results of the maximum bending moment due to inertia and kinematic loading for several pile spacing are shown in Figure 68. The same as for the kinematic load only can be seen, for larger pile spacing the bending moment increases, while the maximum pile displacement at the top is the same for each pile spacing, see Figure 69. The bending moments due to inertia and kinematic loading are approximately a factor of 5 times larger in relation to the maximum kinematic bending moment and pile displacement. The upper bound value of the bending moment, due to rotational and translational fixity of the plate, is still higher than the bending moments obtained with the modelling of inertia loading. So also in this case, the limiting lateral soil resistance was not reached anywhere along the pile.

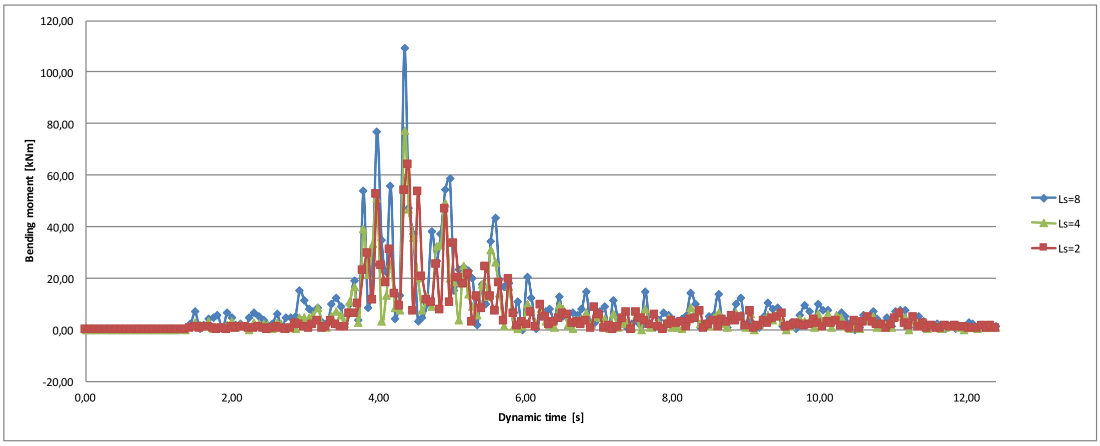

Figure 68 Time history of maximum kinematic and inertia bending moment at pile head for pile spacing 2, 4 and 8m

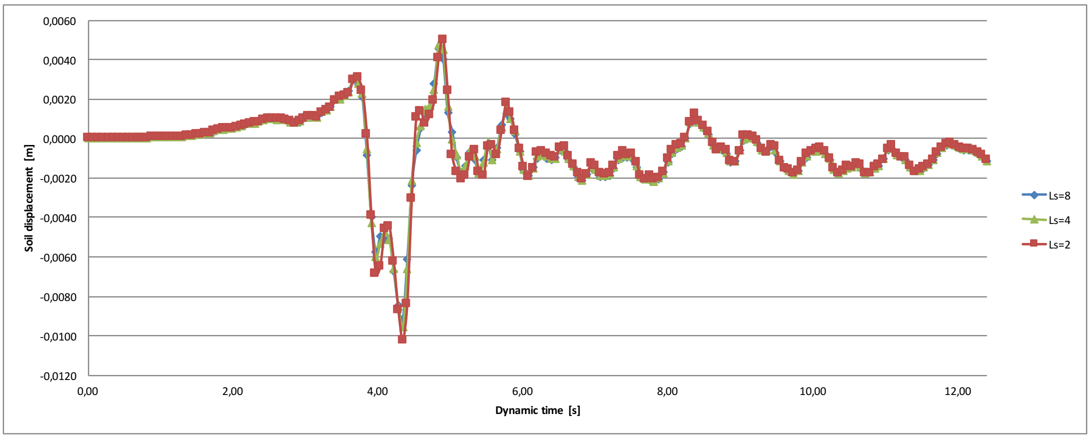

Figure 69 Time history of maximum pile head displacement for pile spacing 2,4 and 8m

4.5 Comparison between cyclic pile load behaviour in 2D and 3D

Since a 3D fully integrated volume pile with the scaled Huizinge signal could not be calculated, the damping (hysteresis) in the pile-soil system was investigated by performing calculations with a cyclic load at pile head. The volume pile in 3D and the embedded beam with two different lateral sliders were loaded with a cyclic 100 kN pile head load. The results are shown in Figure 70. Although the best way of calculating the lateral skin resistance in this study is the API method, a different lateral skin resistance with lower strength was also applied to check its influence on the dynamic behaviour.

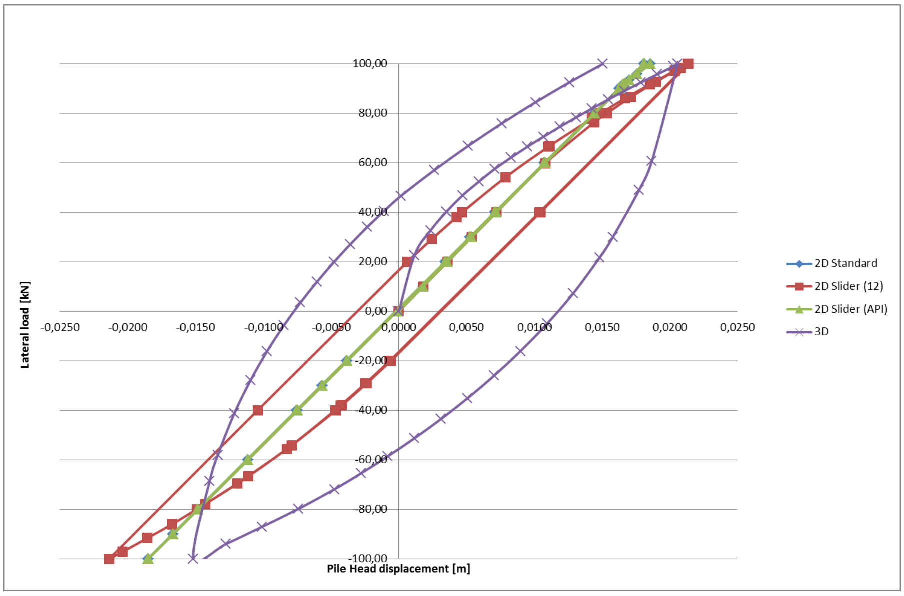

Figure 70 Cyclic pushover characteristics from PLAXIS 2D embedded beam and 3D volume pile

From this analysis it can be seen that for the standard embedded beam and the embedded beam with API slider, there is no hysteretic damping of the pile soil system. For the embedded beam with API slider it is known from Figure 30 (left) that at a point load of 100 kN, the limiting soil resistance profile is not reached yet. So the embedded beam is still showing linear elastic behaviour in which no extra damping by the cyclic load is observed.

The red line in Figure 70 shows the hysteretic behaviour of the embedded beam with a weaker limiting lateral soil resistance. The result shows there is now some damping visible, however not as much as observed in the 3D situation. It is therefore unlikely that the 2D embedded beam, with or without lateral slider, shows the same behaviour as the 3D Volume pile, without changing the way the interface stiffness factor is determined.

4.6 Conclusion and Recommendations

Several studies were performed on the 2D embedded beam row behaviour in dynamic loading situations, either by kinematic load only or by extra inertia loading incorporated. The main conclusion of this part of the research shows there is room for improvement in the way the embedded beam incorporates the stiffness between the pile and the soil. Based on two alternative calculation methods, analytical and pseudo static, the kinematic bending moment for a PGA of 0.146 was overestimated by the 2D Embedded beam row.

Apart from the maximum bending moment calculated with embedded beam, the bending moment along the pile in the pseudo static situation also shows some deviations. This was explained by the fact that the interface stiffness factor should be less near ground level and increasing with depth. This was shown by reducing the ISF, where eventually the upper part of the shear force distribution could be matched with D-Sheet piling calculations.

The influence of several pile spacing with kinematic and inertia load, showed peculiar results in accordance with the static calculations in chapter 3. With increased pile spacing the default interface stiffness factor will become less, however also the weight (or load) is distributed over this pile spacing. So for high pile spacing, the applied load is decreasing but the resulting bending moments in the embedded beam are also increasing. This effect could be explained, as was done in chapter 3, by the fact that although the load is decreasing the determination of the stiffness of the soil is not proportional or equal to ratio of decrease in applied load. This could mean that there could be a wrong assumption in the way the ISF is determined.

Apart from the kinematic bending moment calculations, the cyclic behaviour of the 2D embedded beam was not comparable with the 3D volume pile situation. When the limiting lateral soil resistance is not reached anywhere along the pile, the embedded beam does not show hysteretic damping but behaves linear. So the dynamic load does not have an effect on the displacement of the pile.

Based on the above conclusions it is doubted that the current version of the 2D embedded beam has capabilities as far as dynamic loading is concerned. It is recommended to improve the default ISF and check the results from PLAXIS 2D embedded beam and 3D volume pile with real measurement data or a “geocentrifuge” experiment.

5. Conclusions and Recommendations

This chapter will elaborate the conclusions and recommendations of this study and the objectives / research goals will be evaluated, followed by some general conclusion encountered during this research.

Research goal and objectives

- *Evaluate the behaviour of the embedded beam with a lateral (static) pile head load and evaluate the influence and determination of the later slider*

For large pile spacing the embedded beam is still not able to model the correct 3D pile displacement / forces. However, a first approximation of the expected displacement can be given for small loads, where the outcome of the displacements and forces are conservative (overestimated). For large expected lateral pile loads and for a pile spacing divided by its diameter greater than 4, it is wise to check the results with alternative calculation methods like D-Pile Group.

The determination of the limiting lateral soil resistance is depending a lot on the engineering judgement and checks with other calculation methods. For different soil types and saturation conditions, this resistance needs to be altered. For this thesis the best way for determining the limiting lateral soil resistance was the API methods, this was compared with D-Pile Group, which also uses this code. Other methods for determining this soil resistance showed too soft soil behaviour and were not comparable with the 3D results.

In this thesis it was shown that the stiffness behaviour of the embedded beam 2D, for small loads, is less than in the 3D volume pile and D-Pile Group calculations. The implementation of the limiting lateral soil resistance did not influence the stiffness behaviour much, but the ultimate strength could be well approximated and was similar to the strength found in D-Pile Group. However, when researching this ultimate strength, the bending moment become so large that it is unlikely that the modelled pile can resist this. After implementation of a plastic capacity moment in the pile, the results were sudden bends in the pile displacement behaviour and the forming of plastic 'hinges' in the pile. Therefore, incorporating this plastic moment only shows whether or not you have reached the maximum capacity, but PLAXIS will stop calculating. In earthquake engineering however this incorporation of maximum bending moment capacity could be useful. Performance based design is a method which specifies the maximum displacement of a structure. To obtain a good approximation of the displacement, both the best soil behaviour and pile behaviour should be incorporated. Assuming linear elastic behaviour for the pile underestimates this pile displacements, when no plasticity is taken into account. Although in the current version of the 2D embedded beam the pile can only be modelled as linear elastic perfectly plastic, therefore it will only tell you when the pile is about to fail and if that will occur during an earthquake loading.

It was shown, by reducing the lateral ISF factor, that the pile displacement could be better be approximated at the top, however unrealistic pile toe behaviour occurred at the same time. For a better working of the embedded beam, with or without limiting lateral soil resistance, it is therefore advised to change the default lateral ISF factor. This could be done by making the lateral ISF independent of the axial ISF factor and incorporate either stress or strain dependency.

- *Evaluate the soil behaviour during an earthquake (free field site response)*

In order to compare and perform the site response analysis, several investigations have been performed on the use of EERA and PLAXIS in combination with its settings and boundary conditions. For this part the deconvolution and scaling of the Huizinge signal was used as input at 30m depth. For the determination of the base boundary condition, a linear elastic model of the Huizinge soil profile was adopted in EERA and PLAXIS. Since the signal measured in Huizinge was assumed to be at ground level, this could be seen as an outcrop motion (both the upward and downward wave). Performing a deconvolution on the signal will obtain an inside motion at 30m depth. However, only the upward wave needs to be modelled in both EERA and PLAXIS, since at 30m depth no bedrock is present and there will also be a downward travelling wave.

In this thesis it was shown that the compliant base boundary in PLAXIS, with a factor of 0.5 on the signal, and the outcrop motion in EERA selected, could be well compared with each other. For further research on the behaviour of pile foundations or embankments during the Groningen earthquakes, these boundaries are recommended to use. The magnitude of the earthquake was determined based on site response analysis of the Huizinge signal. For the soil profile of Huizinge, the peak acceleration at 30 m depth of 0.146g would lead to an acceleration at ground level of approximately 0.25g. However, when applying the motion at the base of the one layered clay layer in this study the same acceleration was obtained at ground level. So rather an attenuation of the input signal than an increase of PGA is expected based on the low plasticity clayey soil.

The dynamic behaviour of the soil was compared by its modulus reductions curves, which are of vital importance in the linear equivalent EERA model. Good agreement of the modulus reduction curve of the clay deposit with HS small parameters with the curves from Vucetic & Dobry (1991) are obtained. However, at high levels of strain the modulus reduction curve from the HS small model is overestimating the damping. Here the specified curves from PLAXIS were used in the EERA model for better agreement.

The time histories of both the PLAXIS models an EERA showed similar behaviour, as was the case for the Fourier-, acceleration- and displacement-spectra.

- *Evaluate the behaviour of the embedded beam during earthquake loading*

In this thesis the kinematic bending moments due to an earthquake in Groningen was researched. Three methods for calculating the kinematic bending moment were evaluated and compared. The results show an overestimation of the bending moments of the 2D embedded beam and the limiting lateral soil resistance was not reached anywhere along the pile, for both kinematic and inertia loading. This means that the behaviour of the embedded beam is still within the elastic region and, as was shown in the static part. The behaviour is likely to be over predicting the displacement of the pile and bending moment (less stiff behaviour for small loads).

- *Compare and validate the behaviour of the embedded beam using a PLAXIS 3D calculation*

Performing 3D dynamic calculations with a compliant base boundary and volume pile, proved to be a computational challenge. The extended calculation time in combination with some limitations in PLAXIS 3D were the main problems. A full 3D result could therefore not be obtained with the provided resources. Since no large scale earthquake loading could be applied, a simple cyclic test was performed in both 2D and 3D situations. A load of 100 kN was moving the pile head back and forth in order to determine its load displacement behaviour. Based on this one could observe some hysteretic behaviour of the soil-pile system in the 3D situation, however no damping was observed with the embedded beam (standard and with API slider).

- *Analyse the possibilities and limitations of the embedded beam in PLAXIS 2D when used for modelling soil-pile interaction during an earthquake, with application to the Groningen case.*

The main goal of this thesis was to determine the possibilities and limitation of the embedded beam in PLAXIS 2D for dynamic application. Several steps were conducted in order to define the dynamic situation. The static loading behaviour was firstly elaborated and it became clear that for large pile spacing and small loads the pile displacement and forces of the embedded beam was not able to model the 3D behaviour appropriately.

The free field site response analysis showed that the soil profile, chosen in this study, did not increase the acceleration of the input signal as is assumed in most cases concerning earthquake loading in Groningen. The maximum acceleration in this study therefore was 0.146 g, on which all the conclusions and recommendations are based. For this magnitude the 2D embedded beam overestimates the displacement, force distribution and bending moments along the pile, since the behaviour of the pile and interface is still in the elastic part.

Despite the results in this thesis, the embedded beam (row) still has possibilities for approximating lateral loaded pile behaviour. But there are also several important limitations, which one has to keep in mind when using the 2D embedded beam row.

Possibilities:

- For small pile spacing, the embedded beam is in better agreement with the 3D situation, probably because of the higher interface stiffness factor. However, several other methods for modelling piles in 2D show similar results, as was shown in other studies (i.e. plate with reduced stiffness or node-to-node anchor);
- The embedded beam was originally only applicable for axial loaded piles. Improving on the determination of lateral stiffness and limiting lateral soil resistance, could result in a time efficient way of modelling lateral pile behaviour;
- The calculation time is definitely favourable when compared to other methods, in either 2D or 3D. However, a lot of extra parameters has to be specified in order to obtain the right pile displacements.
- If the dynamic pile response of the embedded beam can be improved, the calculated displacements from the embedded beam can then be used in, for example, Performance Based Earthquake Design methods.

Limitations:

- **Main limitation is the default lateral interface stiffness factor**
- The determination of the lateral skin resistance is very time consuming and different for other soil types and loading conditions. Only after checks with other calculation methods, or comparison with a 3D calculation, one can be sure on the right behaviour of the embedded beam with lateral slider;
- For large pile spacing (Ls/D>8) the results tent to be in less agreement with the 3D situation, the application area specified by Sluis is therefore not changed by the implementation of the lateral skin resistance;
- In dynamic calculations a reduction in the limiting lateral soil resistance cannot be incorporated, it is only possible to specify one (linear or multi-linear) limiting lateral soil resistance profile. It is likely that, for example a clay, will show softening after a certain amount of cycles or strain level;
- It is doubted if the current embedded beam is capable of modelling the right dynamic behaviour, based on calculating of kinematic bending moment and the cyclic loading response of the embedded beam in comparison with the 3D volume pile.

General conclusion

Making undrained (A) calculation in PLAXIS means a proper definition of effective strength parameters, which represents the undrained shear strength. In this thesis a small investigation was performed on the working and right determination of these effective strength parameters for a silty clay layer. Using the PLAXIS triaxial test facilities on the chosen clay profile, the undrained shear strength was determined. It is suggested to perform this kind of test to check whether or not the right undrained soil behaviour is calculated within PLAXIS.

Performing earthquake analysis in PLAXIS 2D and 3D proved to be a greater challenge than anticipated on. The behaviour of the chosen Hardening Soil small strain model was most appropriate at the time of the start of this thesis, but later the new “Generalized Hardening soil model” became available to model even better dynamic soil behaviour. It is quite hard to pinpoint exactly where certain behaviour originates from in the output of either EERA or PLAXIS, due to the high uncertainties in the assumptions in both methods.

The main question was whether or not the 2D embedded beam could be used in models where the soil is moved with a Groningen earthquake signal. Based on several static, pseudo static and dynamic calculations, the 2D embedded beam overestimates the displacement, force distribution and bending moments along the pile. The embedded beam (row) in 2D does show capabilities for modelling (dynamic) lateral loaded pile behaviour, when the interface stiffness factor and the limiting lateral soil resistance (for dynamic loading situations) are optimized. In this way the plastic behaviour of the pile-soil system should be improved and show similar behaviour as expected in the 3D situation.

This study performed an evaluation and validation of the newly implemented functions of the 2D embedded beam in both static and dynamic loading situations. The research questions could be answered sufficiently, but a lot of new question also appeared during this thesis. In the next chapter some topics for further and future research are summarized.

6. Future research

The future research is separated into three different focusses: Lateral skin resistance of the embedded beam, free field site response and dynamic loading of the embedded beam in PLAXIS 2D.

Recommendations for future research regarding the lateral skin resistance of the PLAXIS 2D embedded beam:

- There are several methods specified in literature to determine the limiting lateral soil resistance. The influence of different limiting lateral soil resistance applied as lateral slider for the embedded beam should be verified with actual soil data and 3D calculations.;
- It is suggested to improve the way the stiffness behaviour is now incorporated between the pile and the soil. Main factor determining this stiffness behaviour is the interface stiffness factor. To overcome the too soft behaviour for small loads and large pile spacing, the ISF should be made stress or depth dependent. The influence of the altered ISF factor in combination with the lateral slider should be a topic for further research;
- In this thesis only a continuous clay layer was applied. It should be investigated what this influence of other types of soil and layered soil profiles have on the behaviour of the embedded beam;

Recommendations for future research regarding the free field site response:

- The applied and scaled Groningen signal can be seen as a moderate to weak earthquake signal with a maximum of 0.146 g. Further research should focus on the influence of stronger motions on the effects in either EERA and PLAXIS;
- In this research the Hardening Soil small strain model was applied. It should be checked if the generalized hardening soil model improves the dynamic soil behaviour. Also the influence on this 2D embedded beam should be evaluated;

Recommendations for future research regarding the dynamic loading of the embedded beams in PLAXIS 2D:

- The influence of different limiting lateral soil resistances, with incorporation of cyclic hardening or softening, for the embedded beam should be evaluated and verified with actual soil data and 3D calculations;
- The influence of the altered ISF factor in combination with the lateral slider and its effect on the cyclic loading behaviour should be a topic for further research.

7. Literature

API RP 2A-WSD. (2010). *Planning, designing and constructing fixed offshore platforms - working stress design.* Washington: API Publishing Services.

Bardet, J.P., Ichii, K., & Lin, C.H. (2000). *EERA: A computer Program for Equivalent-linear Eartquake site Response Analyses of layered Soils Deposits.* Univeristy of southern California.

Benz, T. (2007). *Small-Strain Stiffness of Soils and its Numerical Consequences.* PhD thesis, Institut für Geotechniek der Universität Stuttgart, Stuttgart.

Besseling, F. (2012). *Soil-structure interaction modelling in performance based seismic jetty design.* Msc Thesis, Delft University of Technology , Delft.

Bijnagte, J., & Luger, H. (2010). *D-Pile Group manual, 3D modelling of single piles and pile groups.* Deltares, Delft.

Boulanger, R.W., Curras, C.J., Kutter, B.L., Wilson, D.W., & Abghari, A. (1999, september). *Seismic soil-pile-structure interaction experiments and analyses.* Journal of geotechnical and geoenvironmental engineering, p.750-759.

Brinch Hansen, J. (1961). *The ultimate resistance of rigid piles against transversal forces.* Danish Geotechnical Institute, Copenhagen, Danmark.

Brinkgreve, R.B.J. (2014). *CIE 4361: Behaviour of Soils and Rocks.* Lecture slides and course document. Delft University of Technology, Delft.

Brinkgreve, R.B.J., Engin, E., & Swolfs, W.M. (2015). *Manual Plaxis 2D / 3D.* Plaxis BV, Delft

Brinkgreve, R.B.J., Kappert, M.H., & Bonnier, P.G. (2007). *Hysteretic damping in a small-strain stiffness model.* Numerical Models in Geomechanics – NUMOG X – Pande & Pietruszczak (eds), p. 737 - 742. London.

Broms, B.B. (1964a). *Lateral resistance of piles in cohesionless soils.* Journal of Soil Mechanics and Foundations Div., Vol. 90, p. 123-156, ASCE.

Broms, B.B. (1964b). *Lateral resistance of piles in cohesive soils.* Journal of Soil Mechanics and Foundations Div.,Vol. 90, p. 27-63, ASCE.

CUR 228. (2010). *Ontwerprichtlijn door grond horizontaal belaste palen.* Stichting CURNET, Gouda.

Dao, T.P.T. (2011). *Validation of PLAXIS Embedded Piles For Lateral Loading.* Delft University of Technology, Delft.

Das, B.M., & Ramana, G.V. (2011). *Principles of Soil Dynamics, Second Edition, International SI Edition.* Stamford, USA: Cengage Learning.

Davisson, M.T. (1970). *Lateral load capacity of piles.* Highway Research Record, *No. 333*, p. 104-112.

de Greef, J. (2015). *Interaction between pipelines and flood defences subject to induced eathquake loads in Groningen.* Delft University of Technology, Delft.

de Jong, F.K., Hartmann, D., & Kaspers, E.J. (2015). *Rapport RA14234c2: Geotechnical Base Report.* CRUX Engineering BV, Amsterdam.

Di Laora, R., & Rovithis, E. (2014). *Kinematic bending moment of fixed-head piles in non-homogeneous soil*, Proceedings of 2nd European Conference on Earthquake Engineering and Seismolog. paper No. 2739, Istanbul.

Dost, B., & Kraaijpoel, D. (2013). *The August 16, 2012 earthquake near Huizinge (Groningen).* KNMI, De Bilt.

Dost, B., Caccavale, M., Eck, T., & Kraaijpoel, D. (2013). *Report on the expected PGV and PGA values for induced earthquakes in Groningen Area.* KNMI.

Engin, H.K., Septanika, E.G., & Brinkgreve, R.B.J. (2007). *Improved embedded beam elements for modelling of piles.* Proc. 10th Int. Symp. on Numerical Models in Geotechnical Engineering - NUMOG X. Rhodes (Greece).

Fan, K.G., Gazetas, G., Kaynia, A., Kausel, E., & Ahmad, S. (1991). *Kinematic seismic response of single piles and pile groups.* J. Geotechnical Engineering 117, p. 1860-1879.

Fleming, W.G.K., Randolph, A.J., & Elson, W.K. (2008). *Piling Engineering*. Taylor & Francis e-Library .

Forsythe, G.E., & Wasow, W.R. (2004). *Finite difference methods for partial differential equations*.

Hardin, B.O., & Drnevich, VP. (1972). *Shear modulus and damping soils*. Proc. ASCE: Journal of the Soil Mechanics and Foundations Division, p. 1531-1537.

Hermans, J. J. (2014). *Validation of the Embedded Pile Row in PLAXIS 2D for passive lateral loading.* Delft University of technology, Delft.

Hudson, M., Idriss, I.M., & Beikae, M. (1994). *QUAD4M - A computer program to evaluate the seismic response of soil structures using finite element procedures and incorporating a compiant base. Center for Geotechnical Modeling.* Dept. of Civil & Environmental Engineering, Davis, California.

Idriss, I.M. and Sun J.I. (1992). *SHAKE91: a computer program for conducting equivalent linear seismic response analyses of horizontally layered soil deposits, User's Guide.* University of California, Davis.

KNMI. (2005). *Aardbevingen.* KNMI, De Bilt.

Kottke, A.R., & Rathje, E.M. (2009). *Technical Manual for Strata.* University of California, College of Engineering. Pacific Earthquake Engineering Research Center, Berkeley.

Kramer, S.L. (1996). *Geotechnical Earthquake Engineering.* Prentice-Hall Inc, New Jersey, USA.

Kruse, H.M.G., & Hölscher, P. (2010). *Schade aan buisleiding door aardbeving.* Deltares, Delft.

Kuhlemeyer, R.L., & Lysmer, J. (1973). *Finite Element Method Accuracy for Wave Propagation Problems*. Journal of the Soil Mechanics and Foundations Division, p. 421-427.

Liyanapathirana, D.S., & Poulos, H.G. (2005, December). *Seismic Lateral Response of Piles in Liquefying Soil.* Journal of Geotechnical and Geoenvironmental Engineering, p. 1466-1479.

Makris, N., & Gazetas, G. (1992). *Dynamic Pile Soil Interaction part 2: lateral and Seismic Response.* Earthquake Engineering & Structural Dynamics, p. 145-162.

Margason, E., & Holloway, D.M. (1977). *Pile Bending during Earthquake.* Proc. Sixth World Conference on Earthquake Engineering, p. 1690 - 1696. Sarita Prakashan, Meerut, India.

Matlock, H. (1970). *Correlations for design of laterally loaded piles in soft clay*. Preprints Second Annual Offshore technology Conference, p. 577-58, Housten.

Meijers, P., Steenbergen, R.D.J.M., & Kruse, H.M.G. (2014). *Handreiking voor het uitvoeren van studies naar het effect van aardbevingen, voor bedrijven in de industriegebieden Delfzijl en Eemshaven.* Deltares, Delft.

Mylonakis, G., & Nikolaou, S. (2002). *Design methods for earthquake-induced pile bending.* DFI 2002 Conference, p. 1-9, New York.

Mylonakis, G., Nikolaou, A., & Gazetas, G. (2000). *Seismic Soil-structure interaction: Beneficial or detrimental?* Journal of Earthquake Engineering, p. 277-301.

NEN 9997-1. (2011). *Geotechnisch ontwerp van constructies - Deel 1: Algemene regels.* Nederlands Normalisatie Instituut, Delft.

NERHP. (1997). *Recommended Provisions for Seismic Regulations for New Buildings and other Structures.* Washington: FEMA, Building Seismic Safety Council.

Nikolaou, A., Mylonakis, A., & Gazetas, G. (1995). *Kinematic Bending Moments in Seismically Stressed Piles.* National Center for Earthquake Engineering Research. State Univesity of New York, New York.

Nikolaou, S., Mylonakis, G., Gazetaz, G., & Tazoh, T. (2001). *Kinematic pile bending during earthquakes: analysis and field measurements*. Géotechnique 51, p.425-440.

Plaxis. (2015). *2D: Reference Manual.*

Poulos, H.G., & Davis, E. G.(1980). *Pile foundation analysis and design poulos davis.* Wiley, New York.

Randolph, M., & Gouvernec, S. (2011). *Offshore Geotechnical Engineering*, p. 211 - 235. CRC Press, Hoboken.

Roijakkers, R.H.G. (2015). *Seismische Inspectie en Rehanilitatie Constructieve en Bouwkundige scan.* ABT/Wassenaar ingenieurs.

Septanika, E., Bonnier, P.G., Brinkgreve, R.B.J., & Bakker, K.J. (2007). *An efficient 3D modelling of (multi) Pile-soil interaction.* International Geomechanics Conference, p. 8, Nessebar.

Skempton, A.W. (1951). *The bearing capacity of clays. Building Research Congress, London Institution of Civil Engineers Vol 1.,* p. 180-189.

Sluis, J. (2012). *Validation of Embedded Pile Row in PLAXIS 2D.* Delft University of Technology, Delft.

Terzagi, K.V. (1955). *Evaluation of coefficient of subgrade reaction .* Geotechnique Vol. 5, p. 297-326.

Tschuchnigg, F. (2009). *Embedded Piles - 1. REPORT.* Arbeitsgruppe Numerische Geotechnik Institut für Bodenmechanik und Grundbau Technische Universität Graz. Graz University of Technology, Graz.

Tschuchnigg, F. (2009). *Embedded Piles - 2. REPORT.* Arbeitsgruppe Numerische Geotechnik Institut für Bodenmechanik und Grundbau Technische Universität Graz. Graz University of Technology, Graz.

Verruijt, A. (2008). *Soil Dynamics.* Delft University of Technology, Delft.

Visschedijk, M.A.T., & Trompille. (2010). *D-Sheet Piling, Design of Diaphragm and Sheet Pile Walls.* Delft: Deltares.

Visschedijk, M.A.T., Meijers, P., Meij, R., Chbab, E.H., Kruse, H.M.G., Zuada Coelho, B.E., Nugroho, D.S., Wesselius, D.S., de Lange, W.J., van den Ham, G.A. (2014). *Groningse kades en dijken bij geïnduceerde aardbevingen.* Deltares, Delft.

Vucetic, M. (1992). *Soil properties and seismic response*. Earthquake Engineering, Tenth World Conference 1992, p. 1199-1204, Rotterdam.

Vucetic, M., & Dobry, R. (1991). *Effect of Soil Plasticity on Cyclic Response.* Journal of Geotechnical Engineering - ASCE, p. 89-107.

Zienkiewicz, O.C., & Tayler, R.L. (2000). *The Finite Element Method.* Butterworth Heinemann, Barcelona, Spain.

Appendix A

Determination of effective strength parameters for the use in PLAXIS undrained (A) calculation

For three different values of Cu (at a reference stress of 100 kPa), empirical formulas are derived from clay samples from levees around Marken in the Netherlands (parameter study comes from Den Haan, (2011)[1], which were examined in laboratory tests to determine undrained shear strength for dike stability research.

Based on the classification of the soil (qc~0.7-1) and the correlations of table 2b NEN9997, the Cu was set to 40 kPa at a reference stress of 100 kPa for a weak compacted silty clay. The empirical formulas for the depth dependent Cu values are shown below (red boxed):

Cu based on empirical data

Table 6 Undrained shear strength relation (Annex 3)

Classification from EC7	normalized shear strength from EC7	Undrained shear strength relation
[-]	[kPa]	[-]
Peaty clays (moderate compression)	25	$c_{u\_ref} = s_u = 2{,}8 + 0{,}22\sigma'_{v0}$
Clays, poor sandy (weak compression)	40	$c_{u\_ref} = s_u = 2{,}8 + 0{,}37\sigma'_{v0}$
Clays, poor sandy (weak to moderate compression)	55	$c_{u\_ref} = s_u = 2{,}8 + 0{,}52\sigma'_{v0}$
Clays, poor sandy (moderate compression)	80	$c_{u\_ref} = s_u = 2{,}8 + 0{,}77\sigma'_{v0}$

Table 7 Undrained shear strength expressed in c'corr for Undrained A (Annex 3)

Classification from EC7	normalized shear strength from EC7	corrected c' value
[-]	[kPa]	[kPa]
Peaty clays (moderate compression)	25	$c'_{corr} = \frac{2{,}8 + (0{,}22 + 0{,}5sin^2\varphi' - sin\varphi')\sigma'_1}{cos\varphi'}$
Clays, poor sandy (weak compression)	40	$c'_{corr} = \frac{2{,}8 + (0{,}37 + 0{,}5sin^2\varphi' - sin\varphi')\sigma'_1}{cos\varphi'}$
Clays, poor sandy (weak tomoderate compression)	55	$c'_{corr} = \frac{2{,}8 + (0{,}52 + 0{,}5sin^2\varphi' - sin\varphi')\sigma'_1}{cos\varphi'}$
Clays, poor sandy (moderate compression)	80	$c'_{corr} = \frac{2{,}8 + (0{,}77 + 0{,}5sin^2\varphi' - sin\varphi')\sigma'_1}{cos\varphi'}$

Appendix A figure 1 used empirical relations between undrained shear strength and stress level / friction angle

In order to start with the back calculation of the effective strength parameters, the standard Mohr Coulomb formula was used as a first estimate, see figure below:

Cu Based on formula

$$Cu = \sigma'_p . \sin\varphi + c . \cos\varphi \qquad (3.2)$$

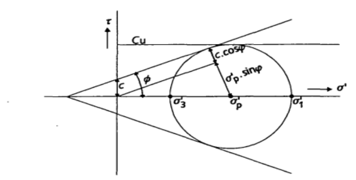

Fig. 3.1 **Ongedraineerde schuifsterkte Cu**

Appendix A figure 2

After some iterations a best estimate of the effective cohesion and friction angle was obtained, see Appendix A table 1 on the next page.

[1] Ongedraineerde sterkte van slappe Nederlandse Grond, deel II, artikel in vakblad Geotechniek, janarie 2011, Deltares, Den Haan

PLAXIS Parameters																				
Groundlayer	Depth m	γ kN/m³	γsat kN/m³	vertical σ'1 kPa	horizontal σ'3 kPa	vert. precon. stress kPa	σ'p kPa	K0	c'corr kPa	c' kPa	φ' Graden	Cu based on empirical data kPa	Cu based on formula MC kPa	Cu based on PLAXIS output kPa	qc MPa	E'50;ref MPa	E'oed;ref MPa	E'ur;ref MPa	G0;ref MPa	γ0,7 -
	0	18	18	0	0,00	0,00	0,00	0,5774	3,09	5	25	2,80	4,53	0,00	1	4,6	2,3	18,4	46,1	0,000280
	0,5	18	18	4	2,31	9,00	3,15	0,5774	3,25	5	25	4,28	5,86	6,19	1	4,6	2,3	18,4	46,1	0,000280
	1	18	18	8	4,62	18,00	6,31	0,5774	3,41	5	25	5,76	7,20	7,85	1	4,6	2,3	18,4	46,1	0,000280
	1,5	18	18	12	6,93	27,00	9,46	0,5774	3,58	5	25	7,24	8,53	9,04	1	4,6	2,3	18,4	46,1	0,000280
	2	18	18	16	9,24	36,00	12,62	0,5774	3,74	5	25	8,72	9,86	10,23	1	4,6	2,3	18,4	46,1	0,000280
	2,5	18	18	20	11,55	45,00	15,77	0,5774	3,90	5	25	10,20	11,20	11,56	1	4,6	2,3	18,4	46,1	0,000280
	3	18	18	24	13,86	54,00	18,93	0,5774	4,06	5	25	11,68	12,53	12,89	1	4,6	2,3	18,4	46,1	0,000280
	3,5	18	18	28	16,17	63,00	22,08	0,5774	4,22	5	25	13,16	13,86	14,22	1	4,6	2,3	18,4	46,1	0,000280
	4	18	18	32	18,48	72,00	25,24	0,5774	4,38	5	25	14,64	15,20	15,55	1	4,6	2,3	18,4	46,1	0,000280
	4,5	18	18	36	20,79	81,00	28,39	0,5774	4,55	5	25	16,12	16,53	16,89	1	4,6	2,3	18,4	46,1	0,000280
	5	18	18	40	23,10	90,00	31,55	0,5774	4,71	5	25	17,60	17,86	18,22	1	4,6	2,3	18,4	46,1	0,000280
	5,5	18	18	44	25,40	99,00	34,70	0,5774	4,87	5	25	19,08	19,20	19,55	1	4,6	2,3	18,4	46,1	0,000280
	6	18	18	48	27,71	108,00	37,86	0,5774	5,03	5	25	20,56	20,53	20,89	1	4,6	2,3	18,4	46,1	0,000280
	6,5	18	18	52	30,02	117,00	41,01	0,5774	5,19	5	25	22,04	21,86	22,22	1	4,6	2,3	18,4	46,1	0,000280
	7	18	18	56	32,33	126,00	44,17	0,5774	5,36	5	25	23,52	23,20	23,56	1	4,6	2,3	18,4	46,1	0,000280
	7,5	18	18	60	34,64	135,00	47,32	0,5774	5,52	5	25	25,00	24,53	24,89	1	4,6	2,3	18,4	46,1	0,000280
	8	18	18	64	36,95	144,00	50,48	0,5774	5,68	5	25	26,48	25,86	26,23	1	4,6	2,3	18,4	46,1	0,000280
	8,5	18	18	68	39,26	153,00	53,63	0,5774	5,84	5	25	27,96	27,20	27,56	1	4,6	2,3	18,4	46,1	0,000280
	9	18	18	72	41,57	162,00	56,79	0,5774	6,00	5	25	29,44	28,53	28,90	1	4,6	2,3	18,4	46,1	0,000280
Clay, poor sandy / silty (weak compression)	9,5	18	18	76	43,88	171,00	59,94	0,5774	6,17	5	25	30,92	29,86	30,23	1	4,6	2,3	18,4	46,1	0,000280
	10	18	18	80	46,19	180,00	63,10	0,5774	6,33	5	25	32,40	31,20	31,57	1	4,6	2,3	18,4	46,1	0,000280
	10,5	18	18	84	48,50	189,00	66,25	0,5774	6,49	5	25	33,88	32,53	32,90	1	4,6	2,3	18,4	46,1	0,000280
	11	18	18	88	50,81	198,00	69,40	0,5774	6,65	5	25	35,36	33,86	34,23	1	4,6	2,3	18,4	46,1	0,000280
	11,5	18	18	92	53,12	207,00	72,56	0,5774	6,81	5	25	36,84	35,20	35,57	1	4,6	2,3	18,4	46,1	0,000280
	12	18	18	96	55,43	216,00	75,71	0,5774	6,98	5	25	38,32	36,53	36,91	1	4,6	2,3	18,4	46,1	0,000280
	12,5	**18**	**18**	**100**	**57,74**	**225,00**	**78,87**	**0,5774**	**7,14**	**5**	**25**	**39,80**	**37,86**	**38,245**	**1**	**4,6**	**2,3**	**18,4**	**46,1**	**0,000280**
	13	18	18	104	60,05	234,00	82,02	0,5774	7,30	5	25	41,28	39,20		1	4,6	2,3	18,4	46,1	0,000280
	13,5	18	18	108	62,36	243,00	85,18	0,5774	7,46	5	25	42,76	40,53		1	4,6	2,3	18,4	46,1	0,000280
	14	18	18	112	64,67	252,00	88,33	0,5774	7,62	5	25	44,24	41,86		1	4,6	2,3	18,4	46,1	0,000280
	14,5	18	18	116	66,98	261,00	91,49	0,5774	7,78	5	25	45,72	43,20		1	4,6	2,3	18,4	46,1	0,000280
	15	18	18	120	69,29	270,00	94,64	0,5774	7,95	5	25	47,20	44,53	44,92	1	4,6	2,3	18,4	46,1	0,000280
	15,5	18	18	124	71,60	279,00	97,80	0,5774	8,11	5	25	48,68	45,86		1	4,6	2,3	18,4	46,1	0,000280
	16	18	18	128	73,90	288,00	100,95	0,5774	8,27	5	25	50,16	47,20		1	4,6	2,3	18,4	46,1	0,000280
	16,5	18	18	132	76,21	297,00	104,11	0,5774	8,43	5	25	51,64	48,53	48,93	1	4,6	2,3	18,4	46,1	0,000280
	17	18	18	136	78,52	306,00	107,26	0,5774	8,59	5	25	53,12	49,86		1	4,6	2,3	18,4	46,1	0,000280
	17,5	18	18	140	80,83	315,00	110,42	0,5774	8,76	5	25	54,60	51,20		1	4,6	2,3	18,4	46,1	0,000280
	18	18	18	144	83,14	324,00	113,57	0,5774	8,92	5	25	56,08	52,53		1	4,6	2,3	18,4	46,1	0,000280
	18,5	18	18	148	85,45	333,00	116,73	0,5774	9,08	5	25	57,56	53,86		1	4,6	2,3	18,4	46,1	0,000280
	19	18	18	152	87,76	342,00	119,88	0,5774	9,24	5	25	59,04	55,20		1	4,6	2,3	18,4	46,1	0,000280
	19,5	18	18	156	90,07	351,00	123,04	0,5774	9,40	5	25	60,52	56,53		1	4,6	2,3	18,4	46,1	0,000280
	20	18	18	160	92,38	360,00	126,19	0,5774	9,57	5	25	62,00	57,86	58,3	1	4,6	2,3	18,4	46,1	0,000280

Appendix A table 1 soil parameters of homogeneous clay profile 0 – 30m depth

The final step of checking whether or not the right effective strength parameters were chosen for the hardening soil model, multiple triaxial test within the PLAXIS test facilities were performed. In the figure below the settings can be seen for the calculation at reference stress of 100 kPa:

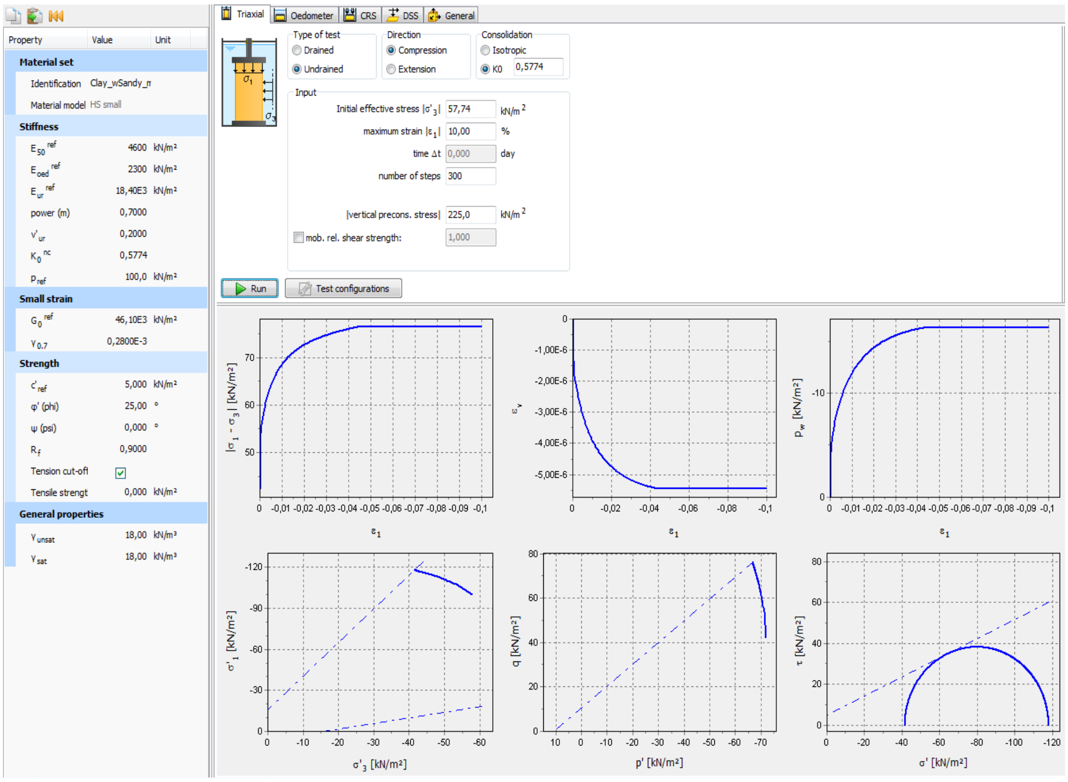

Appendix A figure 3 settings PLAXIS test facilities at 100kPa stress level

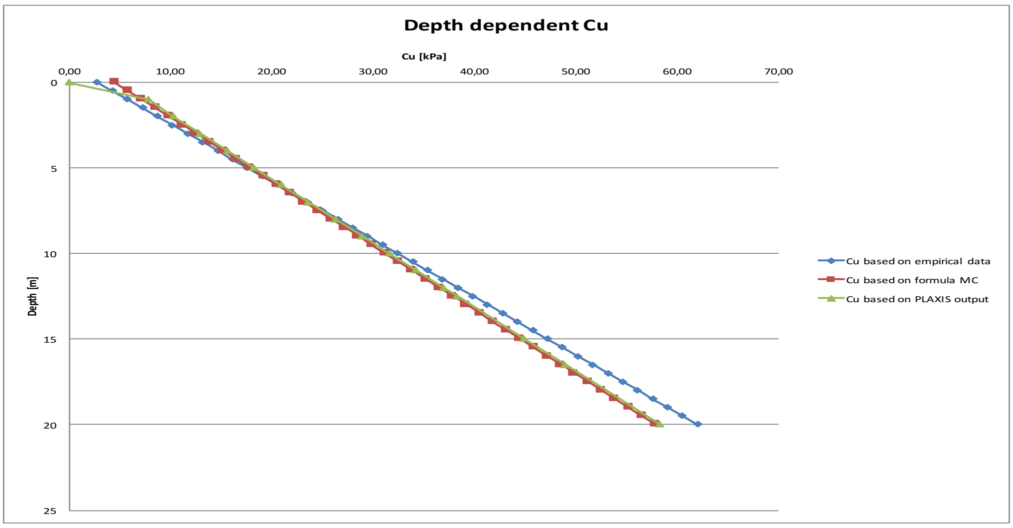

Appendix A figure 4 comparison between undrained shear strength based on empirical formula (blue), Mohr Coulomb formula (red) and PLAXIS undrained triaxial tests (green)

A final comparison of the three different methods, shows a good fit of the chosen effective strength parameters. The stiffnesses for the hardening soil model, with small strains, was determined based on seismic CPT's of soil investigation data near Loppersum (Groningen) and correlation with table 2b NEN9997, see the resulting parameters in Appendix A table 1.

Appendix B

Determination of limiting lateral soil resistance

For cohesive soils, the lateral bearing capacity depends in most theories on the undrained shear strength c_u. In Appendix A, the undrained shear strength calculated with the PLAXIS test facilities is shown. These values were used for determining the lateral limiting soil resistance for the lateral slider.

The bearing capacity varies between 8 and 12 times $c_u * D$, except for shallow depths where the bearing capacity is lower. Values of 12 are associated with rough piles, however most used in design are values of 9. Depending on the type of clay, uniform or normally consolidated, two limiting lateral resistance profiles can be distinguished (Randolph & Gouvernec, 2011):

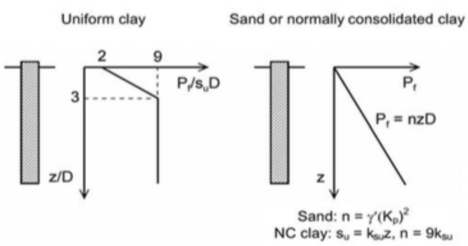

Appendix B figure 1 limiting lateral soil profile for uniform and normally consolidated clay

For the normally consolidated clays, the limiting lateral resistance is determined by 8 to 12 times $c_u * D$, where $c_u$is depth dependent . For uniform clay the profile of limiting pressure goes linear increasing from 2 times $c_u * D$ at surface level to 9 times $c_u * D$ at a depth of 3 pile diameters, where c_u is taken as an average or at reference stress of 100kPa. Below 3 times D the limiting pressure is 9 times $c_u * D$. Equation (B1) and (B2) describes this profile, much as was originally suggested by Broms (1964b):

$$p_u = \left(2 + 7 * \frac{z}{3D}\right) * c_u * D \quad for\ z < 3D \tag{B1}$$

$$p_u = 9 * c_u * D \quad for\ z \geq 3D \tag{B2}$$

With:

- c_u: The undrained shear strength [kN/m^2]
- z : The depth from ground level [m]

Internationally the API standard (2010) is often used, which has a different approach for the lateral bearing capacity for especially cohesionless soils. For cohesive soils the API suggest a set of equations similar to Broms (1964). The ultimate lateral load per unit length varies between 8 and 12 times $c_u * D$, while the initial limiting pressure at ground level is 3 times $c_u * D$.

$$p_u = \left(3 * c_u + \gamma' * z + J * \frac{c_u * z}{D}\right) * D \tag{B3}$$

$$p_u = 9 * c_u * D \tag{B4}$$

With:

- γ': Effective soil weight [kN/m^2]
- J: Dimensionless empirical constant with values ranging from 0,25 to 0,5, determined by field testing [-]

Based on the previous formulas, the values for the limiting soil resistance is shown in the table and visualised in the figure below:

Uniform Clay (Broms, average Cu over 10m)				ay (Broms, Cu at 100kPa)	Normally consolidated Clay (Randolph Pf=9)	Normally consolidated Clay (Randolph Pf=10,5)	Normally consolidated Clay (Randolph Pf=12)	API
epth m	diameter m	Cu kPa	Limiting lateral resistance Pu kN/m	ting lateral resistance Pu kN/m	imiting lateral resistance Pu kN/m	Limiting lateral resistance Pu kN/m	Limiting lateral resistance Pu kN/m	lateral resistance Pu kN/m
0		4,53	18,23	40,00	20,39	23,79	27,19	60,00
0,5		6,19			27,86	32,50	37,14	67,00
1		7,85			35,33	41,21	47,10	74,00
1,5		9,04	82,02	180,00	40,67	47,45	54,23	81,00
2		10,23			46,01	53,68	61,35	88,00
2,5		11,56			52,01	60,68	69,35	95,00
3		12,89			58,01	67,67	77,34	102,00
3,5		14,22			63,99	74,66	85,32	109,00
4		15,55			69,98	81,64	93,30	116,00
4,5		16,89			75,98	88,65	101,31	123,00
5	0,5	18,22			81,99	95,66	109,32	130,00
5,5		19,55			87,99	102,65	117,32	137,00
6		20,89			93,98	109,65	125,31	144,00
6,5		22,22			100,00	116,67	133,34	151,00
7		23,56			106,02	123,69	141,36	158,00
7,5		24,89			112,02	130,69	149,36	165,00
8		26,23			118,01	137,68	157,35	172,00
8,5		27,56			124,02	144,69	165,36	179,00
9		28,90			130,03	151,70	173,37	180,00
9,5		30,23			136,04	158,71	181,38	180,00
10		31,57	82,02	180,00	142,04	165,72	189,39	180,00

Appendix B table 1 values for different limiting soil resistances

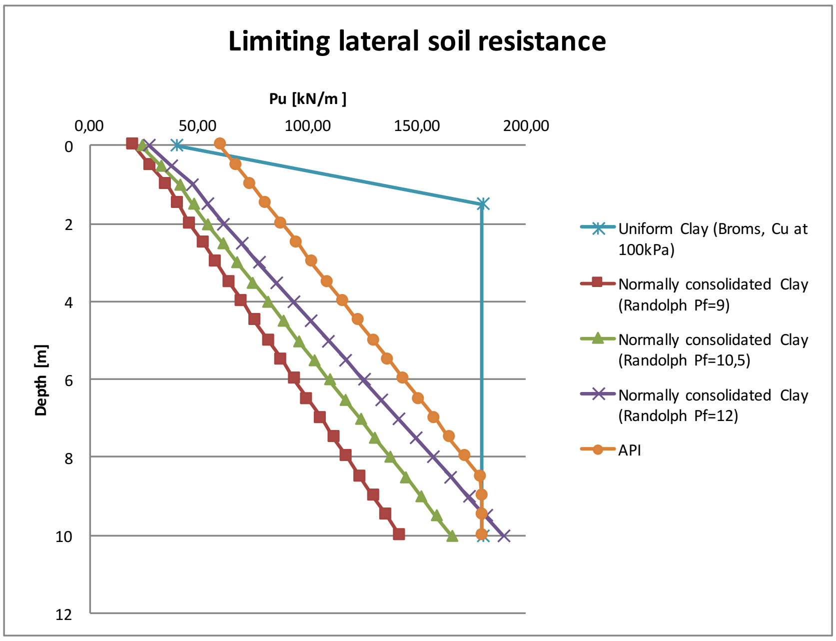

Appendix B figure 2 Visualisation of the limiting lateral resistance profiles

The normally consolidated clay profiles are based on depth dependent c_u values. However, the method of Broms (1964b) is based on c_u values at a reference stress of 100 kPa.These different limiting lateral soil resistances where implemented in PLAXIS and the maximum strength was analysed. The results are shown and compared with the 3D volume pile and the D-Pile Group calculation.

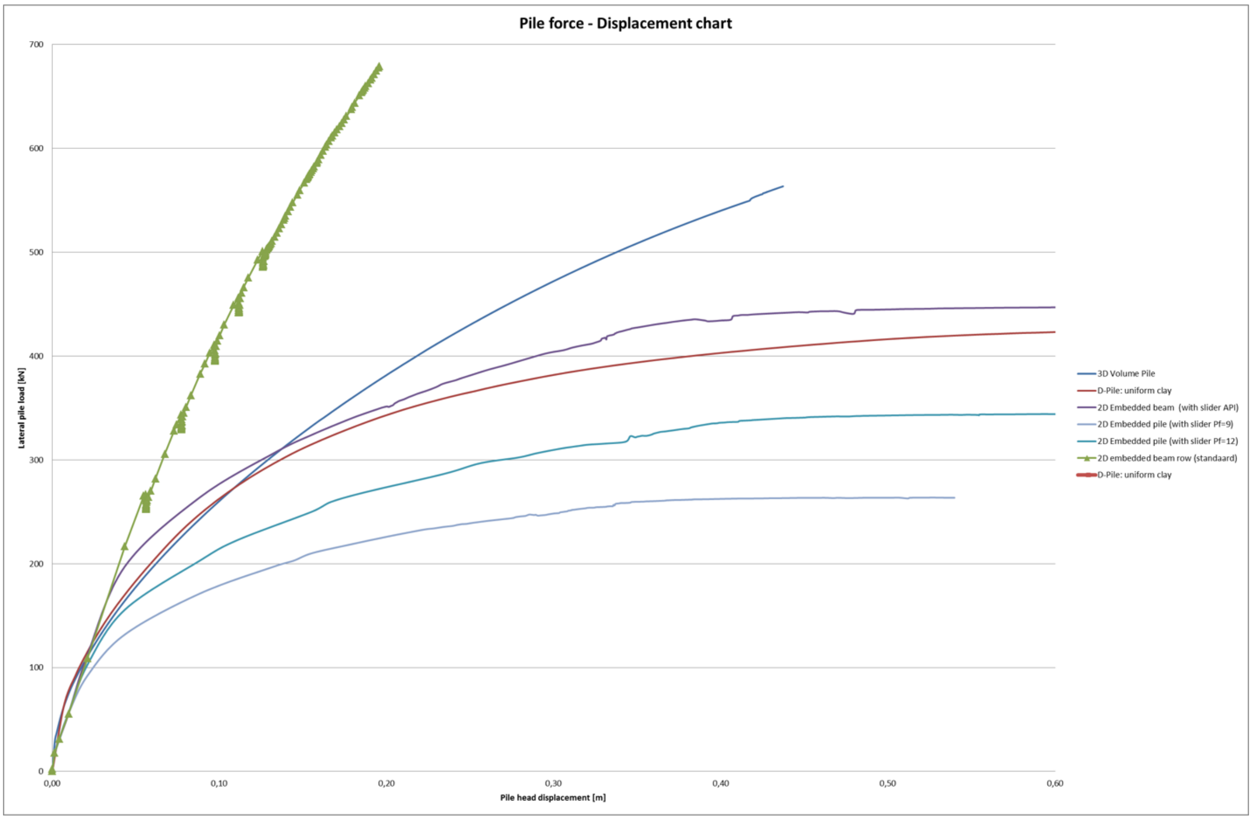

Appendix B figure 3 Results of different lateral sliders and their ultimate strength

From this the best option for the chosen silty clay profile turned out to be the limiting lateral skin resistance determined by the API method. The same was used in the D-Pile Group calculation. The ultimate strength of both the embedded beam with API slider and the D-Pile Group are similar. The difference between stiffnesses for small loads is more visible in Appendix B figure 4. 3D calculation and D-Pile Group results show more stiff behaviour for the loads up until around 110 kN.

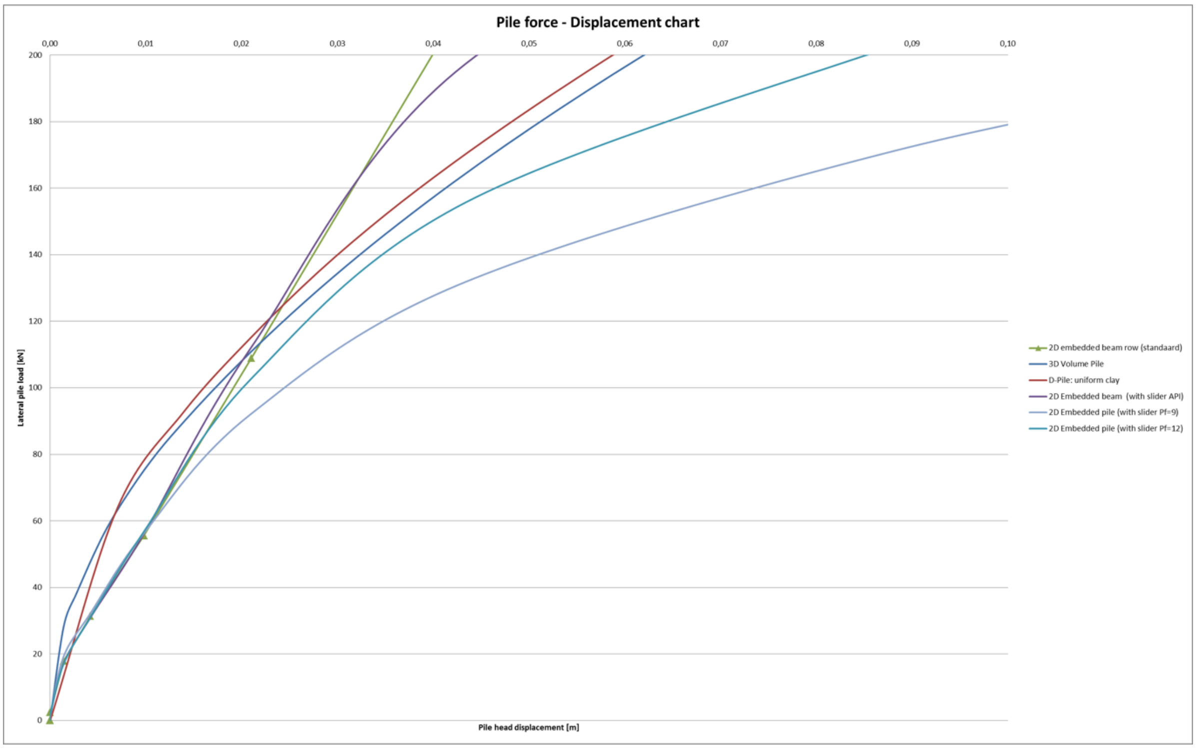

Appendix B figure 4 Difference between pile stiffnesses for small loads

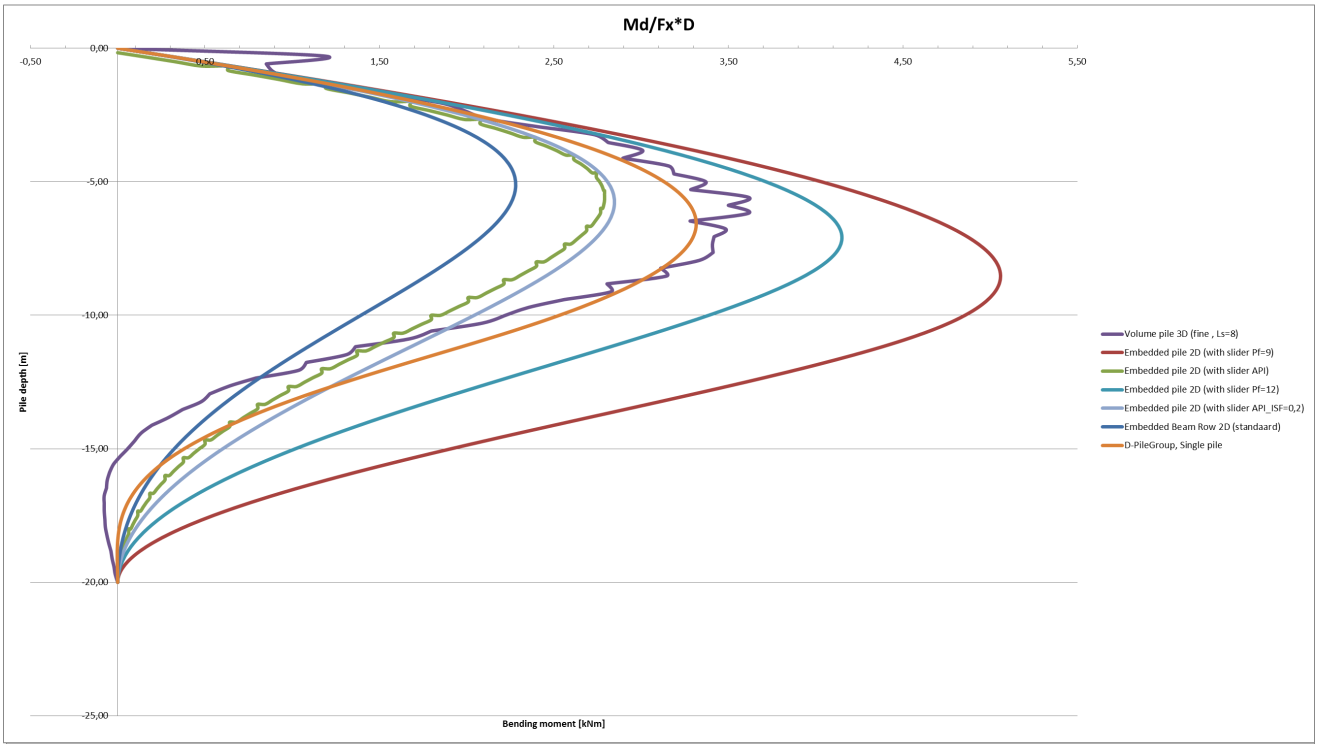

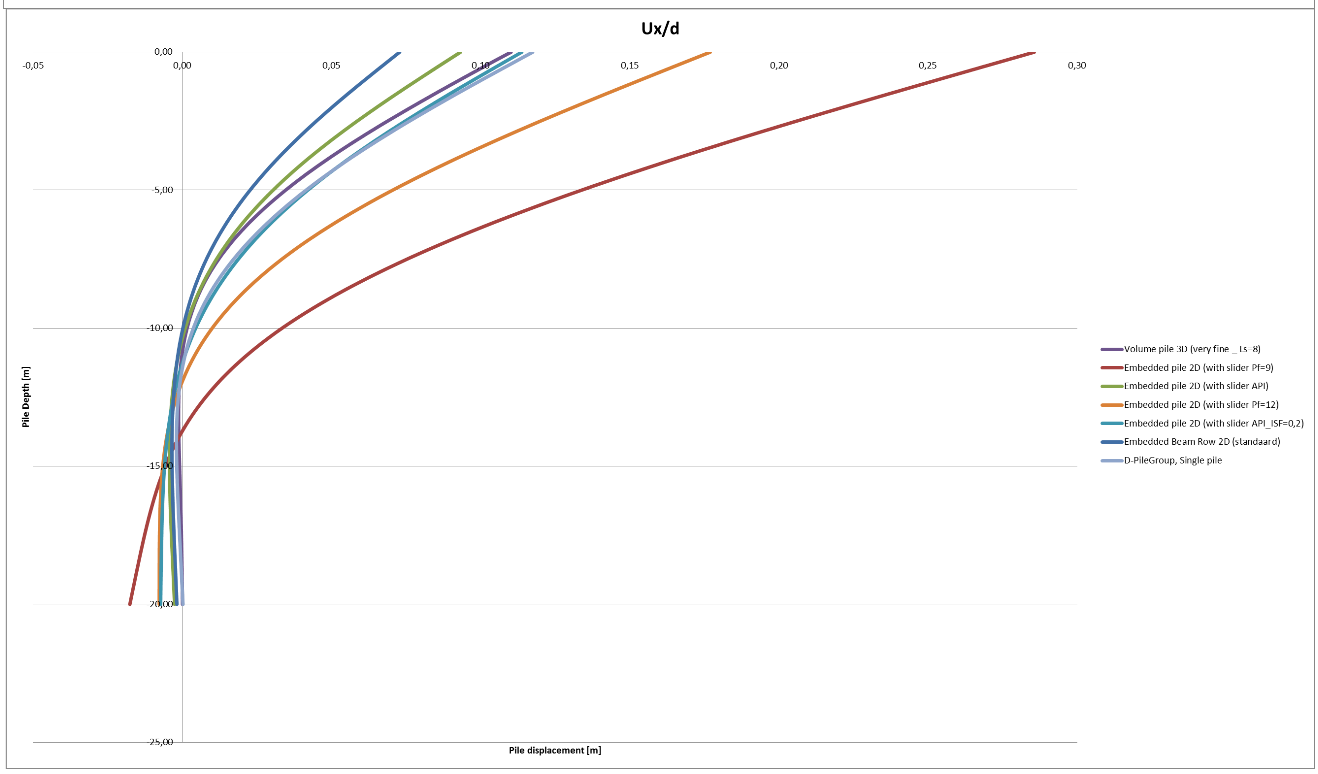

Appendix B figure 5 Bending moment and pile displacement for a 200 kN pile head load for different lateral skin resistances

In Appendix B figure 5 the resulting bending moments and pile displacement along the pile can be compared. It can be concluded that a good approximation of the 3D situation is the embedded beam with API slider.

Appendix C

Results of pile displacement and bending moment for loads from 20 kN till 200 kN and boundary- /mesh-dependency of the 2D model

The results of the different calculations are shown in this appendix. For different pile spacing the results of the bending moments and pile displacements can be seen in the figures below, starting from spacing of 2 m and continuing with 4 m and 8 m.

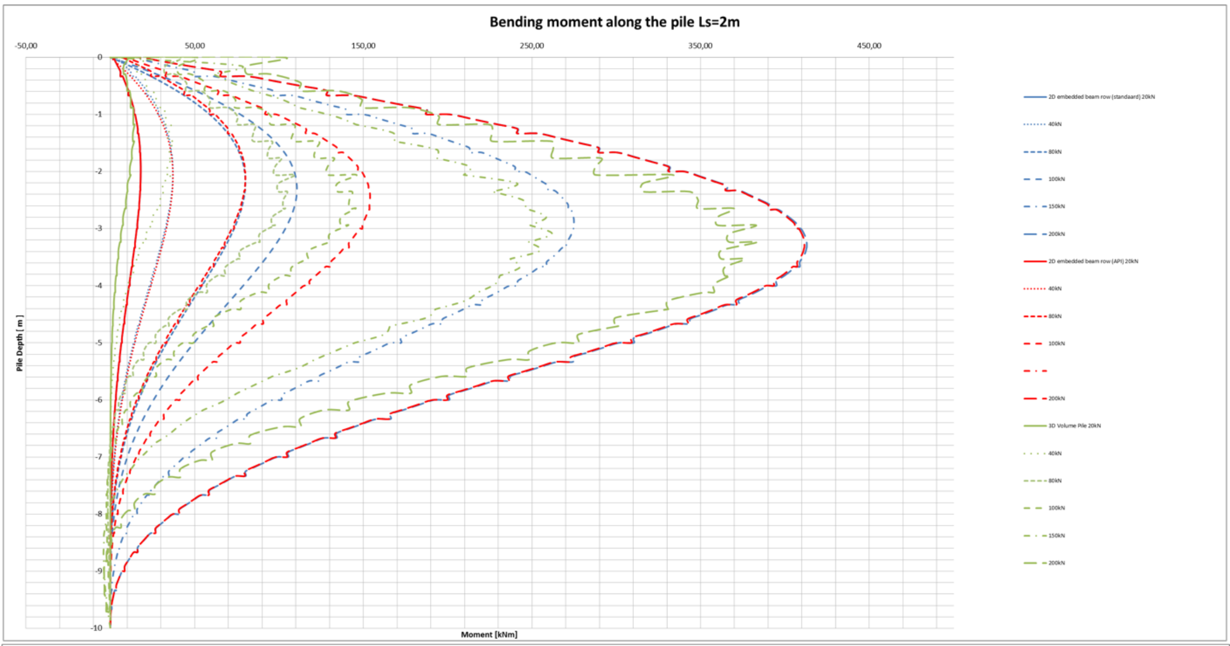

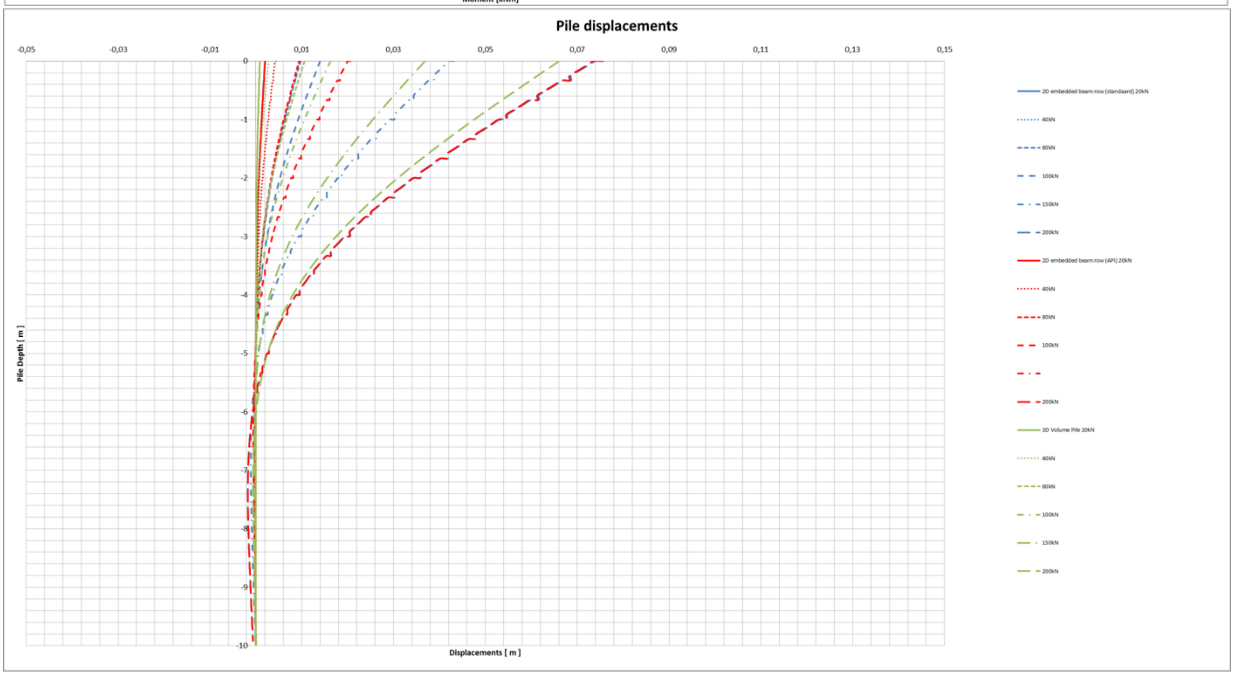

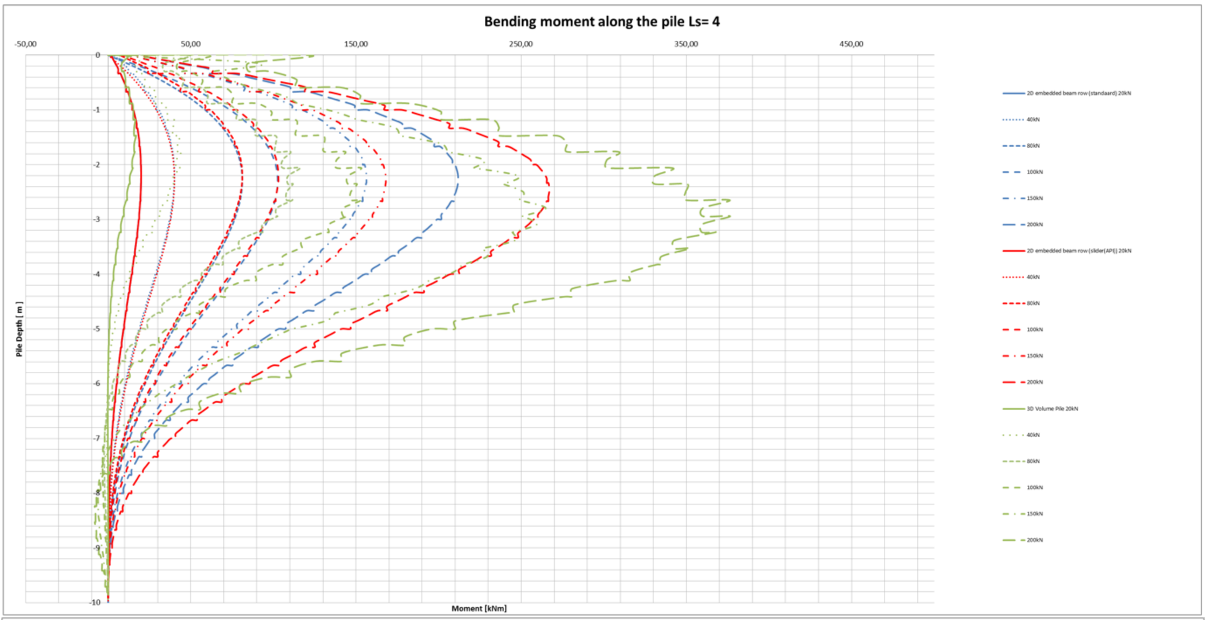
Bending moment along the pile Ls= 4
-50,00
50,00
150,00
250,00
350,00
450,00
0
-1
-2
-3
-4
-5
-6
-7
-8
-9
-10
Pile Depth [m]
Moment [kNm]
2D embedded beam row (standaard) 20kN
40kN
80kN
100kN
150kN
200kN
2D embedded beam row (slider(API)) 20kN
40kN
80kN
100kN
150kN
200kN
3D Volume Pile 20kN
40kN
80kN
100kN
150kN
200kN

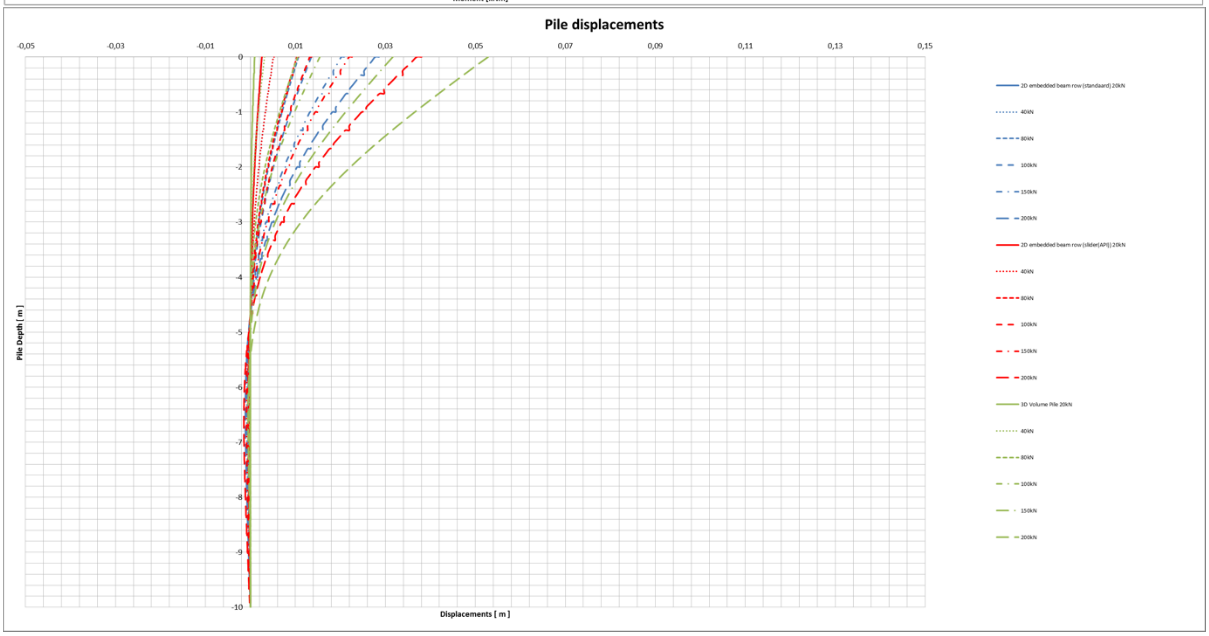
Pile displacements
-0,05
-0,03
-0,01
0,01
0,03
0,05
0,07
0,09
0,11
0,13
0,15
0
-1
-2
-3
-4
-5
-6
-7
-8
-9
-10
Pile Depth [m]
Displacements [m]
2D embedded beam row (standaard) 20kN
40kN
80kN
100kN
150kN
200kN
2D embedded beam row (slider(API)) 20kN
40kN
80kN
100kN
150kN
200kN
3D Volume Pile 20kN
40kN
80kN
100kN
150kN
200kN

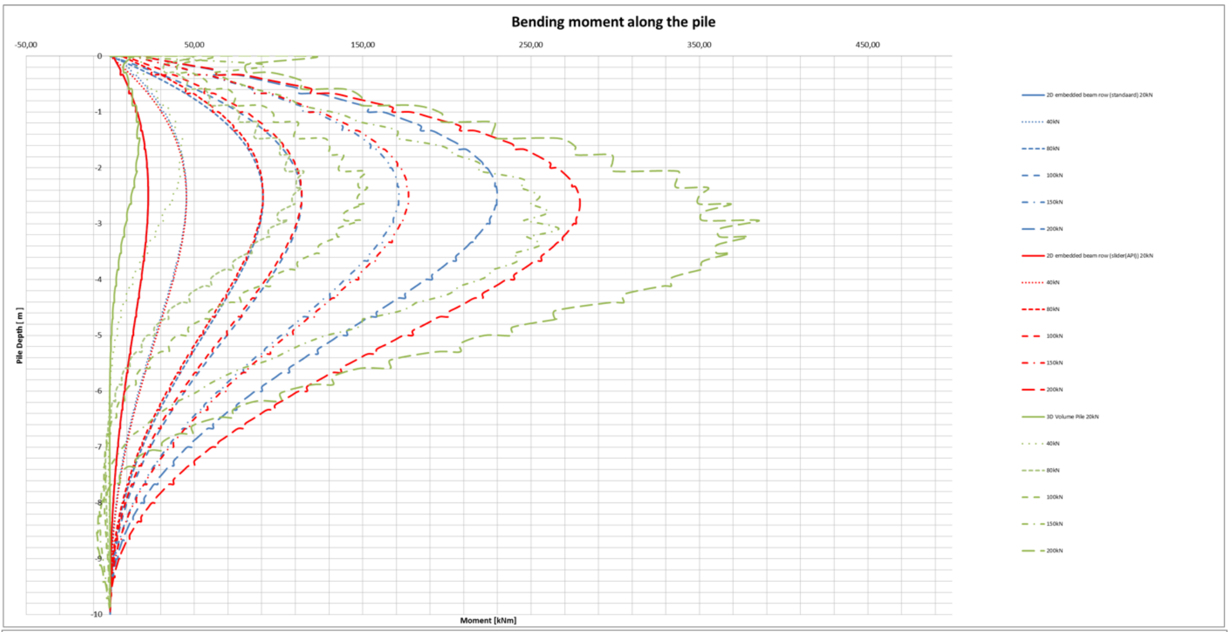

Bending moment along the pile
-50,00
50,00
150,00
250,00
350,00
450,00
Pile Depth [m]
Moment [kNm]

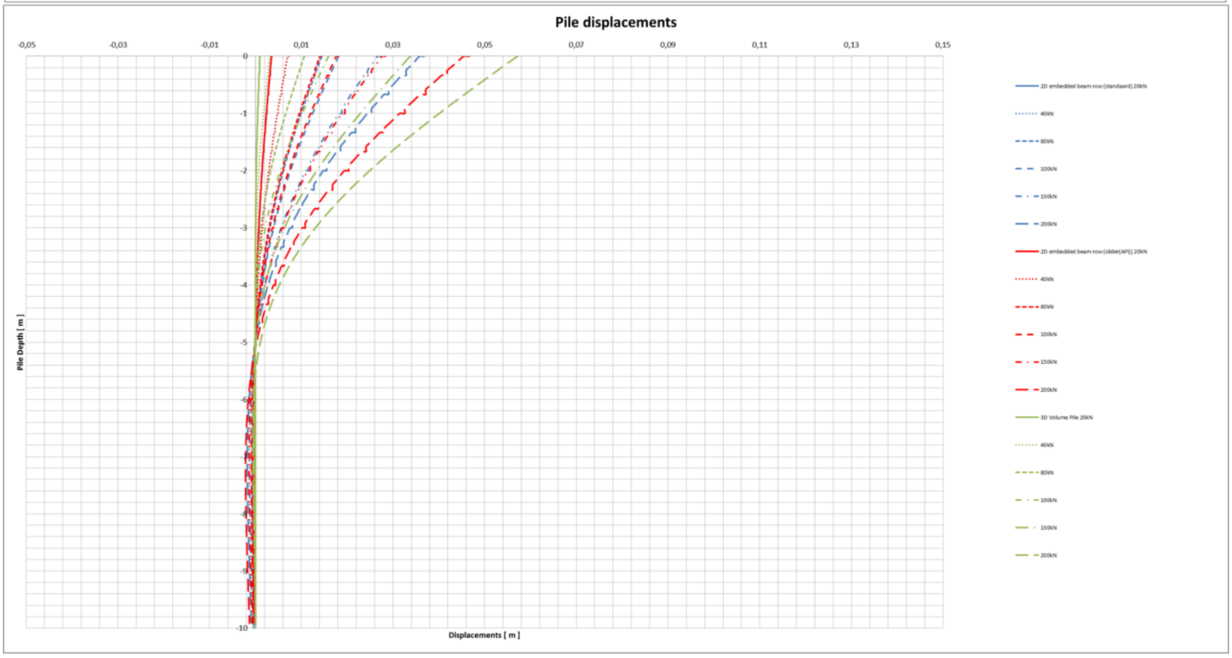

Pile displacements
-0,05
-0,03
-0,01
0,01
0,03
0,05
0,07
0,09
0,11
0,13
0,15
Pile Depth [m]
Displacements [m]

The bending moments are normalized by the applied load and diameter of the pile. The pile displacements are normalized by the pile diameters. These normalized results are summarized in the figure below.

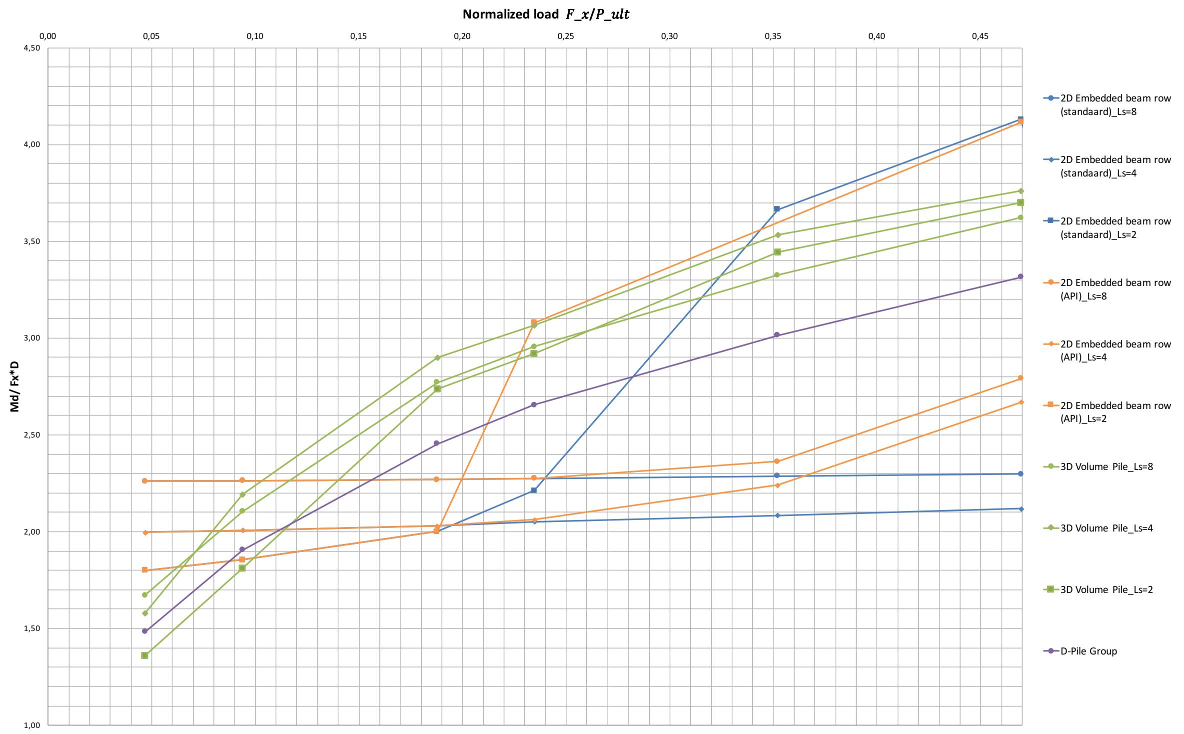

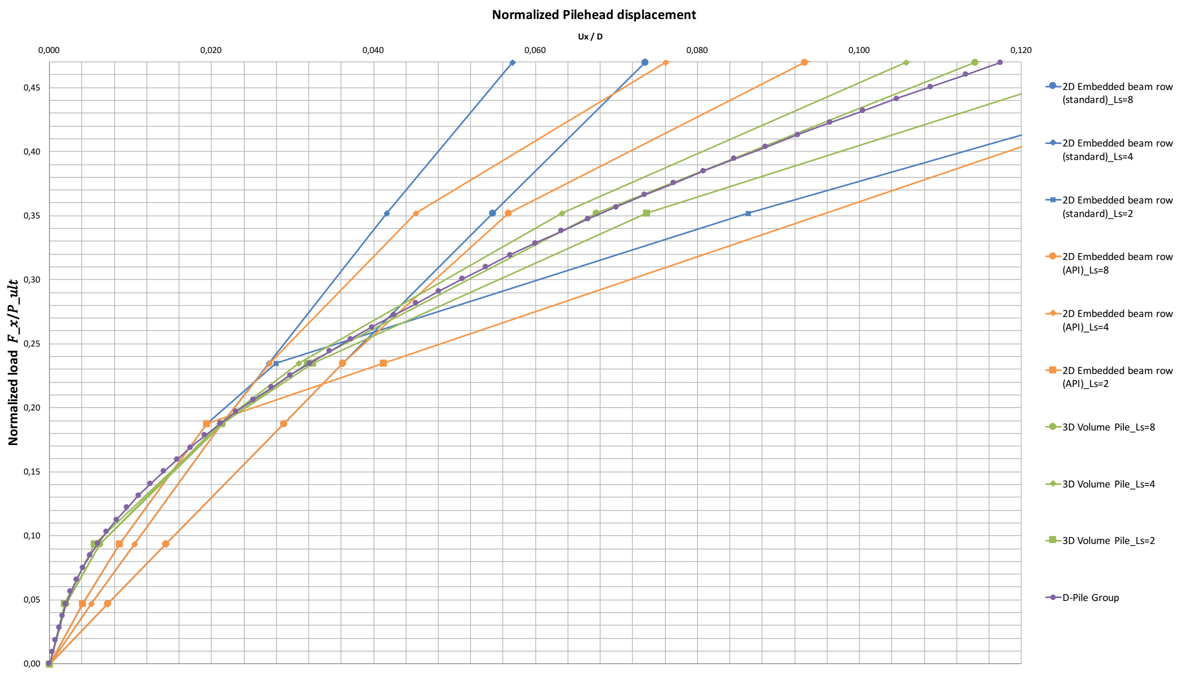

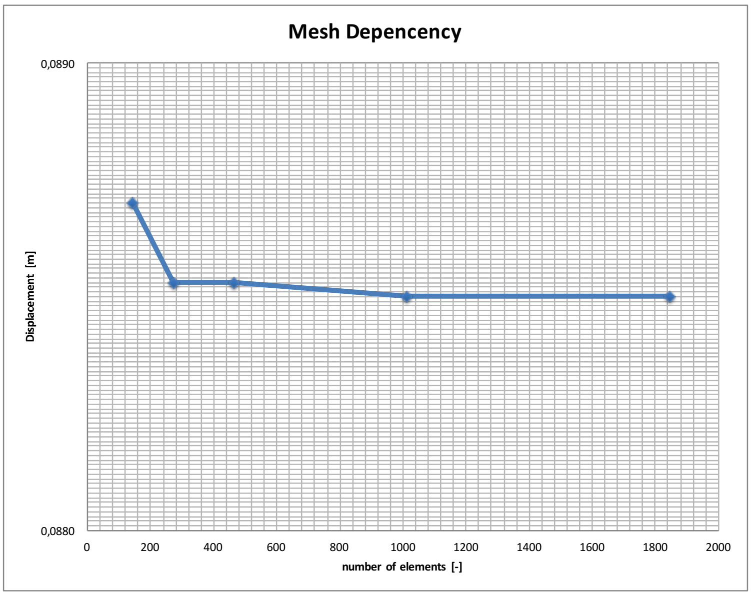

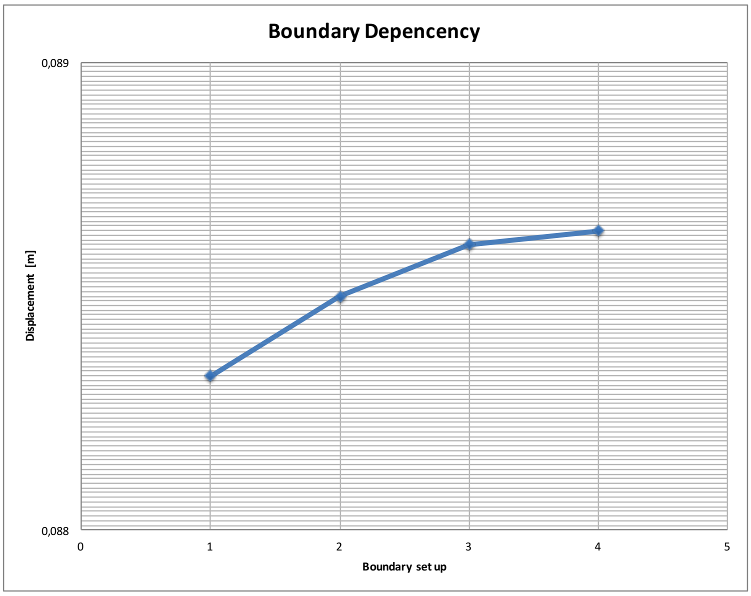

The mesh dependency of the static situation was determined by changing the boundary width and by applying several different meshes. The resulting numbers are shown in the table below:

2D embedded beam with slider (NC12)					
Mesh size (5 standard option PLAXIS)	**number of elements**	**number of nodes**	**kN/m**	**Load**	**Ux**
Very Coarse	143	1232		200	0,0882
Coarse	273	2316		200	0,08853
Medium	463	3880		200	0,08853
fine	1012	8358		200	0,0885
very fine	1846	15122		200	0,0885
Influence boundaries	**Set up**				
20 x 20 m	1			200	0,08833
40 x 20m	2			200	0,0885
60 x 20m	3			200	0,08861
80 x 20m	4			200	0,08864
40 x 40m				200	0,0885

The differences in displacement are negligible for different mesh sizes and boundary widths, in the order of 10^{-4}.

In the figures below two meshes are shown, respectively very coarse and very fine:

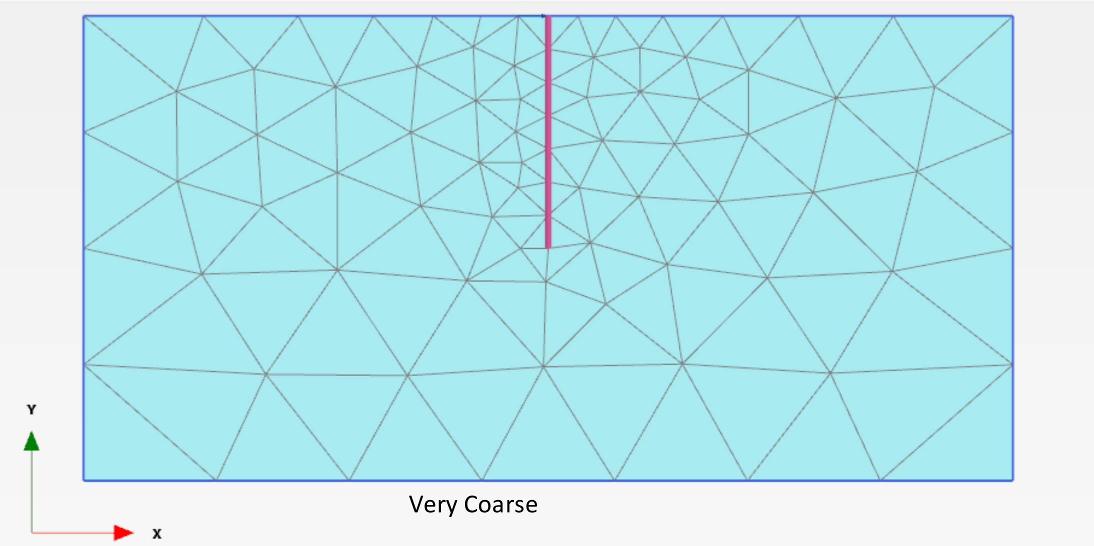

Very Coarse

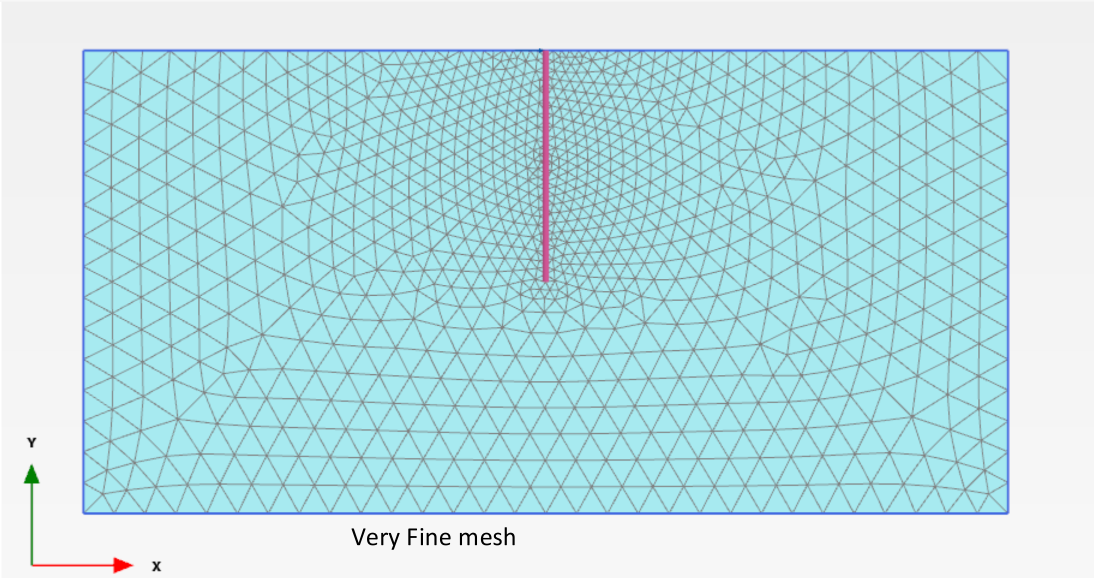

Very Fine mesh

Appendix D

Validation of pile behaviour with 3D volume pile and D-Pile Group

For a pile spacing of 8 m and with an increasing load of 20 kN till 200 kN the different pile head displacements is visualised below:

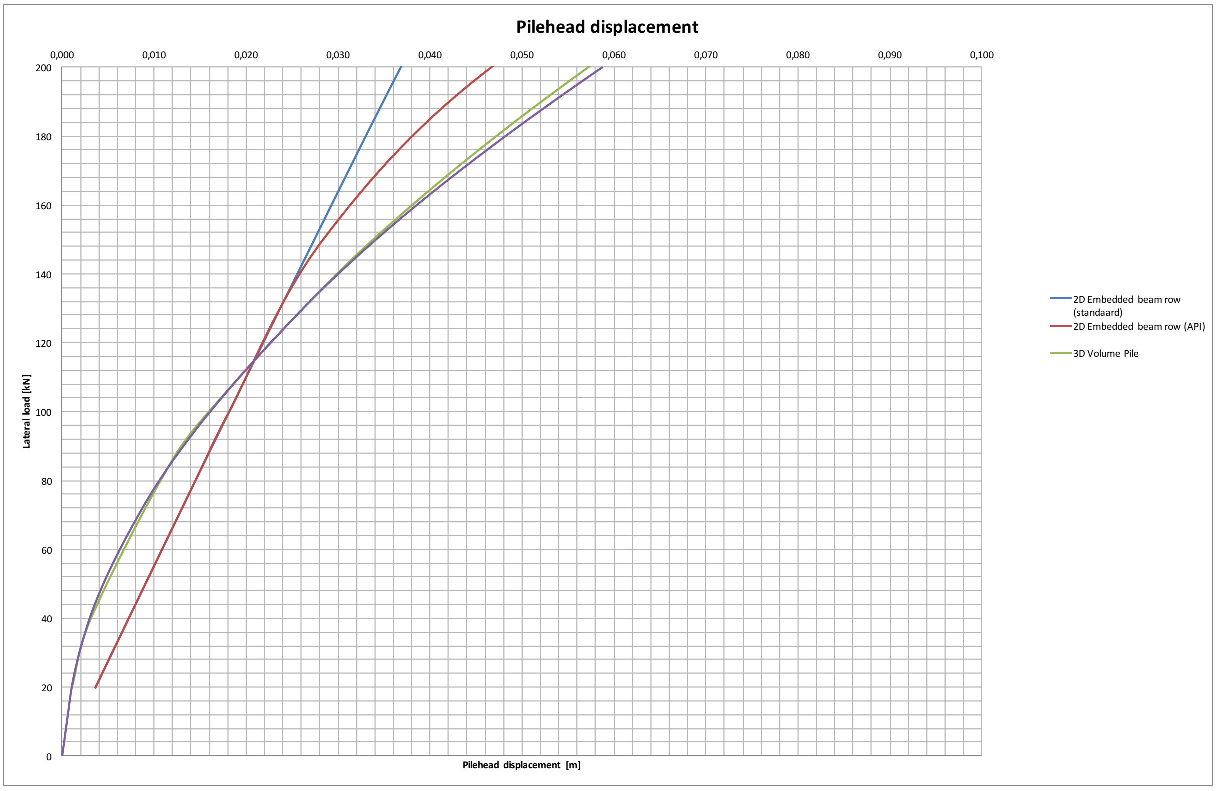

The calculations with D-Pile Group (purple line) were performed using an undrained shear strength of 40kPa, which is the undrained shear strength at reference level. Based on the methods used in D-Pile Group, the lateral slider in PLAXIS was also determined using this API. One can clearly observe that the stiffness of the D-Pile Group, till at least 200 kN (0.47), act almost the same as for the 3D volume pile. Until approximately 140 kN (0.33) the embedded beam with API slider act the same as a standard embedded beam, below 110 kN the stiffness of the pile is underestimated in comparison with the DPile Group and 3D volume pile.

The loads in this thesis where eventually normalized with respect to the lateral bearing capacity according to the API method. For the chosen pile and soil model this was 426 kN. In the previous section the numbers behind the loads express the ratio between the applied load in the model and this bearing capacity. As was also mentioned in the main report, the choice was made to compare the D-Pile Group calculations with an embedded beam with pile spacing of 8 m. This is due to the single pile assumption for this spacing.

In the figures below, one can also see that the moments obtained from the D-Pile Group calculations are quite similar to the ones calculated with the 3D Volume pile.

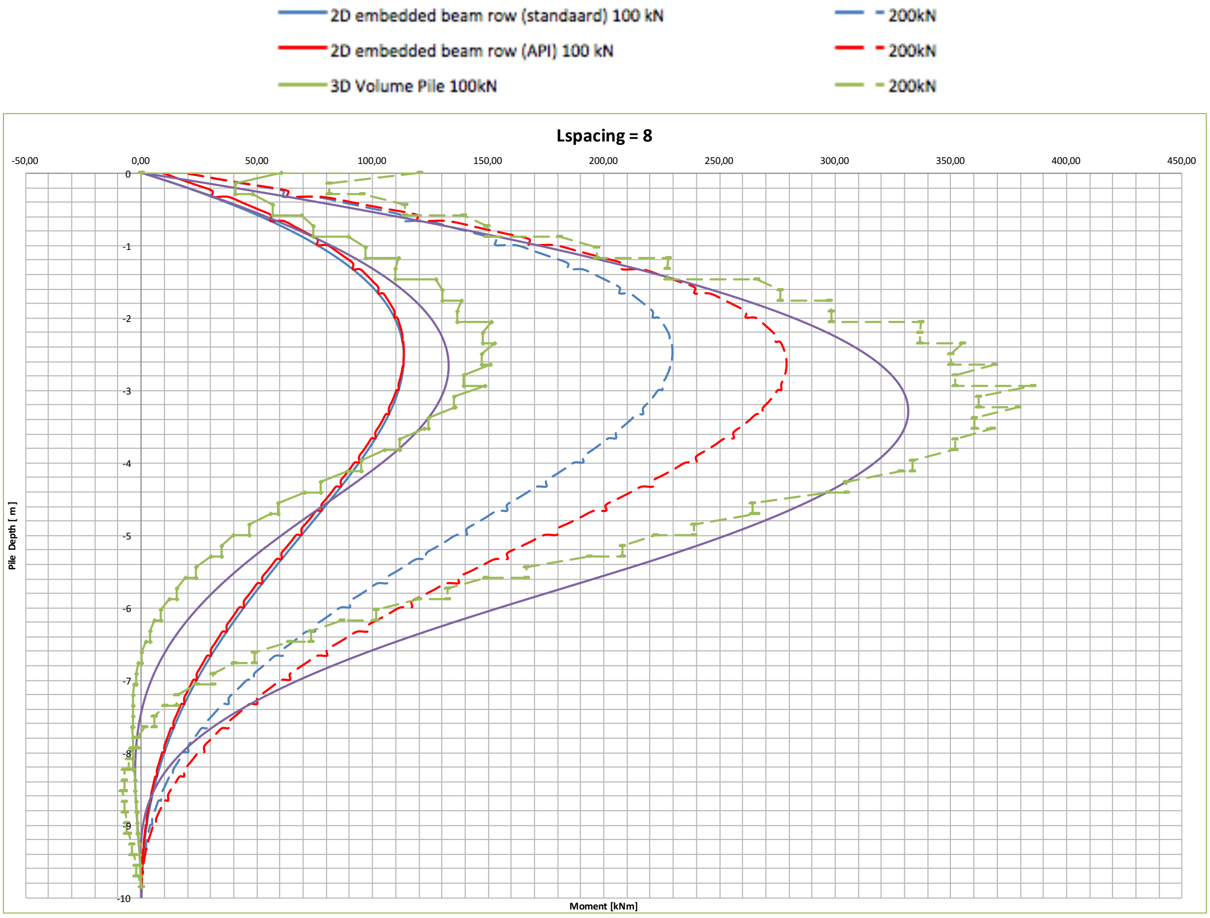

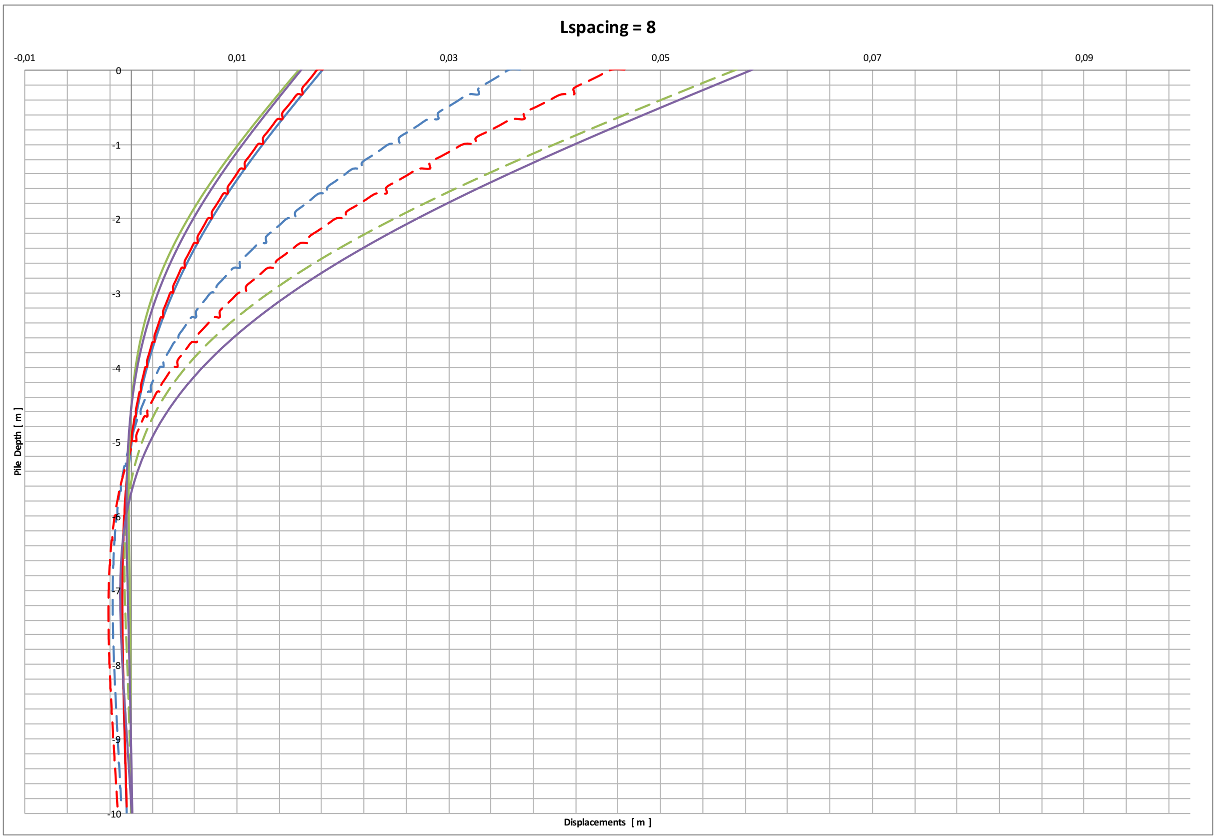

Purple lines are D-Pile Group Calculations for 100 kN (0.235) and 200 kN (0.47) pile head load.

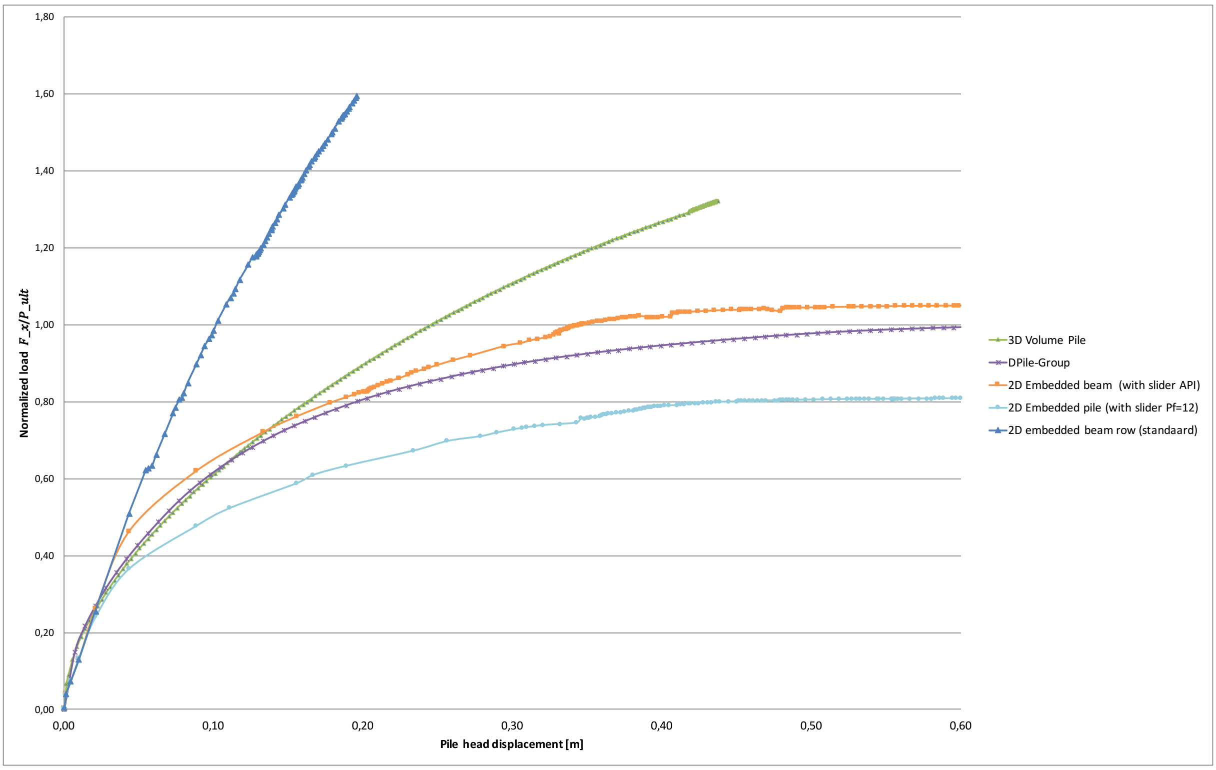

The maximum strength of both the D-Pile Group (using API) and the 2D embedded beam with API slider are quite similar. The input in D-Pile Group can be seen below:

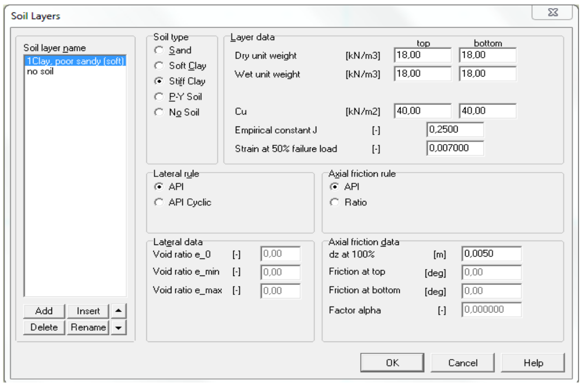

The load-displacement behaviour of both the 3D Volume pile and D-Pile Group match quite exact until approximately 70% of the lateral bearing capacity. Due to this resemblance, the 2D embedded beam behaviour is validated using these two methods.

Validation of pile behaviour with 3D volume pile and 3D embedded pile

Piles in the FE program of PLAXIS in 3D can be modelled in two different ways:

- Embedded pile, which is somewhat similar to the embedded beam in 2D;
- Volume pile, which is a volume element with elastic (non-porous) parameters.

These two methods were compared with one another for a pile spacing of 8 m and a laterally load of 200 kN, the results are shown below:

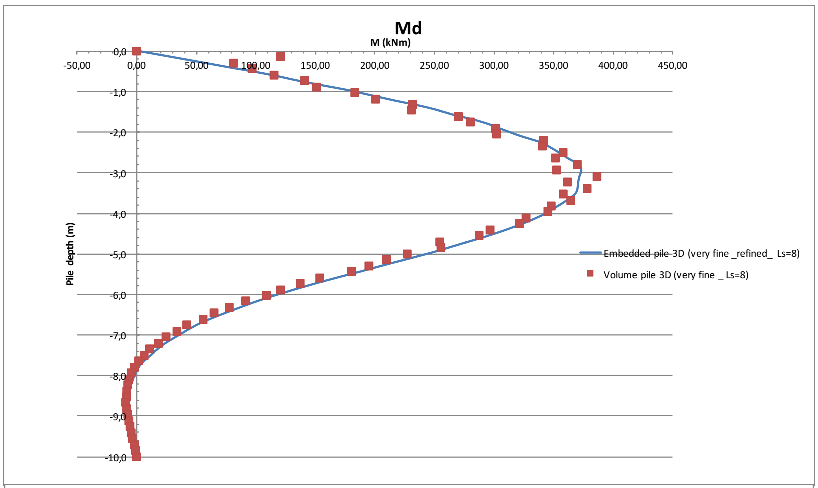

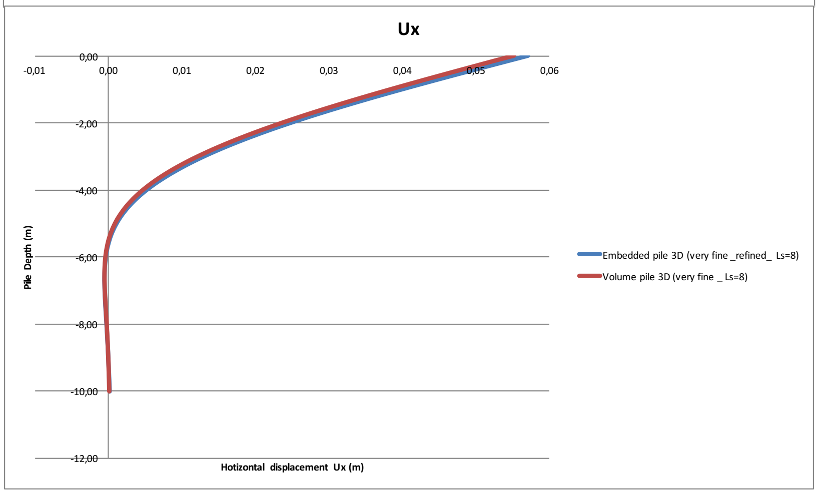

From this figures it can be concluded that the volume pile and embedded pile behave similar, for load up till 200 kN.

The figure below gives an impression of the mesh elements of the 3D model with a volume pile.

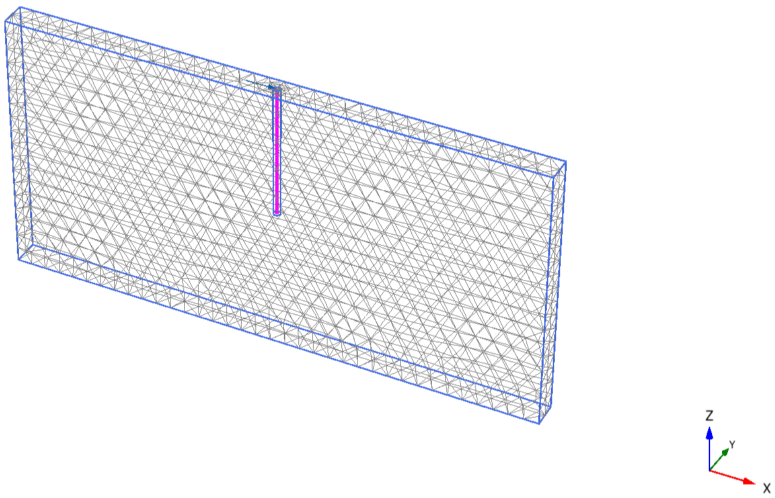

Appendix E

Interaction diagram for circular concrete pile design (Dutch code: GTB 1990)

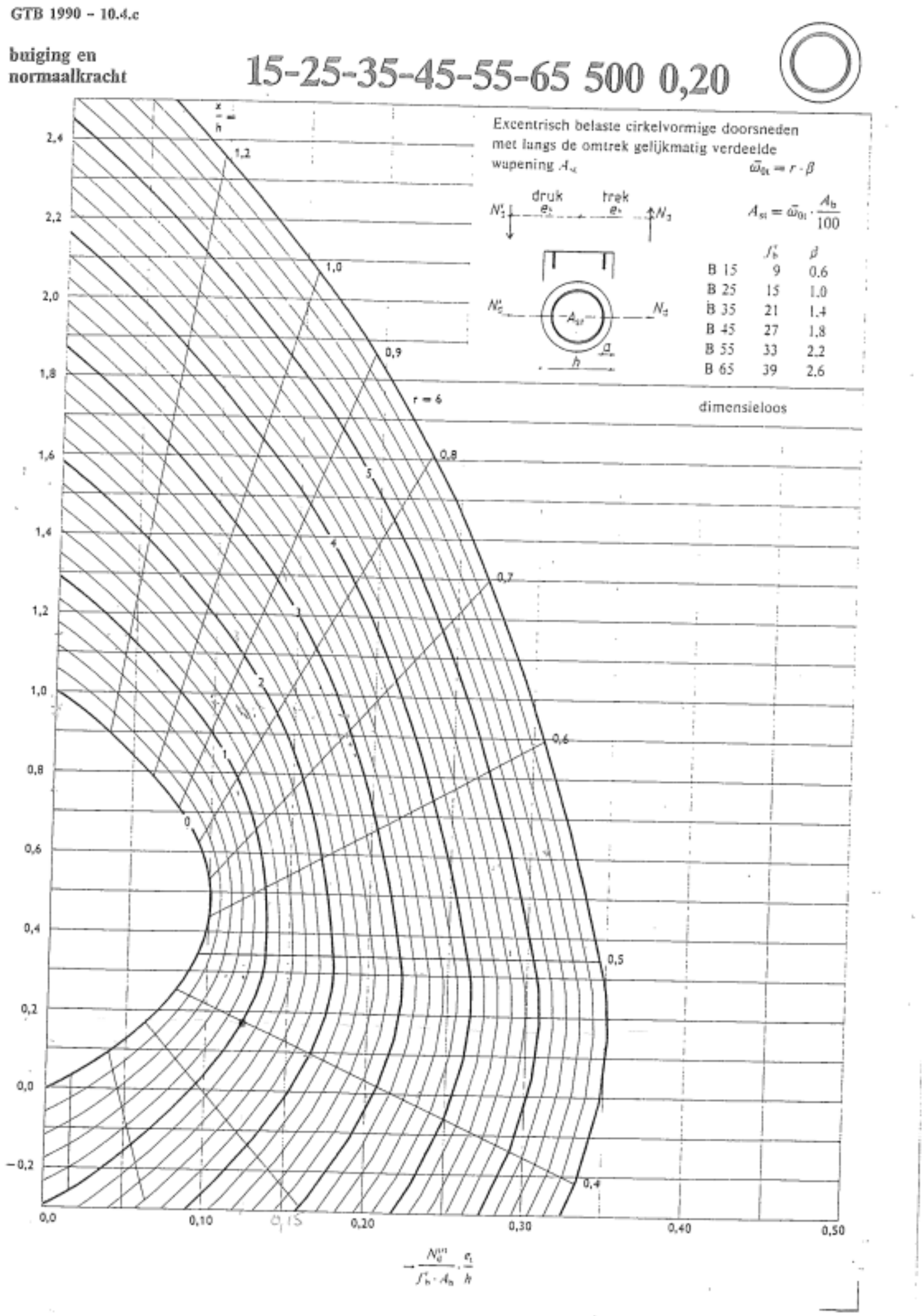

Appendix F

EERA excel data deconvolution Huizinge Signal

Huizinge WSErad signal

Time step ΔT (sec) =	0,005
Desired maximum acceleration (g) =	
Maximum frequency cut-off (Hz) =	25
Use frequency cut-off in calculation ?	Yes
Number of points for FFT =	16384
Import input motion from external file ?	No
Name of input file =	DIAM.ACC
Total number of values read =	7401
Peak Acceleration in input file (g) =	0,0584
Time of peak acceleration (sec) =	5,105
Mean Square Frequency (Hz) =	6,391
Peak acceleration after filtering (g) =	0,059

Time (sec)	Input Acceleration (g)	Scaled Acceleration (g)	Filtered Acceleration (g)
0,000	0	0,00	0,00
0,005	0	0,00	0,00
0,010	0	0,00	0,00
0,015	0	0,00	0,00
0,020	0	0,00	0,00
0,025	0	0,00	0,00
0,030	0	0,00	0,00
0,035	0	0,00	0,00
0,040	0	0,00	0,00
0,045	0	0,00	0,00
0,050	0	0,00	0,00
0,055	0	0,00	0,00
0,060	0	0,00	0,00
0,065	0	0,00	0,00
0,070	0	0,00	0,00
0,075	0	0,00	0,00
0,080	0	0,00	0,00
0,085	0	0,00	0,00
0,090	0	0,00	0,00
0,095	0	0,00	0,00
0,100	0	0,00	0,00
0,105	0	0,00	0,00
0,110	0	0,00	0,00
0,115	0	0,00	0,00
0,120	0	0,00	0,00
0,125	0	0,00	0,00

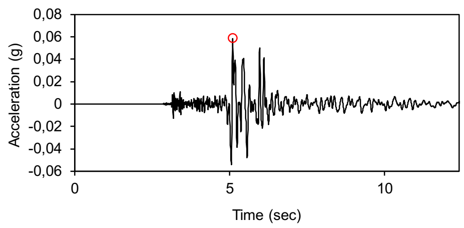

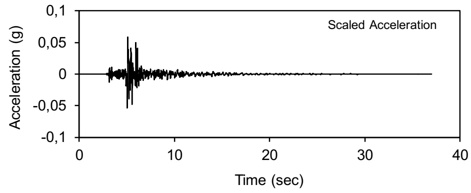

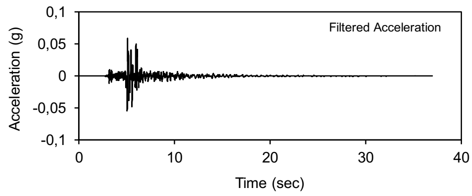

Appendix F figure 1 Earthquake input data

Fundamental period (s) =	0,64
Average shear wave velocity (m/sec) =	204,97
Total number of sublayers =	17

	Layer Number	Soil Material Type	Number of sublayers in layer	Thickness of layer (m)	Maximum shear modulus G_{max} (MPa)	Initial critical damping ratio (%)	Total unit weight (kN/m^3)	Shear wave velocity (m/sec)	Location and type of earthquake input motion	Location of water table	Depth at middle of layer (m)	Vertical effective stress (kPa)
klei	1	1	1	3,4	24,12		14,00	130	Outcrop		1,7	23,80
klei	2	1	1	3,4	24,12		14,00	130			5,1	71,40
zand	3	2	1	1,0	56,15		17,00	180			7,3	103,70
zand	4	2	1	2,0	86,34		17,50	220			8,8	129,70
klei	5	1	1	3,3	29,97		15,00	140			11,4	171,95
zand	6	2	1	2,2	124,04		18,00	260			14,2	216,50
klei	7	1	1	1,5	68,54		16,00	205			16,0	248,30
zand	8	2	1	2,0	120,59		17,50	260			17,8	277,80
klei	9	1	1	3,0	63,96		16,50	195			20,3	320,05
zand	10	2	1	2,5	92,89		18,00	225			23,0	367,30
zand	11	2	1	2,0	124,04		18,00	260			25,3	407,80
zand	12	2	1	1,5	130,93		19,00	260			27,0	440,05
zand	13	2	1	1,5	130,93		19,00	260			28,5	468,55
zand	14	2	1	1,5	130,93		19,00	260			30,0	497,05
zand	15	2	1	1,0	130,93		19,00	260			31,3	520,80
zand	16	2	1	1,0	130,93		19,00	260			32,3	539,80
Bedrock	17	0			4357,80	1	19,00	1500			32,8	549,30

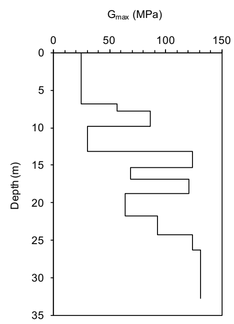

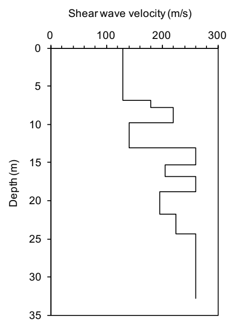

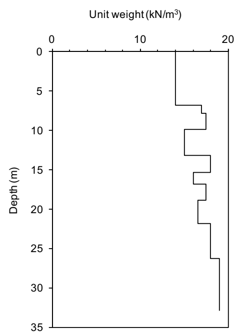

Appendix F figure 2 Soil profile input

Number of iterations : 20
Ratio of effective and maximum shear strain : 0,65
Type of shear modulus = Shake91
Convergence achieved (%) = 3,88E-05

Iteration Number	Sublayer Number	Type	Depth (m)	Maximum Strain (%)	Time of Maximum Strain (sec)	Shear Modulus	G/G_{max}	Damping (%)	Convergence on Shear Modulus (%)	Convergence on Damping (%)	Maximum stress (kPa)	Depth at top of sublayer (m)	Maximum acceleration (g)
1	1	1	1,7	0,005079	5,055	24,11825	1	1	0	0	1,225078		
	2	1	5,1	0,010711	5,435	24,11825	1	1	0	0	2,583377		
	3	2	7,3	0,006495	5,145	56,14679	1	0,24	0	0	3,646615		
	4	2	8,8	0,005033	5,145	86,34047	1	0,24	0	0	4,345098		
	5	1	11,45	0,014589	5,15	29,96942	1	1	0	0	4,372102		
	6	2	14,2	0,002982	4,985	124,0367	1	0,24	0	0	3,698843		
	7	1	16,05	0,006	5,19	68,5423	1	1	0	0	4,112833		
	8	2	17,8	0,003635	5,19	120,5912	1	0,24	0	0	4,383108		
	9	1	20,3	0,007025	4,955	63,95642	1	1	0	0	4,493062		
	10	2	23,05	0,004807	4,945	92,8899	1	0,24	0	0	4,465052		
	11	2	25,3	0,003489	4,935	124,0367	1	0,24	0	0	4,327495		
	12	2	27,05	0,003307	4,925	130,9276	1	0,24	0	0	4,329794		
	13	2	28,55	0,003428	4,92	130,9276	1	0,24	0	0	4,488194		
	14	2	30,05	0,00383	5,25	130,9276	1	0,24	0	0	5,014267		
	15	2	31,3	0,0042	5,255	130,9276	1	0,24	0	0	5,499552		
	16	2	32,3	0,004448	5,255	130,9276	1	0,24	0	0	5,823975		
	17	0	32,8	0,004867	5,265	130,9276	1	1	0	0	6,371809		
2	1	1	1,7	0,005287	5,055	23,42342	0,971191	2,123348	2,880930662	112,3347931	1,238507		
	2	1	5,1	0,011461	5,44	22,33237	0,925953	3,083871	7,404680729	208,387085	2,559577		
	3	2	7,3	0,006874	5,145	52,14855	0,92879	1,797224	7,121044159	648,8433838	3,584615		
	4	2	8,8	0,005112	5,15	82,20431	0,952095	1,500613	4,79052496	525,2553101	4,201982		
	5	1	11,45	0,014732	5,15	27,1889	0,907221	3,481599	9,277850151	248,1598663	4,005555		
	6	2	14,2	0,003131	4,98	120,5546	0,971927	1,161454	2,807272673	383,9391785	3,774348		
	7	1	16,05	0,006239	4,97	65,87518	0,961088	2,337862	3,891216516	133,7861481	4,110229		
	8	2	17,8	0,003728	4,96	116,5542	0,966523	1,269541	3,347706556	428,9753113	4,345119		
	9	1	20,3	0,007984	4,95	60,85631	0,951528	2,540848	4,847221375	154,0848694	4,858646		
	10	2	23,05	0,005352	4,94	88,82939	0,956287	1,447258	4,371313572	503,0242615	4,754527		
	11	2	25,3	0,003844	4,93	120,023	0,967641	1,247182	3,235905409	419,6589966	4,613091		
	12	2	27,05	0,003719	4,92	126,8823	0,969103	1,217943	3,089713573	407,4763794	4,719315		
	13	2	28,55	0,003975	4,915	126,7539	0,968122	1,237566	3,18783164	415,6526794	5,038376		
	14	2	30,05	0,004271	4,91	126,3576	0,965095	1,298099	3,490495682	440,8746948	5,396745		
	15	2	31,3	0,004509	5,26	126,0273	0,962572	1,348552	3,74276042	461,8965149	5,682424		
	16	2	32,3	0,004777	5,26	125,8224	0,961007	1,379855	3,89927268	474,9394226	6,01105		
	17	0	32,8	0,005065	5,27	130,9276	1	1	0	0	6,631787		
3	1	1	1,7	0,005303	5,055	23,36473	0,968757	2,175017	0,243339077	5,166922092	1,239036		
	2	1	5,1	0,011507	5,44	22,2334	0,92185	3,170997	0,410339117	8,71265316	2,558396		
	3	2	7,3	0,006905	5,145	51,85756	0,923607	1,863185	0,518264592	27,48356247	3,580947		
	4	2	8,8	0,005108	5,15	82,08125	0,95067	1,518751	0,142522395	7,557760715	4,192994		
	5	1	11,45	0,01469	5	27,17108	0,906627	3,494224	0,05946181	1,262575388	3,991479		
	6	2	14,2	0,003137	4,98	120,3898	0,970598	1,188041	0,132933632	11,07808304	3,77635		
	7	1	16,05	0,006263	4,97	65,71286	0,95872	2,388142	0,23681049	5,028080463	4,115425		
	8	2	17,8	0,003737	4,96	116,4707	0,965831	1,283383	0,069207311	5,767603397	4,352926		
	9	1	20,3	0,008067	4,95	60,36029	0,943772	2,705523	0,775561392	16,46742249	4,868991		
	10	2	23,05	0,005411	4,94	87,91694	0,946464	1,572277	0,982294858	52,09120178	4,757403		
	11	2	25,3	0,003856	4,93	119,6951	0,964997	1,30005	0,26434797	22,02857399	4,614876		
	12	2	27,05	0,003745	4,92	126,4621	0,965894	1,28213	0,320938051	26,74467468	4,735466		
	13	2	28,55	0,004008	4,915	126,2246	0,964079	1,318412	0,404231846	33,68585968	5,058811		
	14	2	30,05	0,004301	4,91	125,9678	0,962118	1,357649	0,297751695	24,81249046	5,418139		
	15	2	31,3	0,004527	5,26	125,774	0,960638	1,38725	0,193491682	16,12425995	5,693575		
	16	2	32,3	0,004805	5,265	125,2778	0,956848	1,440121	0,415961951	25,11105728	6,019841		
	17	0	32,8	0,005075	5,27	130,9276	1	1	0	0	6,645171		
4	1	1	1,7	0,005304	5,055	23,36043	0,968579	2,178797	0,017801633	0,377949327	1,239075		
	2	1	5,1	0,01151	5,44	22,22758	0,921608	3,176121	0,024136201	0,512413681	2,558313		

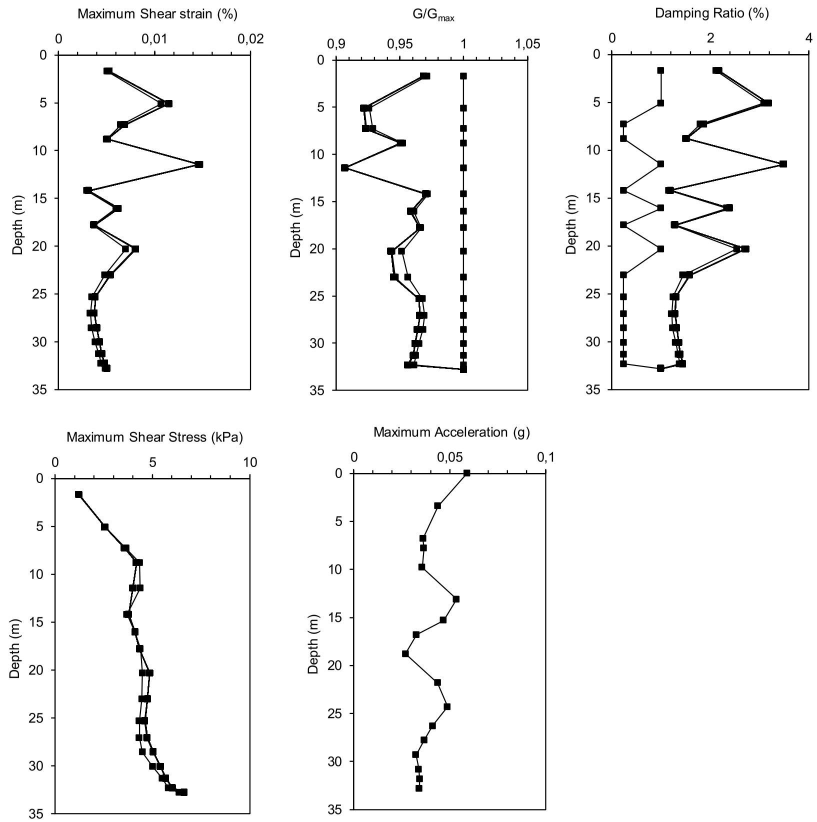

Appendix F figure 3 Iteration settings and strain calculation

Number of sublayer = 17
Type of sublayer = Inside
Depth at top of sublayer (m) = 32,79999924
Maximum acceleration (g) = 0,034
Time of maximum acceleration (sec) = 5,28
Mean Square frequency (Hz) = 8,83
Maximum relative velocity (m/s) = 0,00000
Time of maximum relative velocity (sec) = 0,00
Maximum relative displacement (m) = 0,00000
Time of maximum relative displacement (sec) = 0,00

Time (sec)	Absolute Acceleration (g)	Relative Velocity (m/s)	Relative Displacement (m)
0	-3,94606E-05	0	0
0,005	9,38824E-06	0	0
0,01	5,28674E-05	0	0
0,015	6,54617E-05	0	0
0,02	3,96986E-05	0	0
0,025	-9,42021E-06	0	0
0,03	-5,31528E-05	0	0
0,035	-6,5835E-05	0	0
0,04	-3,99414E-05	0	0
0,045	9,45094E-06	0	0
0,05	5,34398E-05	0	0

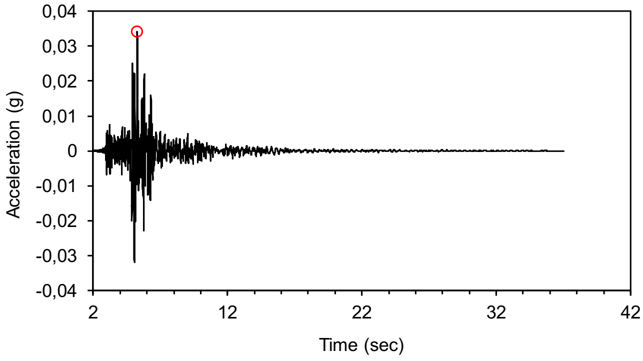

Appendix F figure 4 Output: EERA motion at 30m depth

Appendix G

EERA excel data Huizinge Signal through clay profile

Huizinge 0,25g at ground level

Time step ΔT (sec) = 0,0062
Desired maximum acceleration (g) =
Maximum frequency cut-off (Hz) = 25
Use frequency cut-off in calculation ? Yes
Number of points for FFT = 8192
Import input motion from external file ? No
Name of input file = DIAM.ACC
Total number of values read = 7402
Peak Acceleration in input file (g) = 0,1460
Time of peak acceleration (sec) = 4,073
Mean Square Frequency (Hz) = 7,149
Peak acceleration after filtering (g) = 0,146

Time (sec)	Input Acceleration (g)	Scaled Acceleration (g)	Filtered Acceleration (g)
0,000	-0,000054591	0,00	0,000036346
0,006	0,000216125	0,00	0,000261328
0,012	0,000488029	0,00	0,000482253
0,019	0,000575031	0,00	0,000541464
0,025	0,000373518	0,00	0,000345392
0,031	-0,000047455	0,00	-0,000049737
0,037	-0,000463162	0,00	-0,000443043
0,043	-0,000620851	0,00	-0,000598336
0,050	-0,000402900	0,00	-0,000396515
0,056	0,000082686	0,00	0,000070029
0,062	0,000552593	0,00	0,000533708
0,068	0,000716949	0,00	0,000708123
0,074	0,000462890	0,00	0,000470329
0,081	-0,000066285	0,00	-0,000050420
0,087	-0,000552131	0,00	-0,000541872
0,093	-0,000695410	0,00	-0,000698839
0,099	-0,000402617	0,00	-0,000415701
0,105	0,000153328	0,00	0,000142364
0,112	0,000637220	0,00	0,000637458
0,118	0,000755937	0,00	0,000766366
0,124	0,000436376	0,00	0,000447469
0,130	-0,000131603	0,00	-0,000129290
0,136	-0,000611205	0,00	-0,000619080
0,143	-0,000720825	0,00	-0,000731575
0,149	-0,000399736	0,00	-0,000404046
0,155	0,000159686	0,00	0,000165127

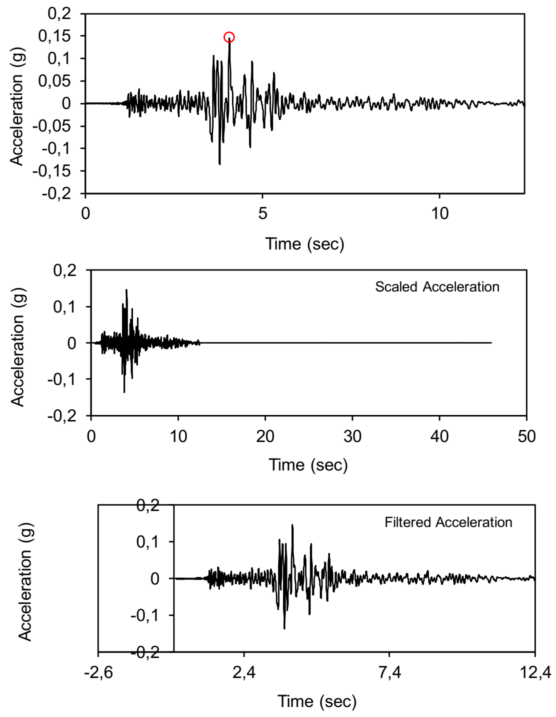

Appendix G figure 1 input and scaling Huizinge signal

Fundamental period (s) = 0,87
Average shear wave velocity (m/sec) = 137,79
Total number of sublayers = 16

	Layer Number	Soil Material Type	Number of sublayers in layer	Thickness of layer (m)	Maximum shear modulus G_{max} (MPa)	Initial critical damping ratio (%)	Total unit weight (kN/m ^{3})	Shear wave velocity (m/sec)	Location and type of earthquake input	Location of water table	Depth at middle of layer (m)	Vertical effective stress (kPa)
Surface	1	1		2,0	11,77		18,00	80,1		W	1,0	8,19
	2	1		2,0	16,39		18,00	94,5			3,0	24,57
	3	1		2,0	20,50		18,00	105,7			5,0	40,95
	4	1		2,0	24,27		18,00	115			7,0	57,33
	5	1		2,0	27,80		18,00	123,1			9,0	73,71
	6	1		2,0	31,15		18,00	130,3			11,0	90,09
	7	1		2,0	34,34		18,00	136,8			13,0	106,47
	8	1		2,0	37,42		18,00	142,8			15,0	122,85
	9	1		2,0	40,41		18,00	148,4			17,0	139,23
	10	1		2,0	43,29		18,00	153,6			19,0	155,61
	11	1		2,0	46,10		18,00	158,5			21,0	171,99
	12	1		2,0	48,81		18,00	163,1			23,0	188,37
	13	1		2,0	51,48		18,00	167,5			25,0	204,75
	14	1		2,0	54,09		18,00	171,7			27,0	221,13
	15	1		2,0	56,64		18,00	175,7			29,0	237,51
Bedrock	16	0			56,64	1	18,00	175,7	Outcrop		30,0	245,70

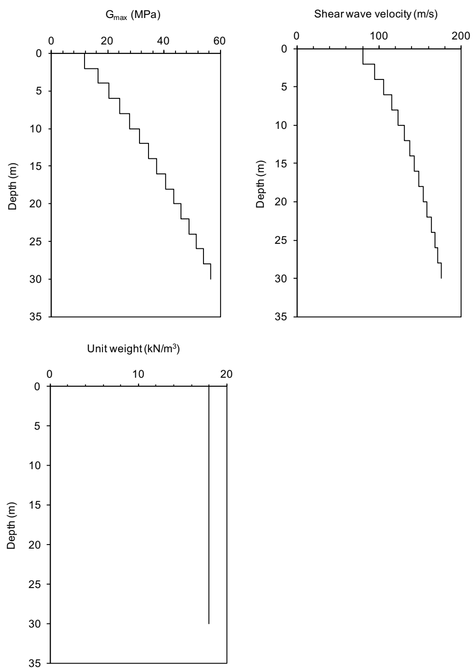

Appendix G figure 2 Clay soil profile

HS small

Strain (%)	G/G_{max}	Strain (%)	Damping (%)
0,000	1,0000	0,000	0,029
0,000	0,9959	0,000	0,087
0,001	0,9864	0,001	0,290
0,003	0,9604	0,003	0,858
0,010	0,8791	0,010	2,732
0,030	0,7080	0,030	7,300
0,100	0,4211	0,100	18,538
0,300	0,1951	0,300	18,538
1,000	0,0678	1,000	18,538
3,000	0,0237	3,000	18,538
10,000	0,0072	10,000	18,538

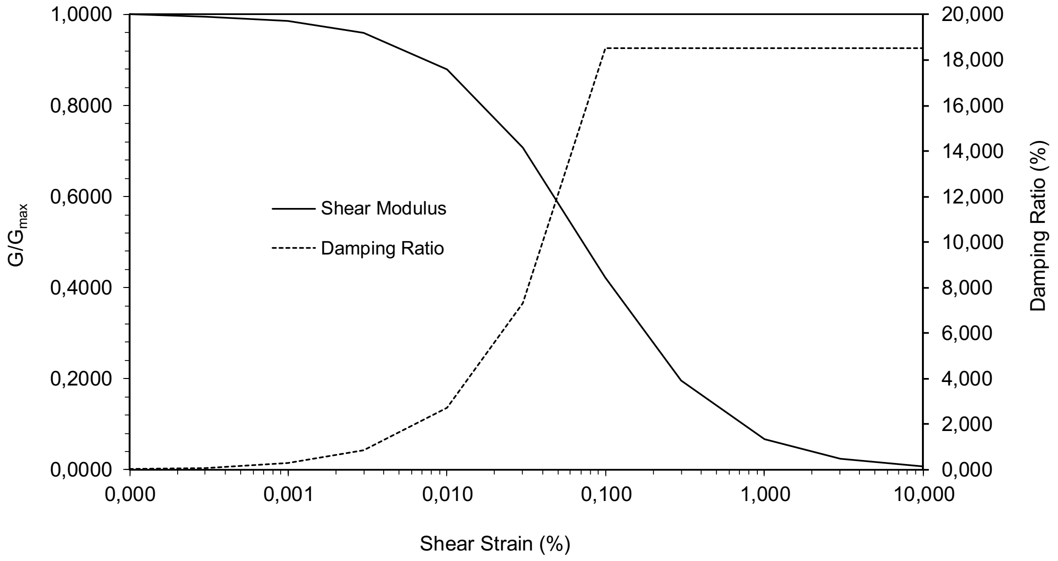

Appendix G figure 3 Modulus reduction curve for the clay profile based on the Hardening Soil small strain model

Number of sublayer = 1
Depth (m) = 1,00
Maximum strain (%) = 0,0249
Effective strain (%) = 0,0162
Number of soil material type = 1
Shear modulus compatible to strain (MPa) = 9,4630
Maximum stress (kPa) = 2,3887
Time of maximum strain and stress (sec) = 4,328

Time (sec)	Strain (%)	Stress (kPa)	Energy (kPa)
0	-8,406E-07	-3,59805E-05	0
0,0062	-9,677E-07	-4,77148E-05	6,06329E-14
0,0124	-1,079E-06	-5,68116E-05	1,2389E-13
0,0186	-1,075E-06	-5,45035E-05	1,21636E-13
0,0248	-9,565E-07	-4,19723E-05	7,19111E-14
0,031	-8,288E-07	-2,97296E-05	3,39477E-14
0,0372	-8,1E-07	-2,84766E-05	2,85954E-14
0,0434	-9,241E-07	-3,93022E-05	7,34455E-14
0,0496	-1,075E-06	-5,22687E-05	1,52123E-13
0,0558	-1,127E-06	-5,4933E-05	1,80802E-13
0,062	-1,029E-06	-4,36203E-05	1,38111E-13
0,0682	-8,644E-07	-2,72465E-05	9,32686E-14
0,0744	-7,82E-07	-1,97515E-05	7,69917E-14
0,0806	-8,62E-07	-2,75727E-05	9,90745E-14
0,0868	-1,039E-06	-4,32974E-05	1,75792E-13
0,093	-1,155E-06	-5,1622E-05	2,3531E-13
0,0992	-1,095E-06	-4,30973E-05	2,09723E-13
0,1054	-9,04E-07	-2,32217E-05	1,6533E-13
0,1116	-7,48E-07	-8,23366E-06	1,52488E-13
0,1178	-7,711E-07	-1,06384E-05	1,54944E-13
0,124	-9,574E-07	-2,7291E-05	2,05781E-13
0,1302	-1,135E-06	-4,11052E-05	2,78696E-13
0,1364	-1,125E-06	-3,61074E-05	2,75103E-13
0,1426	-9,099E-07	-1,2534E-05	2,48164E-13
0,1488	-6,626E-07	1,22468E-05	2,78454E-13
0,155	-5,96E-07	1,88579E-05	2,91012E-13
0,1612	-7,622E-07	4,4779E-06	2,83567E-13
0,1674	-9,856E-07	-1,27177E-05	3,1198E-13
0,1736	-1,01E-06	-8,96853E-06	3,14137E-13
0,1798	-7,355E-07	2,28481E-05	3,76797E-13
0,186	-3,323E-07	6,47981E-05	6,38017E-13
0,1922	-9,497E-08	8,95091E-05	8,50472E-13
0,1984	-1,52E-07	8,76298E-05	8,00489E-13
0,2046	-3,006E-07	8,09764E-05	6,80135E-13
0,2108	-1,511E-07	0,000106501	8,39402E-13
0,217	5,2279E-07	0,000182739	2,07085E-12
0,2232	1,5636E-06	0,000292202	5,11218E-12
0,2294	2,6442E-06	0,000405107	9,48971E-12
0,2356	3,8292E-06	0,000532426	1,57987E-11
0,2418	5,985E-06	0,000759401	3,21701E-11
0,248	1,0481E-05	0,001209517	8,65554E-11
0,2542	1,8089E-05	0,001937236	2,33935E-10
0,2604	2,771E-05	0,002814782	5,04727E-10
0,2666	3,5994E-05	0,003512125	7,95701E-10
0,2728	3,8563E-05	0,003627506	8,88884E-10
0,279	3,2491E-05	0,002925429	7,1124E-10
0,2852	1,8641E-05	0,001541245	4,97788E-10
0,2914	2,1611E-06	-1,23464E-06	4,97991E-10
0,2976	-9,663E-06	-0,001017565	6,18307E-10
0,3038	-1,129E-05	-0,00103433	6,35154E-10
0,31	-2,345E-06	-8,80659E-05	6,27275E-10
0,3162	1,1723E-05	0,001250999	8,03257E-10
0,3224	2,2432E-05	0,002177641	1,03646E-09
0,3286	2,3145E-05	0,002116226	1,05156E-09
0,3348	1,3106E-05	0,001073733	9,4376E-10
0,341	-1,925E-06	-0,000346769	9,95882E-10
0,3472	-1,301E-05	-0,00129764	1,13966E-09
0,3534	-1,341E-05	-0,001199499	1,14449E-09
0,3596	-2,795E-06	-0,000102677	1,13359E-09
0,3658	1,2445E-05	0,001331214	1,33648E-09
0,372	2,2988E-05	0,002222763	1,57081E-09
0,3782	2,2199E-05	0,002006765	1,55498E-09
0,3844	1,0184E-05	0,00077764	1,46155E-09
0,3906	-6,235E-06	-0,000763044	1,58683E-09
0,3968	-1,758E-05	-0,001724954	1,7826E-09
0,403	-1,738E-05	-0,001559077	1,7794E-09
0,4092	-5,951E-06	-0,000381274	1,73583E-09

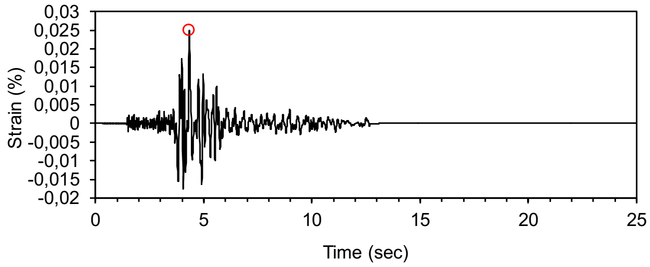

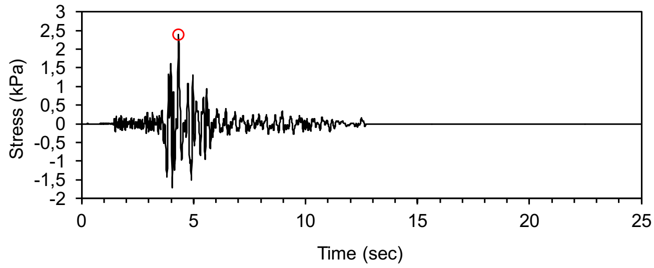

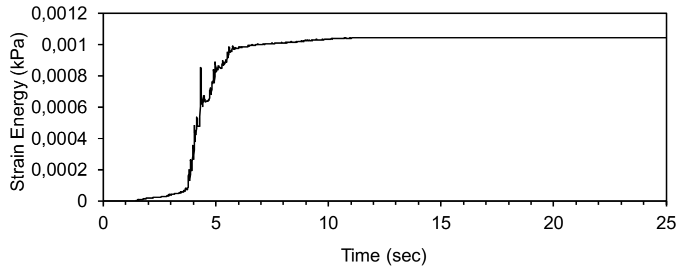

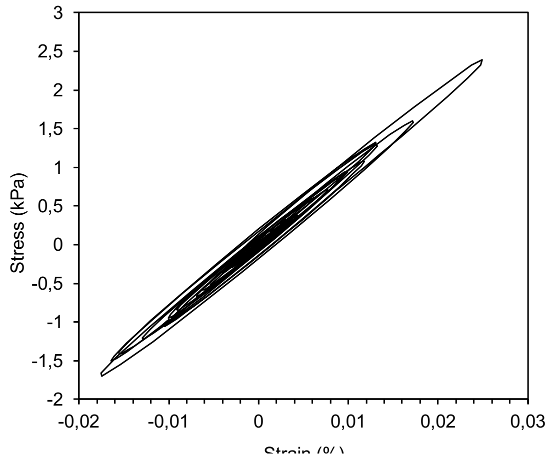

Appendix G figure 4 Output: Strain at ground level

Number of iterations : 50
Ratio of effective and maximum shear strain : 0,65
Type of shear modulus = Shake91
Convergence achieved (%) = 0

Iteration Number	Sublayer Number	Type	Depth (m)	Maximum Strain (%)	Time of Maximum Strain (sec)	Shear Modulus	G/G_{max}	Damping (%)	Convergence on Shear Modulus (%)	Convergence on Damping (%)	Maximum stress (kPa)	Depth at top of sublayer (m)	Maximum acceleration (g)
1	1	1	1	0,031301	4,2966	11,77249	1	0,029158	0	0	3,684935		
	2	1	3	0,044212	4,3028	16,38578	1	0,029158	0	0	7,244528		
	3	1	5	0,04334	4,3214	20,49998	1	0,029158	0	0	8,884654		
	4	1	7	0,039402	3,906	24,26605	1	0,029158	0	0	9,561378		
	5	1	9	0,03632	3,906	27,80479	1	0,029158	0	0	10,0987		
	6	1	11	0,032293	4,278	31,15246	1	0,029158	0	0	10,06008		
	7	1	13	0,030113	4,278	34,33805	1	0,029158	0	0	10,34035		
	8	1	15	0,024982	4,278	37,41622	1	0,029158	0	0	9,347187		
	9	1	17	0,021108	4,2036	40,40836	1	0,029158	0	0	8,529441		
	10	1	19	0,022919	4,216	43,28983	1	0,029158	0	0	9,921721		
	11	1	21	0,022636	4,2222	46,09587	1	0,029158	0	0	10,43417		
	12	1	23	0,01916	4,2284	48,81029	1	0,029158	0	0	9,351838		
	13	1	25	0,016582	3,627	51,47935	1	0,029158	0	0	8,536438		
	14	1	27	0,017321	3,6084	54,09337	1	0,029158	0	0	9,369762		
	15	1	29	0,01761	3,6022	56,64309	1	0,029158	0	0	9,974956		
	16	0	30	0,019152	4,0796	56,64309	1	1	0	0	10,8485		
2	1	1	1	0,025947	4,3276	9,046722	0,768463	5,685363	23,1537323	19398,21875	2,347348		
	2	1	3	0,044377	4,34	11,71026	0,71466	7,121102	28,53398323	24322,1582	5,196672		
	3	1	5	0,045031	4,3524	14,71417	0,717765	7,038241	28,22347069	24037,98242	6,625937		
	4	1	7	0,039839	4,3338	17,77741	0,732604	6,642257	26,73956871	22679,93359	7,082266		
	5	1	9	0,036663	4,3152	20,72275	0,745294	6,303616	25,47055435	21518,54883	7,597597		
	6	1	11	0,031851	4,309	23,78811	0,763603	5,815051	23,6397171	19842,99023	7,576747		
	7	1	13	0,025788	3,7138	26,59448	0,77449	5,524523	22,55101013	18846,61328	6,858209		
	8	1	15	0,023754	3,7014	30,06754	0,803597	4,747803	19,64034653	16182,81543	7,142282		
	9	1	17	0,022639	3,6828	33,53268	0,829845	4,047347	17,01547813	13780,56836	7,591555		
	10	1	19	0,022083	3,6704	35,36866	0,81702	4,389591	18,29799843	14954,30859	7,810573		
	11	1	21	0,021078	3,658	37,75063	0,818959	4,337846	18,10409164	14776,84961	7,957149		
	12	1	23	0,020378	3,6394	41,2415	0,844935	3,644681	15,50653839	12399,60547	8,404322		
	13	1	25	0,01965	3,627	44,65535	0,867442	3,044066	13,25581646	10339,76953	8,774989		
	14	1	27	0,020084	4,1788	46,55531	0,860647	3,225384	13,9352808	10961,60547	9,349995		
	15	1	29	0,020742	4,1602	48,60384	0,858072	3,294111	14,19282818	11197,30957	10,08134		
	16	0	30	0,020991	4,1416	56,64309	1	1	0	0	11,89022		
3	1	1	1	0,025107	4,3276	9,390801	0,79769	4,90542	2,922736645	2674,848145	2,357794		
	2	1	3	0,044674	4,34	11,70077	0,714081	7,136569	0,057956897	53,0410881	5,227199		
	3	1	5	0,045789	4,3524	14,59192	0,711802	7,197381	0,596354067	545,7778931	6,681528		
	4	1	7	0,039956	4,3338	17,73579	0,730889	6,688036	0,171547815	157,0024261	7,086524		
	5	1	9	0,036672	4,3152	20,68203	0,74383	6,3427	0,146463275	134,0413055	7,584572		
	6	1	11	0,031843	4,309	23,855	0,76575	5,757748	0,214732751	196,5226135	7,596115		
	7	1	13	0,024932	3,7138	27,42397	0,798647	4,87989	2,415682316	2210,799805	6,837346		
	8	1	15	0,023473	3,7014	30,36125	0,811446	4,538332	0,784961939	718,3914185	7,126717		
	9	1	17	0,022846	3,6828	33,09183	0,818935	4,338485	1,091004252	998,4707031	7,560171		
	10	1	19	0,021824	3,6704	35,61926	0,822809	4,235117	0,578877449	529,7758789	7,773583		
	11	1	21	0,020679	3,658	38,26262	0,830066	4,04145	1,110706091	1016,505432	7,912342		
	12	1	23	0,020444	3,6394	40,77255	0,835327	3,901064	0,960764945	879,2790527	8,335434		
	13	1	25	0,020117	3,627	43,29378	0,840993	3,749862	2,64487505	2420,559082	8,709384		
	14	1	27	0,020638	4,1788	45,3084	0,837596	3,840507	2,30509305	2109,595703	9,350874		
	15	1	29	0,02122	4,1664	47,15946	0,832572	3,974579	2,549962997	2333,695313	10,0073		
	16	0	30	0,020779	4,1416	56,64309	1	1	0	0	11,76978		
4	1	1	1	0,024973	4,3276	9,45112	0,802814	4,768691	0,512371838	468,9196777	2,360188		
	2	1	3	0,044788	4,34	11,68374	0,713042	7,164291	0,103883579	95,07687378	5,232929		
	3	1	5	0,04603	4,3524	14,53859	0,7092	7,266802	0,260148674	238,0818634	6,69208		
	4	1	7	0,039976	4,3338	17,72465	0,73043	6,700282	0,045887567	41,99745941	7,085577		
	5	1	9	0,036654	4,3152	20,68094	0,743791	6,343745	0,003916937	3,582406998	7,580359		
	6	1	11	0,031845	4,309	23,85624	0,76579	5,756687	0,003973585	3,639899254	7,597099		
	7	1	13	0,024769	3,7138	27,60458	0,803906	4,739533	0,525967002	481,3597412	6,837256		
	8	1	15	0,023421	3,7014	30,43063	0,8133	4,488849	0,185432196	169,7043915	7,127027		
	9	1	17	0,022883	3,6828	33,03459	0,817519	4,376282	0,141643256	129,6271667	7,559309		

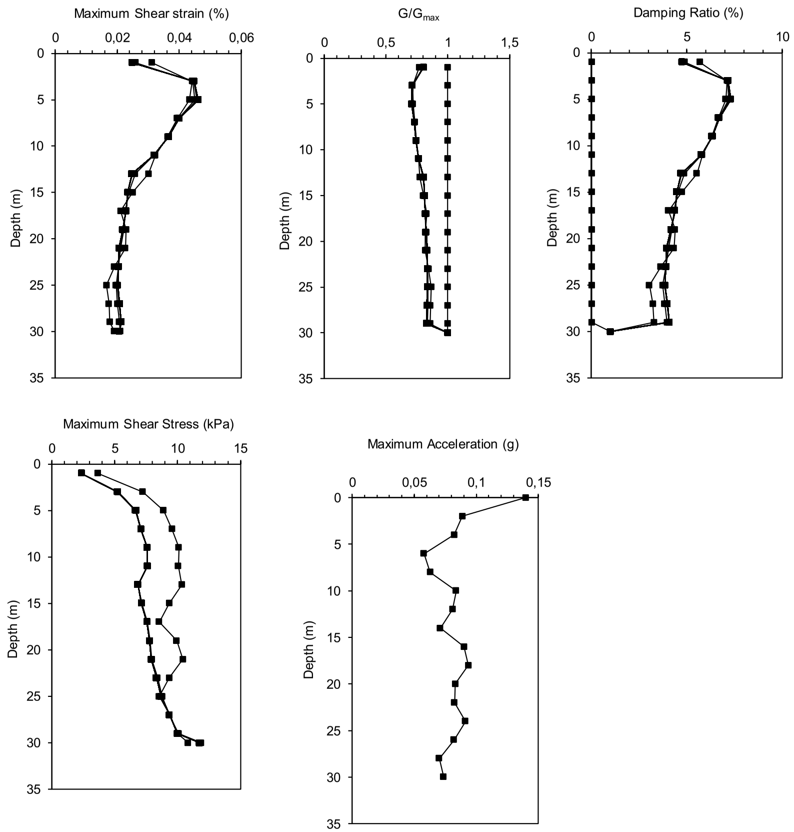

Appendix G figure 5 Iteration setting and calculated maximum damping

TU Delft Delft University of Technology

CRUX

Appendix H

Pile bearing capacity of single pile in continuous one layered clay profile

The assumption here is that the clay layer has an average cone resistance of approximately 1 MPa. Based on the Dutch design code NEN-EN 1997-1 the bearing capacity is then calculated with the values shown in the table below:

NEN 9997-1+C1:2012	Description	Symbol	Value	Kolom1
Skin friction	Circumference of the pile	$O_{s;l;gem}$	1,570796327	m
	Length of the pile	L	10	
	Pile class factor	α_s	0,02	
	Cone resistance	qc	1000	kPa
	Maximum allowable cone resistance	$q_{s;max}$	20	kPa
	Characteristic skin resistance	$R_{s;k}$	314	kN
	Safety factor	γ_b	1,5	
	Design value for skin resistance	$R_{s;d}$	**209**	kN
Pile Tip bearing capacity	Pile surface	Ab	0,196349541	m2
	cone resistance	qc	1000	kPa
	Pile class factor	α_p	1	
	Pile tip factor	β	1	
	Cross sectional factor	s	1	
	Maximum pile tip resistance	$q_{b;max}$	1000	kPa
	Characteristic pile bearing capacity	$R_{b;k}$	196	kN
	Safety factor	γ_s	1,5	
	Design value for bearing capacity	$R_{b;d}$	**131**	kN
Maximum pile bearing capacity	***Design value for pile bearing capacity***	$R_{c;d}$	***340***	***kN***
Weigth of plate in PLAXIS 2D model		**Ls=2**	170	kN/m
		Ls=4	85	kN/m
		Ls=8	42,5	kN/m

Appendix I

Modulus of subgrade reaction by Ménard

Ménard developed an empirical method for determining k_h as given in equation (I1). It is based on in-situ test with a pressiometer. In equation (I1), R and R_0 are pile radius and reference pile radius of 0.3m. E_p is the modulus of elasticity determined with a pressiometer test, or can be related to a CPT test: $E_p \approx \beta \cdot q_c$. Finally, α and β are rheological factors dependent on soil type, see table below:

$$\frac{1}{k_h} = \frac{1}{3E_p} * \left[1.3 * R_0 \left(2.65 \frac{R}{R_0}\right)^{\alpha} + \alpha R\right] \tag{I1}$$

Soil type	α [-]	β [-]
Peat	1	3.0
Clay	2/3	2.0
Silt	1/2	1.0
Sand	1/3	0.7
Gravel	1/4	0.5

Values for α and β according to Ménard (CUR 228, 2010)

Sheet **Horizontale beddingsconstante Ménard v007**
Project
Projectnummer
Onderdeel
Datum
Adviseur

CRUX

#VALUE!

belastingsituatie = statisch ... factor = 1,0 [-] op stijfheid E_m

D_{paal} = 0,500 [m] diameter van de paal — R_{paal} = 0,250 [m] Situatie: R < R_0

h.o.h. dwars = 2,00 [m] paalafstand dwars op belasting
h.o.h. langs = 10,00 [m] paalafstand in richting belasting

e_{side} = 1,00 [-] palenrij "side-by-side"
e_{line1} = 1,00 [-] voorste paal "in-line"
e_{line2} = 1,00 [-] overige palen "in-line"

..

Bepalen met lage waarde van β

Maaiveld = +0,0 [NAP .. m]

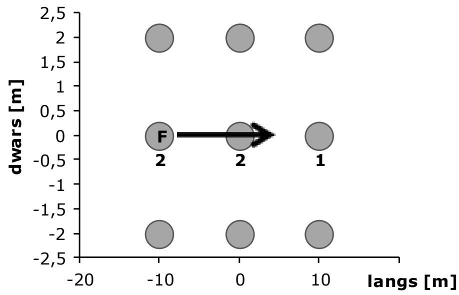

Grondsoort	bk laag [NAP .. m]	ok laag [NAP .. m]	$q_{c;gem}$ [MPa]	α [-]	β [-]	$E_{M;gem}$ [kPa]	$k_{h;alleen}$ [kN/m³]	$k_{h;1}$ [kN/m³]	$k_{h;2}$ [kN/m³]
klei n.c.	+0,00	-20,00	1,0	0,67	2,00	2000	7500	7500	7500